Julius-Maximilians-
UNIVERSITÄT
WÜRZBURG

Julius–Maximilians–Universität Würzburg
Institut für Theoretische Physik und Astronomie
Lehrstuhl für Theoretische Physik II

LHC Phenomenology of Top Partners in Models with SU(6)/Sp(6)

Masterarbeit im Fach Physik

vorgelegt von
Manuel Kunkel

Betreuer:
Prof. Dr. Werner Porod

Abgabe der Arbeit:
27.09.2021

Summary

In the standard model, the Higgs mass m_h receives radiative corrections from high energy scales. To obtain $m_h = 125$ GeV, the coefficient of the Higgs mass term must be fine-tuned with high precision, which goes against the principle of naturalness. Composite Higgs models provide a solution to this by cutting off corrections to m_h at the Higgs compositeness scale. We study a specific composite Higgs model based on the coset $\mathrm{SU}(5) \times \mathrm{SU}(6) \times \mathrm{U}(1)/\mathrm{SO}(5) \times \mathrm{Sp}(6)$ with a fermionic UV completion. To ensure that the top quark can develop a large Yukawa coupling, the model contains composite fermions, so-called top partners, some of which can mix with the top quark. We derive the particle content of the model, calculate parts of the Lagrangian and determine the scalar potential for the pseudo Nambu-Goldstone bosons in the color sector coset $\mathrm{SU}(6)/\mathrm{Sp}(6)$. The latter calculation shows that the neutral color octet π_8 and the charge-2/3 color triplet π_3 generically have different masses, but the mass hierarchy cannot be determined due to the large number of independent coefficients.

Next, we study the phenomenology of the model, focusing on the color octet top partners, which we name "gluonis" in analogy to the gluino in supersymmetry. We show that they can decay via π_3 or π_8 into final states such as $4t$+MET, $2t2j$+MET or $4j$+MET, where the missing energy is due to a stable Majorana color singlet top partner, the "boni". We then formulate simplified models for these decays, implement them in FeynRules and simulate the pair production of gluonis at the LHC. By comparing the results with ATLAS and CMS searches, we derive exclusion bounds in the gluoni-boni-mass plane. For the full gluoni multiplet, these reach up to 2.7 TeV for a massless boni, while the strongest bounds on the boni mass are just below 1.7 TeV. Finally, we discuss how the phenomenology would change if our assumptions about the mass hierachies of the top partners do not hold.

Zusammenfassung

Im Standardmodell erhält die Higgs-Masse Strahlungskorrekturen von hohen Energieskalen. Um $m_h = 125$ GeV zu erhalten, muss der Koeffizient des Higgs-Massenterms sehr genau eingestellt werden, was dem Natürlichkeitsprinzip widerspricht. Composite-Higgs-Modelle lösen dieses Problem, indem sie die Korrekturen zu m_h an der Skala abschneiden, bei der die Bestandteile des zusammengesetzten Higgs berücksichtigt werden müssen. Wir untersuchen ein spezielles Composite-Higgs-Modell mit einer fermionischen UV-Vervollständigung, das auf der Faktorgruppe $\mathrm{SU}(5) \times \mathrm{SU}(6) \times \mathrm{U}(1)/\mathrm{SO}(5) \times \mathrm{Sp}(6)$ basiert. Um sicherzustellen, dass das Top Quark eine hinreichend große Yukawa-Kopplung bilden kann, enthält das Modell zusammengesetzte Fermionen, sogenannte Top Partner, von denen manche Mischungen mit dem Top Quark eingehen können. Wir bestimmen den Teilcheninhalt des Modells und berechnen Teile der Lagrangedichte sowie das skalare Potential für die Pseudo-Nambu-Goldstone-Bosonen in der farbgeladenen Faktorgruppe $\mathrm{SU}(6)/\mathrm{Sp}(6)$. Letztere Rechnung zeigt, dass das neutrale Oktett π_8 und das Triplett π_3 mit Ladung 2/3 im Allgemeinen unterschiedliche Massen haben, aber die Massenhierarchie kann aufgrund der vielen unabhängigen Koeffizienten nicht bestimmt werden.

Des Weiteren untersuchen wir die Phänomenologie des Modells, wobei wir uns auf die Oktett Top Partner konzentrieren. In Analogie zum Gluino in der Supersymmetrie nennen wir diese "Gluonis". Wir zeigen, dass sie über π_3 oder π_8 zerfallen können. Die resultierenden Endzustände sind beispielsweise $4t$+MET, $2t2j$+MET oder $4j$+MET, wobei die fehlende Energie (MET) von dem stabilen Singulett Majorana Top Partner – dem "Boni" – kommt. Anschließend formulieren wir vereinfachte Modelle für die Zerfälle, implementieren diese in FeynRules und simulieren die Paarproduktion von Gluonis am LHC. Durch Vergleich der Ergebnisse mit ATLAS- und CMS-Suchen bestimmen wir Ausschlussgrenzen in der Ebene der Gluoni-Boni-Massen. Für das volle Gluoni Multiplett reichen diese bis zu 2,7 TeV für ein masseloses Boni, während die stärksten Ausschlussgrenzen für die Boni-Masse bis beinahe 1,7 TeV reichen. Abschließend diskutieren wir, wie sich die Phänomenologie ändern würde, wenn unsere Annahmen über die Massenhierarchien der Top Partner nicht zutreffen.

Contents

1 | Introduction

With the discovery of the Higgs boson in 2012 [1, 2], all particles predicted by the standard model (SM) have been observed. However, despite its successes, we know that the SM is not the full story: It includes neither neutrino masses nor dark matter, and the quantum description of gravity breaks down above the Planck scale. The SM should therefore be viewed as an effective field theory that gives an accurate description of nature only up to a scale Λ_{SM}, above which new physics sets in [3]. Besides that, the SM also has several theoretical flaws. For example, it offers no explanation for the strong CP problem, the hierarchy among the fermion masses or the naturalness problem associated with the Higgs mass. The latter in particular has inspired much of the model building beyond the standard model (BSM) of the past decades and provides the primary motivation for this thesis.

The principle of naturalness states, that the parameters of a theory at high energies cannot be correlated with the physics of the effective theory in the infrared [4]. In that sense, the SM is unnatural. To see this, we imagine that we know the fundamental theory replacing the SM above Λ_{SM}. We can then formally compute the Higgs mass from the parameters p_{fund} of the fundamental theory, similar to how the Fermi constant G_F can be computed from the parameters of the electroweak (EW) theory, $G_F = g^2/(4\sqrt{2}m_W^2)$. In general [3],

$$m_h^2 = \int_0^\infty \mathrm{d}E\, \frac{\mathrm{d}m_h^2}{\mathrm{d}E}(E; p_{\text{fund}}) = \int_0^{\lesssim\Lambda_{\text{SM}}} \mathrm{d}E\, \frac{\mathrm{d}m_h^2}{\mathrm{d}E}(E; p_{\text{fund}}) + \int_{\lesssim\Lambda_{\text{SM}}}^\infty \mathrm{d}E\, \frac{\mathrm{d}m_h^2}{\mathrm{d}E}(E; p_{\text{fund}}) \tag{1.1a}$$

$$= \delta_{\text{SM}} m_h^2 + \delta_{\text{BSM}} m_h^2, \tag{1.1b}$$

where the integrand can include both tree-level and loop contributions. By splitting the integral slightly below the cutoff, we obtain an unknown term $\delta_{\text{BSM}} m_h^2$ from physics above Λ_{SM} and a computable contribution from virtual SM particles, which is dominated by top loops,

$$\frac{\delta_{\text{SM}} m_h^2}{m_h^2} \gtrsim \frac{3y_t^2}{8\pi^2}\left(\frac{\Lambda_{\text{SM}}}{m_h}\right)^2 \simeq \left(\frac{\Lambda_{\text{SM}}}{450\ \text{GeV}}\right)^2. \tag{1.2}$$

The quadratic divergence stems from the fact that the Higgs mass term $\mu^2 H^\dagger H$ is a relevant operator. Since the Higgs has a mass of $m_h^2 = 2\mu^2 = (125\ \text{GeV})^2$, the contributions in Eq. (1.1b) have to coincide almost exactly, $\delta_{\text{SM}} m_h^2 \simeq -\delta_{\text{BSM}} m_h^2$, if Λ_{SM} is large. For example, for $\Lambda_{\text{SM}} \sim M_{\text{GUT}} = 10^{15}$ GeV, an enormous cancellation of 24 digits has to take place between the SM and the BSM contribution. But they emerge from completely different energy scales and should therefore not be correlated at all. This is known as the *naturalness problem* of the SM [5, 6].

If nature is to be described by a natural theory, there has to be new physics at the TeV scale resolving the naturalness problem. One promising approach is to assume that the Higgs is a composite particle with an extension of $l_h^{-1} \sim 1$ TeV. The Higgs mass would then be immune

to large corrections, as particles with energy $E \gtrsim l_h^{-1}$ cannot resolve the Higgs but instead see its constituents [3]. In these so-called *composite Higgs models* [7–9], the Higgs emerges as a bound state of a new composite sector. This is a purely fermionic gauge theory in the UV that condenses at the TeV scale. The condensation spontaneously breaks the global symmetry group $\mathcal{G}$ of the composite sector to the subgroup $\mathcal{H}$, leading to (pseudo) Nambu-Goldstone bosons (pNGBs) in the coset $\mathcal{G}/\mathcal{H}$, among them the Higgs. Their potential is generated by interactions between the composite and the elementary sector (the SM minus the Higgs), which explicitly break $\mathcal{G}$. Besides the pNGBs, the composite sector also forms fermionic resonances with masses in the TeV. In order to achieve a sufficiently large Yukawa coupling for the top quark, we assume the physical top quark to be a linear combination of an elementary and a composite state. This is known as *partial compositeness* [10] and requires the composite sector to produce states that can mix with the top quark, so-called *top partners*.

In recent years, the search for UV theories that can deliver a suitable composite sector has seen a lot of activity. In particular, a set of minimal models have been identified as promising candidates [11–13]. In this thesis, we study one of these models, which was named M5 in [13]. It is based on the symmetry breaking pattern

$$\mathcal{G} = \mathrm{SU}(5) \times \mathrm{SU}(6) \times \mathrm{U}(1) \to \mathrm{SO}(5) \times \mathrm{Sp}(6) = \mathcal{H}, \tag{1.3}$$

which offers a rich phenomenology with 29 pNGBs. Among them are an electrically neutral color octet π_8 and a color triplet π_3 with charge 2/3. We classify the leading operators that contribute to the scalar potential of these colored pNGBs with the aim to estimate their masses. The model M5 also includes several non-standard top partners, such as color singlet and octet fermions. We focus on the latter, which we name *gluonis* in analogy to the fermionic partner of the gluon in supersymmetry. Gluonis would be produced by the LHC with an appreciable cross section due to large color factors. Also, to our knowledge, the LHC phenomenology of charged color octet top partners has not yet been studied in the literature. We work out the dominant decay channels of gluonis and implement these in FeynRules [14]. We then simulate gluoni pair production and subsequent decays at the LHC with MadGraph5_aMC@NLO [15]. By comparing the generated events with experimental searches implemented in MadAnalysis5 [16–19] and CheckMATE [20, 21], we derive exclusion bounds on the masses of the new particles.

The remainder of this thesis is structured as follows. In Chapter 2 we review the construction of composite Higgs models and describe the classification of fermionic UV completions. Chapter 3 is dedicated to exploring the model M5. After defining the UV theory we derive the particle content in the IR. We then compute parts of the Lagrangian that are relevant to the phenomenology of gluonis. Furthermore, we classify the leading operators contributing to the scalar potential and compute their contribution to the masses of colored pNGBs. In Chapter 4 we turn to studying the phenomenology of the model, focusing on pair production of gluonis. We describe the tools used for the simulation and analysis, discuss the recasted searches and present the obtained mass bounds. Finally, we summarize our results in Chapter 5 and discuss how this research can be extended.

2 | UV Completions of Composite Higgs Models

This chapter explains the foundations of composite Higgs models (CHMs) and their fermionic UV completions. We begin with the general idea of the composite Higgs scenario, focusing on the low-energy regime first. After introducing the setup of a CHM, we review the low-energy effective theory and discuss how partial compositeness helps with understanding the large top mass. We then discuss which specific UV completions have a chance to be phenomenologically successful.

2.1 Basics of Composite Higgs Models

In the SM, the electroweak symmetry breaking (EWSB) is triggered by an elementary scalar, the Higgs boson. Its mass receives radiative corrections that grow quadratically with the cutoff scale. Thus, the coefficient of the Higgs mass has to be fine-tuned very precisely to reproduce $m_h = 125$ GeV. This *naturalness problem* of the SM has been known for decades [6], and since then theorists have been looking for natural explanations for a light Higgs.

2.1.1 A Naturally Light Higgs

The naturalness problem is intrinsically tied to the Higgs being an elementary scalar, so it can be avoided by constructing a model where the Higgs is a composite state. And there is precedence in nature for a composite scalar inducing spontaneous symmetry breaking [22]: Low-energy QCD with two flavors in the chiral limit ($m_u = m_d = 0$) has a global $\mathrm{SU}(2)_L \times \mathrm{SU}(2)_R$ symmetry that gets broken to $\mathrm{SU}(2)_D$ by the chiral condensate $\langle \overline{q}_R q_L \rangle = \Lambda_{\mathrm{QCD}}^3 \mathbb{1}_2$, yielding massless pions as Nambu-Goldstone bosons. These give mass to the W and Z bosons when the electroweak interactions are turned on, albeit a small one, $m_W = g f_\pi / 2 = 29$ MeV. Here, $f_\pi = 92$ MeV is the pion decay constant.

This motivated early technicolor models [6, 23, 24] to remove the Higgs sector in favor of another strongly interacting "technicolor" gauge group, which is essentially a scaled-up version of QCD [22]. The EW symmetry is then broken dynamically by the condensate of new "technicquarks", giving the vector bosons masses of $m_W = g f_T / 2$. Thus, the technipion decay constant f_T corresponds to the EW scale, $f_T = v$. But if technicolor condensed around v, we would expect a large number of technihadrons with masses $\sim v$ similar to the QCD hadrons around 1 GeV, which have not been observed. This, along with the absence of a light Higgs and difficulties with EW precision tests, is why simple technicolor models have fallen out of favor [25]. However, composite Higgs models [7–9] manage to resolve the phenomenological

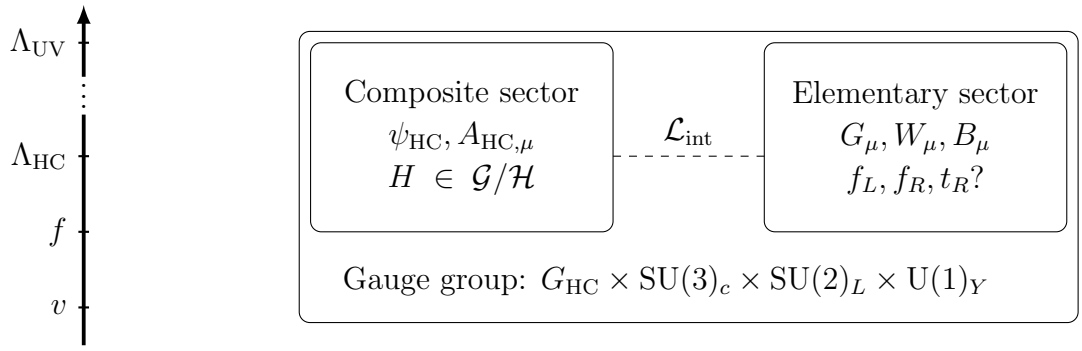

Figure 2.1: Hierarchy of scales (left) and different sectors (right) of a composite Higgs model, adapted from [3]. The gauge group is respected by the complete model, the global symmetry of the composite sector is broken explicitly by interactions with the elementary sector. The Higgs emerges as a pNGB from the composite sector.

problems of technicolor while keeping with the spirit of avoiding elementary scalars. To see how, we have to discuss the setup of a CHM in more detail.

The sectors and energy scales of a CHM are shown in Figure 2.1. As in technicolor, CHMs also assume the presence of a new *composite sector*, which becomes strongly interacting in the IR. It consists of a set of fermions, so-called hyperquarks $\psi_{\rm HC}$, that are charged under a new hypercolor gauge group $G_{\rm HC}$ with coupling $g_{\rm HC}$, and has a global symmetry group $\mathcal{G}$. The composite sector is generated at a high energy scale $\Lambda_{\rm UV} \gg$ TeV where $g_{\rm HC} \ll 1$, so it is close to a free fixed point of its renormalization group equation (RGE) and thereby quasi-conformal. We assume that the composite sector Lagrangian does not contain any strongly relevant operators so as to avoid a new naturalness problem [3]. The composite sector will therefore remain close to its RGE fixed point and hence the evolution of $g_{\rm HC}$ is a slow running. But eventually $g_{\rm HC}$ becomes large and the composite sector starts to condense. The corresponding energy scale $\Lambda_{\rm HC}$ is generated purely from the RG running of a dimensionless coupling. This mechanism is called dimensional transmutation and also occurs in QCD, where $\Lambda_{\rm QCD}$ is generated by the running of g_s. Similar to the hadrons with masses around 1 GeV, the composite sector now forms resonances with a typical mass $\sim \Lambda_{\rm HC}$. But since no such resonances have been observed so far, we expect $\Lambda_{\rm HC}$ to be around 1-5 TeV [26].

As in low-energy QCD, the hyperquark condensate

$$\left\langle \psi^i_{\rm HC} \psi^j_{\rm HC} \right\rangle = \Lambda^3_{\rm HC} \Sigma_0^{ij} \neq 0 \tag{2.1}$$

induces a spontaneous breaking of the global symmetry, $\mathcal{G} \to \mathcal{H}$, where $\mathcal{H}$ is determined by the matrix Σ_0. By the Goldstone theorem [27, 28], this leads to massless scalars in the coset $\mathcal{G}/\mathcal{H}$, so-called Nambu-Goldstone bosons (NGBs). A key characteristic of a CHM is that the Higgs is identified with one of the NGBs, $H \in \mathcal{G}/\mathcal{H}$. To see how the Higgs obtains a mass, we have to take into account the second sector of a CHM, the *elementary sector*. It contains the fields and interactions of the SM – except the Higgs and the Yukawa couplings[1] – and does not respect $\mathcal{H} \subset \mathcal{G}$. Thus, interactions $\mathcal{L}_{\rm int}$ of the composite resonances with elementary fields, e.g. SM gauge interactions, explicitly break $\mathcal{H}$. A further source of explicit breaking are possible hyperquark mass terms. The explicit symmetry breaking turns the NGBs into pseudo NGBs (pNGBs) by giving them mass and generating a scalar potential, which will trigger the EWSB.

[1] And possibly the right-handed top quark, see Section 2.1.3.

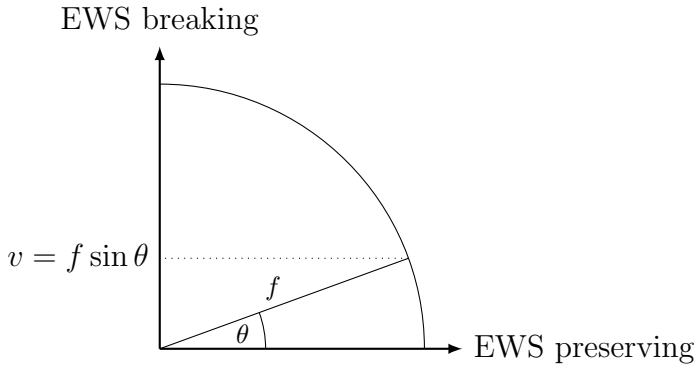

Figure 2.2: Alignment of the vacuum in theories with a composite sector, adapted from [9, 29]. In technicolor, $\theta = \pi/2$ and $f = v$, while the SM is recovered for $\theta \to 0$, which corresponds to $f \to \infty$. CHMs interpolate between the SM and technicolor with $0 < \theta \ll 1$.

We introduce a pNGB decay constant $f \approx \Lambda_{\mathrm{HC}}/(4\pi)$ to characterize the $\mathcal{G} \to \mathcal{H}$ breaking scale, the analog of f_T above. But while technicolor has $f_T \simeq v$, a CHM assumes a separation between the symmetry breaking and EW scales, $v \ll f$ [7]. This is conveniently parameterized with

$$\xi = \frac{v^2}{f^2} = \sin^2\theta \ll 1, \tag{2.2}$$

where θ quantifies the *vacuum misalignment* from the direction that preserves the EW symmetry [9], see Fig. 2.2. Since a CHM reduces to the SM for $\xi \to 0$ and forms a technicolor model for $\xi \simeq 1$, a CHM can be considered an interpolation between the SM and technicolor [22]. By pushing the scale where new resonances are expected above the EW scale, CHMs avoid the phenomenological problems of technicolor.

To summarize, in a CHM the Higgs emerges as a pNGB from the spontaneous breaking of the global symmetry of the composite sector. The Higgs gains a potential and mass from explicit symmetry breaking by interactions with the elementary sector. If the breaking is small, the Higgs is lighter than the symmetry breaking scale f and we can naturally obtain $m_h = 125$ GeV. The vacuum of the composite sector is misaligned with respect to the EW vacuum, leading to a separation between f and the EW scale, $v = f \sin\theta$.

The considerations above imply several constraints on the symmetry breaking pattern [3]: Firstly, the composite sector has to respect the SM gauge group, so we must have $\mathcal{G} \supset \mathcal{H} \supset G_{\mathrm{SM}} = \mathrm{SU}(3)_c \times \mathrm{SU}(2)_L \times \mathrm{U}(1)_Y$. The gauging of G_{SM} means that only a subgroup of $\mathcal{H}$ is gauged. This is an instance of the explicit $\mathcal{H}$ breaking mentioned above. Secondly, to avoid tree-level contributions to $\rho = m_W^2/(m_Z^2 \cos^2\theta_W)$, the composite sector must have a custodial symmetry, so $\mathcal{H} \supset G_{\mathrm{cust}} = \mathrm{SU}(3)_c \times \mathrm{SU}(2)_L \times \mathrm{SU}(2)_R$. And naturally, a suitable representation for the Higgs must be present in the coset, $\mathcal{G}/\mathcal{H} \supset (\mathbf{1}, \mathbf{2}, \mathbf{2})$ of G_{cust}. The simplest coset to satisfy these constraints is

$$\mathrm{SU}(3)_c \times \mathrm{SO}(5)/\mathrm{SU}(3)_c \times \mathrm{SO}(4), \tag{2.3}$$

because $\mathrm{SO}(4) \cong \mathrm{SU}(2)_L \times \mathrm{SU}(2)_R$ and thus $\mathcal{H} = G_{\mathrm{cust}}$. CHMs based on the SO(5)/SO(4) breaking are accordingly called minimal composite Higgs models (MCHMs) [30].

2.1.2 Low-Energy Effective Theory

Assuming we have constructed a CHM with all the features lined out in the previous section, how do we go about testing it against current experimental data? For this, we can integrate out the heavy degrees of freedom and focus solely on the low-energy effective theory.

The physics at an energy scale well below the $\mathcal{G} \to \mathcal{H}$ breaking can be systematically worked out with the Callan-Coleman-Wess-Zumino (CCWZ) construction [31, 32]. Following the presentation in [3], we choose a basis where the generators T^A of $\mathcal{G}$ can be divided into unbroken (T^a) and broken (X^I) ones. We then define the Goldstone matrix

$$U(\Pi) = \exp\left(\mathrm{i}\frac{\sqrt{2}}{f}\Pi^I X^I\right), \tag{2.4}$$

which is a convenient parametrization of the pNGBs Π^I. Under a global transformation $g \in \mathcal{G}$, the Goldstone matrix transforms as

$$U(\Pi) \to U(\Pi^{(g)}) = gU(\Pi)h^{-1}(\Pi, g), \tag{2.5}$$

where $h \in \mathcal{H}$ is a local matrix, $h = h(\Pi(x), g)$. From the Goldstone matrix, we can obtain the d- and e-symbols, which form the basis of the CCWZ construction. To this end, we consider the Maurer-Cartan form constructed from U and separate it into broken and unbroken components,

$$\mathrm{i}U^{-1}(\Pi)\partial_\mu U(\Pi) = d^I_\mu(\Pi)X^I + e^a_\mu(\Pi)T^a \equiv d_\mu(\Pi) + e_\mu(\Pi). \tag{2.6}$$

From Eq. (2.5) it follows that d_μ and e_μ transform under the full group $\mathcal{G}$ as

$$d_\mu \to h d_\mu h^{-1}, \tag{2.7a}$$
$$e_\mu \to h(e_\mu + \mathrm{i}\partial_\mu)h^{-1}. \tag{2.7b}$$

The statement of the CCWZ construction is now that all $\mathcal{G}$ invariant operators can be built from d_μ, e_μ and derivatives – except for the Wess-Zumino-Witten term discussed at the end of this section. But since the d- and e-symbols both transform with h, we only have to find $\mathcal{H}$ invariants. For example, the kinetic term of the pNGBs is obtained by combining two d-symbols,

$$\mathcal{L}^{(2)} = \frac{f^2}{4}d^I_\mu(\Pi)d^{\mu,I}(\Pi) = \frac{1}{2}\partial_\mu\Pi^I\partial^\mu\Pi^I + \cdots, \tag{2.8}$$

where the $\cdots$ contain higher dimensional operators. The superscript on $\mathcal{L}^{(2)}$ indicates the order in the chiral expansion, the appropriate power counting scheme for a theory with pNGBs [33]. And operator's chiral dimension is given by the number of derivatives of pNGBs, or equivalently the factors of pNGB momenta p. We can deduce from Eq. (2.8) that d_μ contributes one factor of p, so $\mathcal{L}^{(2)}$ is the $\mathcal{O}(p^2)$ Lagrangian. In fact, the square of d_μ is the unique two-derivative operator for the minimal coset SO(5)/SO(4), while in general there might be more [3].

So far, we have only dealt with global $\mathcal{G}$ transformations. But the coupling to the SM gauges some of the generators of $\mathcal{G}$. It turns out to be useful to introduce gauge fields for the complete group $\mathcal{G}$, $A_\mu = A^A_\mu T^A$, and to only restrict A_μ to the physical gauge fields after the operator classification. The generalized d- and e-symbols are defined by

$$U^{-1}(\Pi)(A_\mu + \mathrm{i}\partial_\mu)U(\Pi) = d^I_\mu(\Pi, A)X^I + e^a_\mu(\Pi, A)T^a \equiv d_\mu(\Pi, A) + e_\mu(\Pi, A) \tag{2.9}$$

and also transform according to Eq. (2.7). Using $d_\mu(\Pi, A)$ in Eq. (2.8) gives the gauge invariant kinetic term for the pNGBs,

$$\mathcal{L} = \frac{f^2}{4} d_\mu^I(\Pi, A) d^{\mu,I}(\Pi, A) = (D_\mu \Pi)^\dagger D^\mu \Pi + \cdots , \tag{2.10}$$

where $D_\mu \Pi$ is the SM-covariant derivative.

If we want to include some of the hyperbaryons Ψ in the low-energy description, we have to find an adequate covariant derivative. According to Eq. (2.7b), the e-symbol transforms as an adjoint of $\mathcal{H}$. As the hyperbaryons live in irreps of $\mathcal{H}$, we can use $e_\mu(\Pi, A)$ as a generalized gauge field,

$$D_\mu \Psi = \partial_\mu \Psi - \mathrm{i} e_\mu^a(\Pi, A)\, T^a\, \Psi, \tag{2.11}$$

and the kinetic Lagrangian

$$\mathcal{L} = \overline{\Psi}(\mathrm{i}\not{D} - m_\Psi)\Psi \tag{2.12}$$

includes the interactions of Ψ with both the gauge fields and the pNGBs.

There is one term that the CCWZ construction misses, the Wess-Zumino-Witten (WZW) term [34,35]. To see its origin, we follow [36] and return to low-energy QCD, this time including the strange quark and QED. The classical theory has a $\mathrm{SU}(3)_L \times \mathrm{SU}(3)_R$ symmetry, but the axial current $j_A^{\mu,a} = \overline{q}\gamma^\mu\gamma_5 T^a q$ is anomalous,

$$\partial_\mu j_A^{\mu,a} = -\frac{N_c e^2}{16\pi^2} \epsilon^{\mu\nu\rho\sigma} F_{\mu\nu} F_{\rho\sigma}\, \mathrm{Tr}\big(T^a Q^2\big), \tag{2.13}$$

where $N_c = 3$ is the number of colors, $F_{\mu\nu}$ is the QED field strength tensor, $T^a = \lambda^a/2$ are the $\mathrm{SU}(3)_c$ generators and Q is the quark charge matrix, $Q = \mathrm{diag}(\frac{2}{3}, -\frac{1}{3}, -\frac{1}{3})$. So far we have not yet used the condensation of QCD, so Eq. (2.13) holds also at high energies. But it must be reproduced by the low-energy Lagrangian with the same coefficient, since the coefficient of an anomalous conservation law is not renormalized in the RG evolution to the IR [36]. This is achieved by the gauged WZW action, which was shown in [35] to contain the term

$$S_{\text{gauged WZW}} \supset \frac{k e^2}{96\pi^2 f_\pi} \int \mathrm{d}^4 x\, \pi_0 \epsilon^{\mu\nu\rho\sigma} F_{\mu\nu} F_{\rho\sigma}, \tag{2.14}$$

where $\pi_0 \equiv \pi^3$ is the neutral pion, one of the eight pNGBs π^a that emerge from the spontaneous breaking of $\mathrm{SU}(3)_L \times \mathrm{SU}(3)_R \to \mathrm{SU}(3)_D$ when the $\langle \overline{q}_R q_L \rangle$ condensate forms. The axial Noether current (i.e. the one corresponding to $g \to L^\dagger g R$ with $R = -L$) from Eq. (2.14) satisfies

$$\partial_\mu j_A^{\mu,3} = -\frac{k e^2}{96\pi^2} \epsilon^{\mu\nu\rho\sigma} F_{\mu\nu} F_{\rho\sigma}, \tag{2.15}$$

which matches Eq. (2.13) if we choose $k = N_c$. The WZW term has important phenomenological consequences, e.g. Eq. (2.14) induces the decay $\pi_0 \to \gamma\gamma$ of the neutral pion. More generally, the WZW term can allow pNGBs to decay to two vector bosons. Which couplings it includes depends on the symmetry breaking pattern and can for example be computed from the formulation with differential forms given in [12, 37].

2.1.3 Partial Compositeness

Besides triggering the EWSB, one of the crucial roles of the Higgs field in the SM is to generate mass terms for the fermions. But since the Higgs is no longer an elementary scalar in a CHM, we have to find a way to generate the Yukawa couplings dynamically. As the EWSB originates from the composite sector, it must be transmitted to the elementary sector by an appropriate interaction term. Motivated by the SM, one might be tempted to use a bilinear interaction of the form

$$\mathcal{L}_{\text{int}} = -\lambda_t\, \overline{q}_L t_R \mathcal{O}_S^c - \lambda_b\, \overline{q}_L b_R \mathcal{O}_S + \text{h.c.}\,, \tag{2.16}$$

where $\mathcal{O}_S = \overline{\psi}_{\text{HC}}\psi_{\text{HC}}$ is a composite scalar with the quantum numbers of the Higgs [3]. Such interactions are for example generated in extended technicolor [38, 39]. Since we assumed that the composite sector is near a conformal fixed point of its RGE above Λ_{HC}, the evolution of the couplings λ_i from Λ_{UV} where they were generated down to the condensation scale is determined by the dimension of $\mathcal{O}_S$,

$$\lambda_i(\Lambda_{\text{HC}}) \simeq \lambda_i \left(\frac{\Lambda_{\text{HC}}}{\Lambda_{\text{UV}}}\right)^{[\mathcal{O}_S]-1}. \tag{2.17}$$

There are several problems with this approach [3, 22]: Since $\mathcal{L}_{\text{int}}$ must be a small perturbation of the composite sector, there is an upper bound on the λ_i, making it difficult to obtain a large Yukawa coupling for the top if $\Lambda_{\text{UV}} \gg \Lambda_{\text{HC}}$. But Λ_{UV} has to be very large to avoid constraints on flavor-changing neutral currents from a four SM fermion interaction that also gets generated at Λ_{UV}. Also, the large scale separation cannot be counteracted by having $[\mathcal{O}_S]$ close to 1, because then $\mathcal{O}_S^2$ is a relevant operator, leading to a new naturalness problem.

A possible solution is to couple the SM fermions linearly to composite operators, as was first pointed out in [10]. Focusing on the contributions to the top Yukawa coupling, the linear interaction reads [3]

$$\mathcal{L}_{\text{int}} = -\lambda_L \overline{q}_L \mathcal{O}_F^L - \lambda_R \overline{t}_R \mathcal{O}_F^R + \text{h.c.}\,. \tag{2.18}$$

The composite operators are now fermionic and have the same SM quantum numbers as q_L and t_R, i.e. $\mathcal{O}_F^L \in (\mathbf{3},\mathbf{2})_{1/6}$ and $\mathcal{O}_F^R \in (\mathbf{3},\mathbf{1})_{2/3}$. Therefore, the $\mathcal{O}_F^{L,R}$ can excite fermionic resonances Q, T from the vacuum, $\langle 0|\mathcal{O}_F^L|Q\rangle \neq 0$ and $\langle 0|\mathcal{O}_F^R|T\rangle \neq 0$. As Q, T also have the same quantum numbers as q_L, t_R, they are called *top partners* and can mix with the SM fermions. As we will see below, in general the $\mathcal{O}_F^{L,R}$ contain further resonances. Since these emerge from the same $\mathcal{G}$ multiplet as Q, T, we refer to them as top partners as well.

The physical mass eigenstates of the top and bottom quarks are therefore superpositions of elementary and composite fermions, giving this approach the name *partial compositeness*. To see what makes this preferable to the bilinear couplings, we again evolve the UV couplings to the IR,

$$\lambda_i(\Lambda_{\text{HC}}) \simeq \lambda_i \left(\frac{\Lambda_{\text{HC}}}{\Lambda_{\text{UV}}}\right)^{[\mathcal{O}_F^i]-\frac{5}{2}}. \tag{2.19}$$

For $[\mathcal{O}_F^i] \simeq 5/2$, a large Yukawa is possible even for a large scale separation. The difference to $\mathcal{O}_S$ is that for the critical value of $\mathcal{O}_F$, $|\mathcal{O}_F|^2$ is an irrelevant operator, thus retaining naturalness. Furthermore, since there are different $\mathcal{O}_{F,f}$ for each flavor, Eq. (2.19) offers an explanation of flavor hierarchies in the form of larger operator dimensions for the lighter quarks [3].

Having established its viability, let us now investigate the phenomenological consequences of partial compositeness. First we note that both chiralities of the top partners are present

with the same quantum numbers, so they can form a Dirac mass term and are also referred to as vector-like quarks (VLQs). From dimensional analysis, the mass terms for the top and VLQs can be estimated as [3]

$$\mathcal{L}_{\text{mass}} = -m_* \left(\overline{Q}Q + \overline{T}T\right) - \frac{m_*}{g_*}\left(\lambda_L \overline{q}_L Q + \lambda_R \bar{t}_R T + \text{h.c.}\right), \tag{2.20}$$

where $\lambda_{L,R}$ are the IR couplings, $m_* = \Lambda_{\text{HC}}$ is the typical mass of the resonances and g_* a composite sector coupling constant. The mass matrix can be diagonalized by rotating the fields as

$$\begin{pmatrix} q_L \\ Q \end{pmatrix} \to \begin{pmatrix} \hat{Q}_1 \\ \hat{Q}_2 \end{pmatrix} = \begin{pmatrix} \cos\theta_L & \sin\theta_L \\ -\sin\theta_L & \cos\theta_L \end{pmatrix} \begin{pmatrix} q_L \\ Q \end{pmatrix}, \qquad \sin\theta_L = \frac{\lambda_L}{\sqrt{g_*^2 + \lambda_L^2}}, \tag{2.21}$$

with an analogous expression for t_R and T. This results in two massless eigenstates $\hat{Q}_1, \hat{T}_1$, which we identify with the physical q_L and t_R, as well as two heavy resonances $\hat{Q}_2, \hat{T}_2$. The degree of compositeness of the physical SM quarks is determined by $\sin\theta_{L,R}$.

The composite sector Lagrangian contains interactions of the top partners with the pNGBs, among them a term $\overline{Q}T\tilde{H}$. After mixing, this generates the top Yukawa couplings,

$$\mathcal{L}_{\text{comp}} \supset -g_* \overline{Q} T \tilde{H} + \text{h.c.} \supset -g_* \sin\theta_L \overline{\hat{Q}}_1 \sin\theta_R \hat{T}_1 \tilde{H} + \text{h.c.}\,, \tag{2.22}$$

and we can read off the top Yukawa as

$$y_t = g_* \sin\theta_L \sin\theta_R. \tag{2.23}$$

This shows that heavier particles typically have larger compositeness angles $\theta_{L,R}$, which is why we have neglected lighter quarks and leptons so far: While they can have mixing terms with composite states as well, they are strongly suppressed by their small Yukawa. It is however possible for one chirality to have a much larger compositeness fraction than the other. For example, there are models where t_R is a completely composite state [3].

While the CCWZ construction described in Section 2.1.2 is universal in any model with $\mathcal{G}/\mathcal{H}$ symmetry breaking, the details of partial compositeness are model dependent. In particular, we have to specify the $\mathcal{G}$ representations of the composite operators $\mathcal{O}_F^{L,R}$, which affect the top couplings to the Higgs. To illustrate this, we consider a model based on $\mathcal{G} = \text{SU}(3)_c \times \text{SO}(5) \times \text{U}(1)_X \to \text{SU}(3)_c \times \text{SO}(4) \times \text{U}(1)_X = \mathcal{H}$. The $\text{SU}(2)_L$ is taken as one of the factors of $\text{SO}(4) \cong \text{SU}(2)_L \times \text{SU}(2)_R$ and the hypercharge is embedded as $Y = T_R^3 + X$. Compared to the MCHM introduced in Section 2.1.1, this symmetry breaking pattern contains an additional unbroken factor of $\text{U}(1)_X$, which is necessary to accommodate top partners. By choosing the composite operators in the $(\mathbf{3}, \mathbf{5})_{2/3}$ of $\mathcal{G}$, we obtain the model MCHM_5, which was first discussed in [40]. Under $\mathcal{G} \to \mathcal{H} \to G_{\text{SM}}$, this representation decomposes as

$$\mathbf{5}_{2/3} \to \mathbf{4}_{2/3} + \mathbf{1}_{2/3} \to \mathbf{2}_{7/6} + \mathbf{2}_{1/6} + \mathbf{1}_{2/3}, \tag{2.24}$$

where the $\mathbf{3}$ of color is implicit. The last two representations are the desired top partners. The first doublet gives rise to two additional VLQs with electric charges 5/3 and 2/3 after EWSB. As mentioned above, the presence of further top partners is a common feature of CHMs. In fact, the $\mathbf{2}_{7/6}$ is also present in the model M5 that is studied in the following chapters.

To formulate the mixing terms Eq. (2.18) with the composite operators $(\mathcal{O}_F^{L,R})_I \in \mathbf{5}_{2/3}$, it is useful to embed q_L and t_R into incomplete SO(5) fiveplets. In the basis used in [3], the embeddings read

$$\zeta_L = \frac{\lambda_L}{\sqrt{2}}(-\mathrm{i}b_L, -b_L, -\mathrm{i}t_L, t_L, 0)^T, \qquad \zeta_R = \lambda_R(0,0,0,0,t_R)^T. \tag{2.25}$$

The linear couplings can now be written in a formally SO(5) invariant way,

$$\mathcal{L}_{\text{int}} = -(\overline{\zeta}_L)^I(\mathcal{O}_F^L)_I - (\overline{\zeta}_R)^I(\mathcal{O}_F^R)_I + \text{h.c.}\,. \tag{2.26}$$

The advantage of this is that while $\zeta_{L,R}$ do not transform as full representations of SO(5), we are free to act as if they do and only restrict them to their physical values in Eq. (2.25) at the end of any calculation. To this end we define so-called *spurions* by

$$\Xi_{L,R} \in \mathbf{5}_{2/3} \quad \text{with} \quad \Xi_{L,R}\Big|_{\text{phys}} = \zeta_{L,R}. \tag{2.27}$$

The spurions are very useful in the calculation of the effective Lagrangian with the fermionic resonances integrated out, which can be constructed by forming $\mathcal{G}$ invariant operators from the spurions. For top partners in the representation R of $\mathcal{G}$, the result can be written as

$$\mathcal{L}_{\text{int}} = -m_t\bar{t}t - k_t^R\frac{m_t}{v}h\,\bar{t}t - c_2^R\frac{m_t}{v^2}h^2\,\bar{t}t + \cdots\,. \tag{2.28}$$

For the case of fiveplet top partners [3],

$$k_t^{\mathbf{5}} = \frac{1-2\xi}{\sqrt{1-\xi}}, \qquad c_2^{\mathbf{5}} = -2\xi. \tag{2.29}$$

The parameters $\lambda_{L,R}$ were removed by fixing the coefficient of $-\bar{t}t$ as the top mass. We could also have chosen the top partners in the $(\mathbf{3},\mathbf{4})_{1/6}$ of $\mathcal{G}$, as $\mathbf{4}_{1/6} \to \mathbf{2}_{1/6} + \mathbf{1}_{2/3} + \mathbf{1}_{-1/3}$ under $\mathrm{SU}(2)_L \times \mathrm{U}(1)_Y$. In this so-called MCHM$_4$ [30], the couplings are given by [3]

$$k_t^{\mathbf{4}} = \sqrt{1-\xi}, \qquad c_2^{\mathbf{4}} = -\frac{\xi}{2}. \tag{2.30}$$

We note that for both models, we recover the SM coupling of the top quark to the Higgs in the limit $\xi \to 0$, as expected from the discussion in Section 2.1.1.

2.2 Classification of Fermionic UV Completions

Following the introduction of CHMs in the 1980s, the literature has been mostly focused on studying their low-energy effects with the CCWZ construction. Inspired by the AdS/CFT correspondence [41], the 2000s saw the appearance of holographic CHMs with a dual bulk description on five-dimensional Anti-de Sitter space [22,30,42]. But not until the 2010s did the study of the UV theory in four-dimensional models receive a lot of attention. In this section, we summarize the classification of fermionic UV completions of CHMs with partial compositeness that was performed by Ferretti and collaborators [11–13] starting in 2013.

2.2.1 Assumptions and Requirements

We start by describing the framework of the classification [11]. The aim is to find *minimal* UV models that yield a CHM with partially composite top quarks. Thus, we only consider the case of a simple hypercolor group G_{HC}. For the hyperquarks, we limit ourselves to two distinct irreducible representations (irreps) R_i of G_{HC}. That is, $\psi_{\text{HC}} \in n_1 R_1 + n_2 R_2$, where n_i is the number of flavors of the respective irrep. For now, we discuss only (pseudo-)real irreps. We denote the hyperquarks in R_1 and R_2 by ψ and χ respectively, and work with left-handed Weyl fermions. The anomaly-free global symmetry group of these models is $\mathcal{G} = \mathrm{SU}(n_1) \times \mathrm{SU}(n_2) \times \mathrm{U}(1)$. The $\mathrm{SU}(n_i)$ come from rotating the n_i hyperquarks in R_i among each other. Actually, the flavor symmetry is $\mathrm{U}(n_i) \cong \mathrm{SU}(n_i) \times \mathrm{U}(1)$. But only one linear combination of $\mathrm{U}(1)_\psi$ and $\mathrm{U}(1)_\chi$ is anomaly-free, whereas the orthogonal combination induces a $\mathrm{U}(1)G_{\text{HC}}^2$ Adler-Bell-Jackiw (ABJ) anomaly [13].

In the case of a complex irrep, there are n_i pairs of hyperquarks $(\psi, \tilde{\psi})$ or $(\chi, \tilde{\chi})$ in the $(R_i, \overline{R}_i)$ representation. The associated flavor symmetry is $\mathrm{U}(n_i) \times \mathrm{U}(n_i)' \cong \mathrm{SU}(n_i) \times \mathrm{SU}(n_i)' \times \mathrm{U}(1)_A \times \mathrm{U}(1)_V$, where the phase rotations act as

$$\mathrm{U}(1)_A^\psi : \quad \psi \to \mathrm{e}^{\mathrm{i}\alpha}\psi, \quad \tilde{\psi} \to \mathrm{e}^{\mathrm{i}\alpha}\tilde{\psi}, \qquad \mathrm{U}(1)_V^\psi : \quad \psi \to \mathrm{e}^{\mathrm{i}\alpha}\psi, \quad \tilde{\psi} \to \mathrm{e}^{-\mathrm{i}\alpha}\tilde{\psi} \tag{2.31}$$

and identically for $(\chi, \tilde{\chi})$. The axial $\mathrm{U}(1)_A^{\psi/\chi}$ can again be combined with $\mathrm{U}(1)_{\chi/\psi}$ to construct one anomaly-free combination, and the vector-like $\mathrm{U}(1)_V^{\psi/\chi}$ is an additional anomaly-free factor in $\mathcal{G}$ that remains unbroken when G_{HC} condenses [12].

While the SM particles are neutral under G_{HC}, we have to assign SM quantum numbers to the hyperquarks so that Higgs-like and top-like bound states can be formed. To this end, we give EW quantum numbers to the ψ, and QCD color and hypercharge to the χ. This separation is useful for avoiding problems like spontaneous color breaking and light colored pNGBs [13].

There are several technical conditions the models have to satisfy: As the composite sector should condense in the IR, we require the theory to be asymptotically free. For the case of $G_{\text{HC}} = \mathrm{SU}(N)$ ($\mathrm{Sp}(2N)$), the theory must not have gauge (global) anomalies, and G_{SM} must be free of 't Hooft anomalies [11]. Furthermore, the theory must be conformal in the UV to be able to generate a large anomalous dimension for the top partner. On the other hand, a conformal theory cannot become strongly interacting in the IR. A possible solution is to look for theories that lead to a valid CHM with top partners but are *not* conformal [13]. The theory is then brought into the conformal window by adding additional hyperfermions with mass $\sim \Lambda_{\text{HC}}$. These explicitly break the conformal invariance in the IR, but the theory is conformal in the UV. Following this approach, we look for models outside of the conformal window. However, for this we have to rely on some heuristics, as it is not yet possible to identify the conformal region for a non-supersymmetric gauge theory [12].

2.2.2 Minimal Cosets

The global symmetry group is spontaneously broken by the chiral condensates $\langle\psi\psi\rangle$ and $\langle\chi\chi\rangle$. We denote the unbroken subgroups by $\mathcal{H}_{\psi/\chi}$. The symmetry breaking pattern depends on the reality of the hyperquark irreps: $\mathrm{SU}(n) \to \mathrm{SO}(n)$ for a real (R), $\mathrm{SU}(2n) \to \mathrm{Sp}(2n)$ for a pseudo-real (PR), and $\mathrm{SU}(n) \times \mathrm{SU}(n)' \times \mathrm{U}(1)_V \to \mathrm{SU}(n)_D \times \mathrm{U}(1)_V$ for a complex (C) irrep [12].

Since the ψ form the EW sector, $\mathcal{H}_\psi$ must contain the custodial $\mathrm{SU}(2)_L \times \mathrm{SU}(2)_R \cong \mathrm{SO}(4)$ to protect the ρ-parameter from tree-level contributions. Furthermore, the coset must contain

	$\psi \in \mathrm{R}$	$\psi \in \mathrm{PR}$	$\psi \in \mathrm{C}$
$\chi \in \mathrm{R}$	$\frac{\mathrm{SU}(5)}{\mathrm{SO}(5)}\,\frac{\mathrm{SU}(6)}{\mathrm{SO}(6)}$	$\frac{\mathrm{SU}(4)}{\mathrm{Sp}(4)}\,\frac{\mathrm{SU}(6)}{\mathrm{SO}(6)}$	$\frac{\mathrm{SU}(4)\times\mathrm{SU}(4)'}{\mathrm{SU}(4)_D}\,\frac{\mathrm{SU}(6)}{\mathrm{SO}(6)}$
$\chi \in \mathrm{PR}$	$\frac{\mathrm{SU}(5)}{\mathrm{SO}(5)}\,\frac{\mathrm{SU}(6)}{\mathrm{Sp}(6)}$	$\frac{\mathrm{SU}(4)}{\mathrm{Sp}(4)}\,\frac{\mathrm{SU}(6)}{\mathrm{Sp}(6)}$	$\frac{\mathrm{SU}(4)\times\mathrm{SU}(4)'}{\mathrm{SU}(4)_D}\,\frac{\mathrm{SU}(6)}{\mathrm{Sp}(6)}$
$\chi \in \mathrm{C}$	$\frac{\mathrm{SU}(5)}{\mathrm{SO}(5)}\,\frac{\mathrm{SU}(3)\times\mathrm{SU}(3)'}{\mathrm{SU}(3)_D}$	$\frac{\mathrm{SU}(4)}{\mathrm{Sp}(4)}\,\frac{\mathrm{SU}(3)\times\mathrm{SU}(3)'}{\mathrm{SU}(3)_D}$	$\frac{\mathrm{SU}(4)\times\mathrm{SU}(4)'}{\mathrm{SU}(4)_D}\,\frac{\mathrm{SU}(3)\times\mathrm{SU}(3)'}{\mathrm{SU}(3)_D}$

Table 2.1: Minimal cosets for CHMs with hyperquarks in two distinct irreps of G_{HC}, split into real (R), pseudo-real (PR), and complex (C) irreps [12]. Each coset includes an additional U(1) that is spontaneously broken. For each complex irrep there is also a U(1) factor of $\mathcal{G}$ that remains unbroken. For the grayed-out cosets, the models cannot form top partners.

a $(\mathbf{2},\mathbf{2})$ of the custodial group to accommodate a Higgs. The minimal cosets fulfilling these requirements are SU(5)/SO(5), SU(4)/Sp(4) and $\mathrm{SU}(4)\times\mathrm{SU}(4)'/\mathrm{SU}(4)_D$. The second set of hyperquarks χ carry QCD color and hypercharge, so we need $\mathcal{H}_\chi \supset \mathrm{SU}(3)_c \times \mathrm{U}(1)_X$. This leads to the minimal cosets SU(6)/SO(6), SU(6)/Sp(6) and $\mathrm{SU}(3)\times\mathrm{SU}(3)'/\mathrm{SU}(3)_D$ for the color sector[2] [12]. All possible combinations of EW and colored cosets are shown in Tab. 2.1, neglecting the spontaneously broken anomaly-free U(1) that is common to all cases. Of those, three cosets can be excluded as the corresponding models cannot form top partners, leaving six minimal cosets.

Suppose we have chosen a G_{HC} and irreps R_1, R_2 in accordance with the requirements from the previous section. Then one important question we have not discussed yet is whether the theory will actually form condensates that lead to the desired symmetry breaking pattern, as opposed to e.g. breaking G_{HC}. This can be addressed with the MAC hypothesis [43], a heuristic for identifying symmetry breaking patterns in a condensing gauge theory. Applied to our case, it works as follows [11]: We form the three products $R_i \times R_j = \sum_k R'_k$ corresponding to the bilinears $\psi\psi, \chi\chi, \psi\chi$. Each (R_i, R_j, R'_k) represents a possible channel for the condensation. The MAC hypothesis states that the first channel to condense, called the *maximally attractive channel* (MAC), is the one with the lowest value of $C_2(R'_k) - C_2(R_i) - C_2(R_j)$, where $C_2(R)$ is the quadratic Casimir of R. The irreps in the MAC are removed and the process is iterated until none are left. If the MAC hypothesis favors a condensate that breaks G_{HC} or $\mathrm{SU}(3)_c$, the model is discarded.

Before listing the possible UV completions of CHMs, we impose a final constraint. A common phenomenological hurdle for CHMs is avoiding large contributions to the $Zb_L\bar{b}_L$ coupling, which can easily arise due to the large coupling of the $q_L = (t_L, b_L)$ doublet to the composite sector. But it was shown in [44] that the $Zb_L\bar{b}_L$ coupling is protected if the custodial SO(4) is enlarged to $\mathrm{O}(4) \cong \mathrm{SO}(4)\times\mathrm{Z}_2$, where Z_2 corresponds to the parity transformation P_{LR} that exchanges $L \leftrightarrow R$. We therefore require top partners to be eigenstates of P_{LR}, which excludes models where they come in a $(\mathbf{2},\mathbf{1})$ of $\mathrm{SU}(2)_L \times \mathrm{SU}(2)_R$. For the present class of models, this concerns models with top partners of type $\chi\psi\chi$ with ψ in a complex irrep [12].

[2]Note that the complex coset has an additional unbroken factor of $\mathrm{U}(1)_V$, so that $\mathrm{SU}(3)\times\mathrm{SU}(3)'\times\mathrm{U}(1)_V \to \mathrm{SU}(3)_D \times \mathrm{U}(1)_V \equiv \mathrm{SU}(3)_c \times \mathrm{U}(1)_X$.

Name	G_{HC}	ψ	χ	Coset	Top Partners
M1	SO(7)	$5 \times \mathbf{F}$	$6 \times \mathbf{Spin}$	(R, R)	$\chi\psi\chi$
M2	SO(9)	$5 \times \mathbf{F}$	$6 \times \mathbf{Spin}$	(R, R)	$\chi\psi\chi$
M3	SO(7)	$5 \times \mathbf{Spin}$	$6 \times \mathbf{F}$	(R, R)	$\psi\chi\psi$
M4	SO(9)	$5 \times \mathbf{Spin}$	$6 \times \mathbf{F}$	(R, R)	$\psi\chi\psi$
M5	Sp(4)	$5 \times \mathbf{A}_2$	$6 \times \mathbf{F}$	(R, PR)	$\chi\psi\chi$
M6	SU(4)	$5 \times \mathbf{A}_2$	$3 \times (\mathbf{F}, \overline{\mathbf{F}})$	(R, C)	$\chi\psi\chi$
M7	SO(10)	$5 \times \mathbf{F}$	$3 \times (\mathbf{Spin}, \overline{\mathbf{Spin}})$	(R, C)	$\chi\psi\chi$
M8	Sp(4)	$4 \times \mathbf{F}$	$6 \times \mathbf{A}_2$	(PR, R)	$\psi\chi\psi$
M9	SO(11)	$4 \times \mathbf{Spin}$	$6 \times \mathbf{F}$	(PR, R)	$\psi\chi\psi$
M10	SO(10)	$4 \times (\mathbf{Spin}, \overline{\mathbf{Spin}})$	$6 \times \mathbf{F}$	(C, R)	$\psi\chi\psi$
M11	SU(4)	$4 \times (\mathbf{F}, \overline{\mathbf{F}})$	$6 \times \mathbf{A}_2$	(C, R)	$\psi\chi\psi$
M12	SU(5)	$4 \times (\mathbf{F}, \overline{\mathbf{F}})$	$3 \times (\mathbf{A}_2, \overline{\mathbf{A}}_2)$	(C, C)	$\psi\chi\psi$

Table 2.2: Possible UV completions of a CHM with a partially composite top quark, based on [12,13]. The shown models satisfy all requirements from the previous sections. In particular, they are asymptotically free, likely non-conformal and protect to the $Zb_L\bar{b}_L$ coupling. We denote by **F**, $\mathbf{A}_2$ and **Spin** the fundamental, two-index antisymmetric and spinoral irreps, respectively. The column "Coset" indicates the reality of the (ψ, χ) irreps, which determines the coset by Tab. 2.1.

2.2.3 Possible Models

Determining the possible UV models of partial compositeness is now a matter of listing all combinations of irreps of the simple Lie groups and checking which ones satisfy all requirements laid out in the previous sections. For each group, we consider only the lowest-dimensional R, PR and C irreps. All in all, there are 12 promising models, shown in Tab. 2.2 with the names introduced in [13]. More detailed lists with likely conformal models included are given in [12,13].

Only few of these models have been studied in the literature: In [45], the model M8 was constructed independently of the classification in [11]. Its symmetry breaking was analyzed and the top partner was argued to have a scaling dimension sufficiently close to 5/2. A more detailed investigation was performed for the model M6 in [46], studying both the UV and IR regime. Phenomenological studies have so far been focused on signatures common to several models, e.g. [13, 47–51]. In the remainder of this thesis, the model M5 is studied in detail with a particular focus on the LHC phenomenology of fermionic resonances.

3 | The Composite Higgs Model M5

In this chapter we explore a specific composite Higgs model in detail, which was named M5 in [13]. We start by presenting the field content of the UV theory and the symmetry breaking pattern. Following [52], we then describe the composite particles after the UV theory has condensed and work out a part of the Lagrangian. Finally, we classify the operators that contribute to the scalar potential using the spurion method.

3.1 Model Definition

The model M5 is based on the gauge group $G_{\text{HC}} = \text{Sp}(4) \times \text{SU}(3)_c \times \text{SU}(2)_L \times \text{U}(1)_Y$. The hyperquarks are shown in Tab. 3.1 as two-component spinors. The five EW sector hyperquarks ψ_i transform under the real two-index antisymmetric irrep $\mathbf{A}_2$ of Sp(4) and form a $\mathbf{5}$ of the global SU(5) flavor symmetry. Using the notation of [53], we arrange the ψ_i into two $\text{SU}(2)_L$ doublets $\psi_d^{\pm}$ with hypercharge $\pm 1/2$ and the SM neutral ψ_s,

$$\psi_d^+ = \big(\psi_1, \psi_2\big)^T, \qquad \psi_d^- = \big(\psi_3, \psi_4\big)^T, \qquad \psi_s = \psi_5. \tag{3.1}$$

The color sector hyperquarks χ_i live in the pseudoreal fundamental irrep $\mathbf{F}$ of Sp(4) and come in six flavors, thus forming a $\mathbf{6}$ of SU(6). We split them into a color triplet $\chi_{\mathbf{3}}$ and antitriplet $\chi_{\bar{\mathbf{3}}}$,

$$\chi_{\mathbf{3}} = \big(\chi_1, \chi_2, \chi_3\big)^T, \qquad \chi_{\bar{\mathbf{3}}} = \big(\chi_4, \chi_5, \chi_6\big)^T. \tag{3.2}$$

In addition to the rotations in flavor space, we can perform a simultaneous phase rotation of all ψ_i or χ_i. By assigning the charges under the corresponding $\text{U}(1)_{\psi,\chi}$ groups as in the last column of Tab. 3.1, we can construct one anomaly-free U(1) as a linear combination of $\text{U}(1)_\psi$ and $\text{U}(1)_\chi$. Therefore, the total global symmetry group of M5 is $\text{SU}(5) \times \text{SU}(6) \times \text{U}(1)$.

	Sp(4)	$\text{SU}(3)_c$	$\text{SU}(2)_L$	$\text{U}(1)_Y$		SU(5)	SU(6)	$\text{U}(1)_{\psi,\chi}$
$\psi_{1,2}$	$\mathbf{A}_2$	$\mathbf{1}$	$\mathbf{2}$	$1/2$	⎫			
$\psi_{3,4}$	$\mathbf{A}_2$	$\mathbf{1}$	$\mathbf{2}$	$-1/2$	⎬	$\mathbf{5}$	$\mathbf{1}$	$-\frac{3}{5}q_\chi$
ψ_5	$\mathbf{A}_2$	$\mathbf{1}$	$\mathbf{1}$	0	⎭			
$\chi_{1,2,3}$	$\mathbf{F}$	$\mathbf{3}$	$\mathbf{1}$	x	⎫	$\mathbf{1}$	$\mathbf{6}$	q_χ
$\chi_{4,5,6}$	$\mathbf{F}$	$\bar{\mathbf{3}}$	$\mathbf{1}$	$-x$	⎭			

Table 3.1: Quantum numbers of the hyperquarks in M5 under the gauge group $G_{\text{HC}} = \text{Sp}(4) \times \text{SU}(3)_c \times \text{SU}(2)_L \times \text{U}(1)_Y$ and the flavor symmetries $\text{SU}(5) \times \text{U}(1)_\psi$ and $\text{SU}(6) \times \text{U}(1)_\chi$.

When the Sp(4) gauge theory condenses, the condensates $\langle\psi\psi\rangle$ and $\langle\chi\chi\rangle$ spontaneously break the flavor symmetries, SU(5) $\to$ SO(5) and SU(6) $\to$ Sp(6) respectively, as well as the anomaly-free U(1). All in all, the symmetry breaking pattern is

$$\mathcal{G} = \mathrm{SU}(5) \times \mathrm{SU}(6) \times \mathrm{U}(1) \to \mathrm{SO}(5) \times \mathrm{Sp}(6) = \mathcal{H}. \tag{3.3}$$

In the EW sector, we identify the $\mathrm{SU}(2)_L \times \mathrm{SU}(2)_R$ subgroup of SO(5) with the custodial group and gauge the $\mathrm{SU}(2)_L$ factor. The gauged color group and the X-charge are embedded in the color sector, $\mathrm{Sp}(6) \supset \mathrm{SU}(3)_c \times \mathrm{U}(1)_X$, and the EW hypercharge Y is a gauged combination of $\mathrm{U}(1)_X$ and $\mathrm{SU}(2)_R$, $Y = X + T^3_R$.

3.2 Particle Content

In the low-energy regime, the hyperquarks form composite resonances. Among them are the pNGBs in the coset $\mathcal{G}/\mathcal{H}$ and three-hyperquark bound states of the form $\psi\chi\chi$, from which we obtain the top partners. While vector resonances can also occur [3], we limit ourselves to scalar and fermionic ones in this work. In this section, we work out which composite states are present and define our notation.

3.2.1 Pseudo Nambu-Goldstone Bosons

The pNGBs come from the cosets SU(5)/SO(5), SU(6)/Sp(6) and from the global U(1).

Global U(1) The spontaneous breaking of the anomaly-free U(1) gives rise to a SM neutral pNGB a. This state is present in all models in Tab. 2.2, making it an interesting object for general studies [13, 47, 51]. However, we do not consider it further because it does not couple to the color octet fermions that are the focus of this thesis.

Color Sector The colored hyperquark condensate

$$\langle\chi_i\chi_j\rangle \propto \Sigma^{ij}_{0,\chi}, \qquad \Sigma_{0,\chi} = \begin{pmatrix} 0 & -\mathbb{1}_3 \\ \mathbb{1}_3 & 0 \end{pmatrix} \tag{3.4}$$

breaks SU(6) $\to$ Sp(6). Of the 35 generators of SU(6), 21 unbroken ones T^A preserve the vacuum and generate Sp(6),

$$T^A\Sigma_{0,\chi} + \Sigma_{0,\chi}(T^A)^T = 0, \tag{3.5}$$

while 14 broken generators X^I instead satisfy

$$X^I\Sigma_{0,\chi} - \Sigma_{0,\chi}(X^I)^T = 0. \tag{3.6}$$

The generators of the $\mathrm{SU}(3)_c \times \mathrm{U}(1)_X$ subgroup of Sp(6) are

$$\mathrm{SU}(3)_c: \quad \frac{1}{\sqrt{2}}\begin{pmatrix} T^a & 0 \\ 0 & -(T^a)^T \end{pmatrix}, \tag{3.7a}$$

$$\mathrm{U}(1)_X: \quad T_X = N_X\begin{pmatrix} \mathbb{1}_3 & 0 \\ 0 & -\mathbb{1}_3 \end{pmatrix}, \tag{3.7b}$$

where T^a are the SU(3) generators in the fundamental irrep and we need $N_X = -1/3$ for the correct embedding of the hypercharge. The broken generators are conveniently expressed as

$$X^I = X^a = \frac{1}{\sqrt{2}}\begin{pmatrix} T^a & 0 \\ 0 & (T^a)^T \end{pmatrix}, \quad a = 1, \dots, 8 \tag{3.8a}$$

$$X^I = X^{8+j} = \frac{1}{2\sqrt{2}}\begin{pmatrix} 0 & -t^j \\ t^j & 0 \end{pmatrix}, \quad j = 1, 2, 3 \tag{3.8b}$$

$$X^I = X^{11+j} = \frac{1}{2\sqrt{2}}\begin{pmatrix} 0 & \mathrm{i}t^j \\ \mathrm{i}t^j & 0 \end{pmatrix}, \quad j = 1, 2, 3 \tag{3.8c}$$

where we chose a basis that helps identifying the color multiplets in Eq. (3.11). The t^j are antisymmetric 3×3 matrices,

$$t^1 = \begin{pmatrix} 0 & -1 & 0 \\ 1 & 0 & 0 \\ 0 & 0 & 0 \end{pmatrix}, \quad t^2 = \begin{pmatrix} 0 & 0 & -1 \\ 0 & 0 & 0 \\ 1 & 0 & 0 \end{pmatrix}, \quad t^3 = \begin{pmatrix} 0 & 0 & 0 \\ 0 & 0 & -1 \\ 0 & 1 & 0 \end{pmatrix}, \tag{3.9}$$

and the X^I are normalized as

$$\mathrm{Tr}\big(X^I X^J\big) = \frac{1}{2}\delta^{IJ}. \tag{3.10}$$

The pNGBs $\Pi_\chi \in \mathrm{SU}(6)/\mathrm{Sp}(6)$ form a **14** of Sp(6), which decomposes as

$$\mathbf{14} \to \mathbf{8}_0 + \mathbf{3}_{2x} + \bar{\mathbf{3}}_{-2x} \equiv \pi_8 + \pi_3 + \pi_3^* \tag{3.11}$$

under $\mathrm{SU}(3)_c \times \mathrm{U}(1)_{\mathrm{em}}$. Since the Π_χ are singlets under the custodial group, their electric charge is simply given by their X-charge. In the next section we will see that we need to choose $x = 1/3$ to obtain top partners. Thus, π_8 is an electrically neutral color octet and π_3 is a color triplet with charge 2/3. The π_8 and π_3 can be interpreted as scalar partners of the gluon and the top quark, respectively. Using the naming convention of the supersymmetry (SUSY) literature, we refer to them as *sgluon* and *stop*.

According to Eq. (3.11), the matrix representation $\Pi_\chi = \Pi_\chi^I X^I$ of the pNGBs can be split into a color octet part,

$$\Pi_{\mathbf{8}} = \sum_{I=1}^{8} \pi_8^I X^I = \frac{1}{\sqrt{2}}\begin{pmatrix} \pi_8^a T^a & 0 \\ 0 & \pi_8^a (T^a)^T \end{pmatrix}, \tag{3.12}$$

and a matrix for the triplet and antitriplet,

$$\Pi_{\mathbf{3}+\bar{\mathbf{3}}} = \begin{pmatrix} 0 & \kappa^\dagger \\ \kappa & 0 \end{pmatrix}, \qquad \kappa_{ij} = \frac{1}{2}\epsilon_{ijk}\pi_3^k, \tag{3.13}$$

where the generators corresponding to π_3 and π_3^* are linear combinations of X^{8+j} and X^{11+j}. The total matrix of the colored pNGBs is now given by

$$\Pi_\chi = \Pi_{\mathbf{8}} + \Pi_{\mathbf{3}+\bar{\mathbf{3}}}. \tag{3.14}$$

The normalization was chosen such that

$$\mathrm{Tr}\big(\Pi_\chi^\dagger \Pi_\chi\big) = \frac{1}{2}\pi_8^a \pi_8^a + \pi_3^\dagger \pi_3 \tag{3.15}$$

has the canonical normalization of a mass term. By exponentiating Π_χ, we obtain the Goldstone matrix,

$$U_\chi = \mathrm{e}^{\mathrm{i}\Pi_\chi^I X^I/(2f_\chi)}, \tag{3.16}$$

which transforms as $U_\chi \to g U_\chi h^{-1}$ with $g \in \mathrm{SU}(6)$ and $h \in \mathrm{Sp}(6)$.

To make the connection with the vacuum $\Sigma_{0,\chi}$, we have another look at the condensate in Eq. (3.4). Considering only the SU(6) irreps, the two-hyperquark operator

$$\mathbf{6} \times \mathbf{6} \ni \chi_i\chi_j = \frac{1}{2}(\chi_i\chi_j - \chi_j\chi_i) + \frac{1}{2}(\chi_i\chi_j + \chi_j\chi_i) \in \mathbf{15} + \mathbf{21} \tag{3.17}$$

can be split into the two-index antisymmetric (**15**) and symmetric (**21**) irreps. As the vacuum is antisymmetric, only the **15** contributes to the symmetry breaking. The pNGBs can therefore be parametrized by a scalar field Σ_χ in the **15** of SU(6) with $\langle\Sigma_\chi\rangle = \Sigma_{0,\chi}$. This field transforms as $\Sigma_\chi \to g\Sigma_\chi g^T$ with $g \in \mathrm{SU}(6)$. This is achieved by "dressing" the vacuum with the Goldstone matrix,

$$\Sigma_\chi = U_\chi \Sigma_{0,\chi} U_\chi^T = \mathrm{e}^{\mathrm{i}\Pi_\chi^I X^I/f_\chi}\Sigma_{0,\chi} \tag{3.18a}$$

$$= \Sigma_{0,\chi} + \frac{\mathrm{i}}{f_\chi}\begin{pmatrix} -\kappa^* & -\frac{1}{\sqrt{2}}\pi_8^a T^a \\ \frac{1}{\sqrt{2}}\pi_8^a (T^a)^T & -\kappa \end{pmatrix} + \mathcal{O}(\Pi_\chi^2), \tag{3.18b}$$

which is antisymmetric by construction. Since Sp(6) is unbroken, the pNGBs do not develop a vacuum expectation value (vev), which ensures $\langle\Sigma_\chi\rangle = \Sigma_{0,\chi}$, and the correct transformation is guaranteed by the Goldstone matrix.

EW Sector The EW pNGBs Π_ψ live in the coset SU(5)/SO(5), which results from[1] [53]

$$\langle\psi_i\psi_j\rangle \propto \Sigma_{0,\psi}^{ij}, \quad \Sigma_{0,\psi} = \begin{pmatrix} & \mathrm{i}\sigma_2 & \\ -\mathrm{i}\sigma_2 & & \\ & & 1 \end{pmatrix}. \tag{3.19}$$

The vacuum preserves the custodial symmetry $\mathrm{SU}(2)_L \times \mathrm{SU}(2)_R \subset \mathrm{SO}(5)$, whose generators are embedded as

$$T_L^i = \frac{1}{2}\begin{pmatrix} \mathbb{1}_2 \otimes \sigma^i & \\ & 0 \end{pmatrix}, \qquad T_R^i = \frac{1}{2}\begin{pmatrix} \sigma^i \otimes \mathbb{1}_2 & \\ & 0 \end{pmatrix}. \tag{3.20}$$

The pNGBs form a **14** of SO(5), which decomposes as

$$\mathbf{14} \to (\mathbf{3},\mathbf{3}) + (\mathbf{2},\mathbf{2}) + (\mathbf{1},\mathbf{1}) \tag{3.21a}$$

$$\to \mathbf{3}_1 + \mathbf{3}_0 + \mathbf{3}_{-1} + \mathbf{2}_{1/2} + \mathbf{2}_{-1/2} + \mathbf{1}_0 \tag{3.21b}$$

$$\equiv \pi_+ + \pi_0 + \pi_- + H + \tilde{H} + \eta \tag{3.21c}$$

under $\mathrm{SO}(5) \to \mathrm{SU}(2)_L \times \mathrm{SU}(2)_R \to \mathrm{SU}(2)_L \times \mathrm{U}(1)_Y$ since the ψ_i do not carry X-charge. The π_i are $\mathrm{SU}(2)_L$ triplets with hypercharge ± 1 and 0,

$$\pi_0 = \frac{1}{\sqrt{2}}\pi_0^i\sigma^i = \frac{1}{\sqrt{2}}\begin{pmatrix} \frac{1}{\sqrt{2}}\pi_0^3 & \pi_0^+ \\ \pi_0^- & -\frac{1}{\sqrt{2}}\pi_0^3 \end{pmatrix}, \qquad \pi_\pm = \pi_\pm^i\sigma^i = (\pi_\mp)^\dagger, \tag{3.22}$$

[1] There is another inequivalent choice for the vacuum with $1 \to -1$ in $\Sigma_{0,\psi}$ [53]. For simplicity, we only consider the form in Eq. (3.19).

where we have set $\pi_i^{\pm} = \frac{1}{\sqrt{2}}(\pi_i^1 \mp \mathrm{i}\pi_i^2)$. H is the Higgs doublet, $\tilde{H} = \mathrm{i}\sigma^2 H^*$ is its dual, and η is SM neutral. The EW pNGB matrix can be compactly expressed as

$$\Pi_\psi = \Pi_\psi^I X^I = \frac{1}{2}\begin{pmatrix} \frac{\eta}{\sqrt{10}}\mathbb{1}_2 + \pi_0 & \pi_+ & H \\ \pi_- & \frac{\eta}{\sqrt{10}}\mathbb{1}_2 - \pi_0 & -\tilde{H} \\ H^\dagger & -\tilde{H}^\dagger & -\frac{4}{\sqrt{10}}\eta \end{pmatrix}, \tag{3.23}$$

and exponentiating yields the Goldstone matrix,

$$U_\psi = \mathrm{e}^{2\mathrm{i}\Pi_\psi^I X^I / f_\psi}. \tag{3.24}$$

Finally, we construct a matrix

$$\Sigma_\psi = U_\psi \Sigma_{0,\psi} U_\psi^T = \mathrm{e}^{4\mathrm{i}\Pi_\psi^I X^I / f_\psi}\Sigma_{0,\psi} \tag{3.25}$$

so that $\langle\Sigma_\psi\rangle = \Sigma_{0,\psi}$. By analogous reasoning to the color sector, Σ_ψ is in the two-index symmetric representation **15** of SU(5) and transforms as $\Sigma_\psi \to g\Sigma_\psi g^T$ with $g \in \mathrm{SU}(5)$.

Note that the colored and EW pNGBs have different decay constants. As these are dynamically determined quantities, their ratio can in principle be calculated on the lattice [13]. However, no lattice data is available yet, so we have to resort to less reliable methods. For example, in [13] their ratio was estimated with the MAC hypothesis to be $f_\psi/f_\chi = 2.8$. Another approach is to use holographic techniques, by which a strongly coupled gauge theory can be mapped to a weakly coupled gravitational theory on a higher dimensional space. This allows for the calculation of some observables which would otherwise not be feasible. This idea was applied in [26] to study the spectra of CHMs, yielding $f_\psi/f_\chi = 1.7$ for M5. These estimates should be treated with care, however, and in the following we keep both f_ψ and f_χ as free parameters.

The matrix $\Sigma_{0,\psi}$ gives the orientation of the SO(5) preserving vacuum within SU(5). But the true vacuum $\tilde{\Sigma}_{0,\psi}$ of the theory is misaligned from the EW preserving vacuum by an angle θ due to the vev of the Higgs [53],

$$\tilde{\Sigma}_{0,\psi} = \Omega_\theta \Sigma_{0,\psi} \Omega_\theta^T = \begin{pmatrix} 0 & 0 & 0 & 1 & 0 \\ 0 & -s_\theta^2 & -c_\theta^2 & 0 & \frac{\mathrm{i}}{\sqrt{2}}s_{2\theta} \\ 0 & -c_\theta^2 & -s_\theta^2 & 0 & -\frac{\mathrm{i}}{\sqrt{2}}s_{2\theta} \\ 1 & 0 & 0 & 0 & 0 \\ 0 & \frac{\mathrm{i}}{\sqrt{2}}s_{2\theta} & -\frac{\mathrm{i}}{\sqrt{2}}s_{2\theta} & 0 & c_{2\theta} \end{pmatrix}, \tag{3.26}$$

where $s_\theta = \sin\theta = v/f_\psi$ and the misalignment matrix is given by

$$\Omega_\theta = \mathrm{e}^{4\mathrm{i}X^h\frac{\theta}{2}} = \begin{pmatrix} 1 & 0 & 0 & 0 & 0 \\ 0 & c_{\theta/2}^2 & s_{\theta/2}^2 & 0 & \frac{\mathrm{i}}{\sqrt{2}}s_\theta \\ 0 & s_{\theta/2}^2 & c_{\theta/2}^2 & 0 & -\frac{\mathrm{i}}{\sqrt{2}}s_\theta \\ 0 & 0 & 0 & 1 & 0 \\ 0 & \frac{\mathrm{i}}{\sqrt{2}}s_\theta & -\frac{\mathrm{i}}{\sqrt{2}}s_\theta & 0 & c_\theta \end{pmatrix}, \quad X^h = \frac{1}{2\sqrt{2}}\begin{pmatrix} & & & & 0 \\ & & & & 1 \\ & & & & -1 \\ & & & & 0 \\ 0 & 1 & -1 & 0 & \end{pmatrix}. \tag{3.27}$$

We define the pNGBs with respect to the misaligned vacuum. This way, no pNGB develops a vev. We also have to rotate the Goldstone matrix

$$\tilde{U}_\psi = \Omega_\theta U_\psi \Omega_\theta^{-1}, \tag{3.28}$$

and dressing the rotated vacuum with $\tilde{U}_\psi$ yields

$$\tilde{\Sigma}_\psi = \tilde{U}_\psi \tilde{\Sigma}_{0,\psi} \tilde{U}_\psi^T = \Omega_\theta \Sigma_\psi \Omega_\theta^T. \tag{3.29}$$

In Eq. (3.21c), we have written the pNGBs as gauge eigenstates. However, the Higgs vev breaks the $\mathrm{SU}(2)_L \times \mathrm{SU}(2)_R$ symmetry to the custodial $\mathrm{SU}(2)_D$, so when we use the misaligned vacuum, we should express the pNGBs as custodial eigenstates. The Higgs bidoublet becomes $(\mathbf{2},\mathbf{2}) \to \mathbf{3}+\mathbf{1} \equiv \phi + h$, where the triplet $\phi = (\phi^+, \phi^0, \phi^-)$ contains the longitudinal components of the $W^\pm, Z$ and h is the physical Higgs boson. They are related to the Higgs doublet by

$$H = \begin{pmatrix} \phi^+ \\ \frac{1}{\sqrt{2}}(h + \mathrm{i}\phi^0) \end{pmatrix}. \tag{3.30}$$

The bitriplet decomposes under the custodial $\mathrm{SU}(2)_D$ as

$$(\mathbf{3},\mathbf{3}) \to \mathbf{5} + \mathbf{3} + \mathbf{1} \equiv \eta_5 + \eta_3 + \eta_1. \tag{3.31}$$

The change of basis is given by

$$\pi_+^+ = \eta_5^{++}, \quad \pi_+^0 = \frac{\mathrm{i}\eta_3^+ - \eta_5^+}{\sqrt{2}}, \quad \pi_0^+ = \frac{\mathrm{i}\eta_3^+ + \eta_5^+}{\sqrt{2}} \tag{3.32a}$$

$$\pi_0^3 = \frac{\eta_1^0 - \sqrt{2}\eta_5^0}{\sqrt{3}}, \quad \pi_+^- = \frac{\sqrt{2}\eta_1^0 + \eta_5^0}{\sqrt{6}} + \mathrm{i}\frac{\eta_3^0}{\sqrt{2}} \tag{3.32b}$$

and $\pi_-^- = (\pi_+^+)^\dagger$, $\pi_-^0 = (\pi_+^0)^\dagger$, $\pi_-^+ = (\pi_+^-)^\dagger$ and $\pi_0^- = (\pi_0^+)^\dagger$ [53].

3.2.2 Top Partners

In M5, top partners occur in three-hyperquark bound states of the form $\psi\chi\chi$. More concretely, the combinations $\psi\chi\chi$, $\psi\bar{\chi}\bar{\chi}$ and $\psi\chi\bar{\chi}$ are possible. The respective representations under the global symmetries read

$$\psi\chi\chi \in (\mathbf{5},\mathbf{15})_\mathcal{G} + (\mathbf{5},\mathbf{21})_\mathcal{G} \to (\mathbf{5},\mathbf{14})_\mathcal{H} + (\mathbf{5},\mathbf{1})_\mathcal{H} + (\mathbf{5},\mathbf{21})_\mathcal{H} \equiv \mathcal{B}_{14}^1 + \mathcal{B}_1^1 + \mathcal{B}_{21}^1, \tag{3.33a}$$

$$\psi\bar{\chi}\bar{\chi} \in (\mathbf{5},\overline{\mathbf{15}})_\mathcal{G} + (\mathbf{5},\overline{\mathbf{21}})_\mathcal{G} \to (\mathbf{5},\mathbf{14})_\mathcal{H} + (\mathbf{5},\mathbf{1})_\mathcal{H} + (\mathbf{5},\mathbf{21})_\mathcal{H} \equiv \mathcal{B}_{14}^2 + \mathcal{B}_1^2 + \mathcal{B}_{21}^2, \tag{3.33b}$$

$$\psi\chi\bar{\chi} \in (\mathbf{5},\mathbf{35})_\mathcal{G} + (\mathbf{5},\mathbf{1})_\mathcal{G} \to (\mathbf{5},\mathbf{14})_\mathcal{H} + (\mathbf{5},\mathbf{21})_\mathcal{H} + (\mathbf{5},\mathbf{1})_\mathcal{H} \equiv \mathcal{B}_{14}^3 + \mathcal{B}_{21}^3 + \mathcal{B}_1^3, \tag{3.33c}$$

where we used

$$\mathbf{15}_{\mathrm{SU}(6)} \to \mathbf{14}_{\mathrm{Sp}(6)} + \mathbf{1}_{\mathrm{Sp}(6)}, \quad \mathbf{21}_{\mathrm{SU}(6)} \to \mathbf{21}_{\mathrm{Sp}(6)}, \quad \mathbf{35}_{\mathrm{SU}(6)} \to \mathbf{14}_{\mathrm{Sp}(6)} + \mathbf{21}_{\mathrm{Sp}(6)} \tag{3.34}$$

and we neglected the global U(1) in $\mathcal{G}$, which is irrelevant for the following. We decompose the SO(5) and Sp(6) irreps further under $\mathrm{SU}(2)_L \times \mathrm{SU}(2)_R$ and $\mathrm{SU}(3)_c \times \mathrm{U}(1)_X$ respectively,

$$\mathbf{5}_{\mathrm{SO}(5)} \to (\mathbf{2},\mathbf{2}) + (\mathbf{1},\mathbf{1}), \tag{3.35a}$$

$$\mathbf{14}_{\mathrm{Sp}(6)} \to \mathbf{8}_0 + \mathbf{3}_{2x} + \overline{\mathbf{3}}_{-2x}, \tag{3.35b}$$

$$\mathbf{21}_{\mathrm{Sp}(6)} \to \mathbf{8}_0 + \mathbf{6}_{-2x} + \overline{\mathbf{6}}_{2x} + \mathbf{1}_0, \tag{3.35c}$$

to identify the irreps that contain partners of $q_L \in (\mathbf{3},\mathbf{2})_{1/6}$ and $t_R^c \in (\overline{\mathbf{3}},\mathbf{1})_{-2/3}$. Note that we work with two-component spinors in this chapter. The $\mathbf{14}_{\mathrm{Sp}(6)}$ contains a color triplet and antitriplet. Pairing the $\mathbf{3}$ with the $(\mathbf{2},\mathbf{2})$ and the $\overline{\mathbf{3}}$ with the EW singlet, we obtain

$$(\mathbf{3},\mathbf{2})_{2x+1/2}, \quad (\mathbf{3},\mathbf{2})_{2x-1/2}, \quad (\overline{\mathbf{3}},\mathbf{1})_{-2x} \tag{3.36}$$

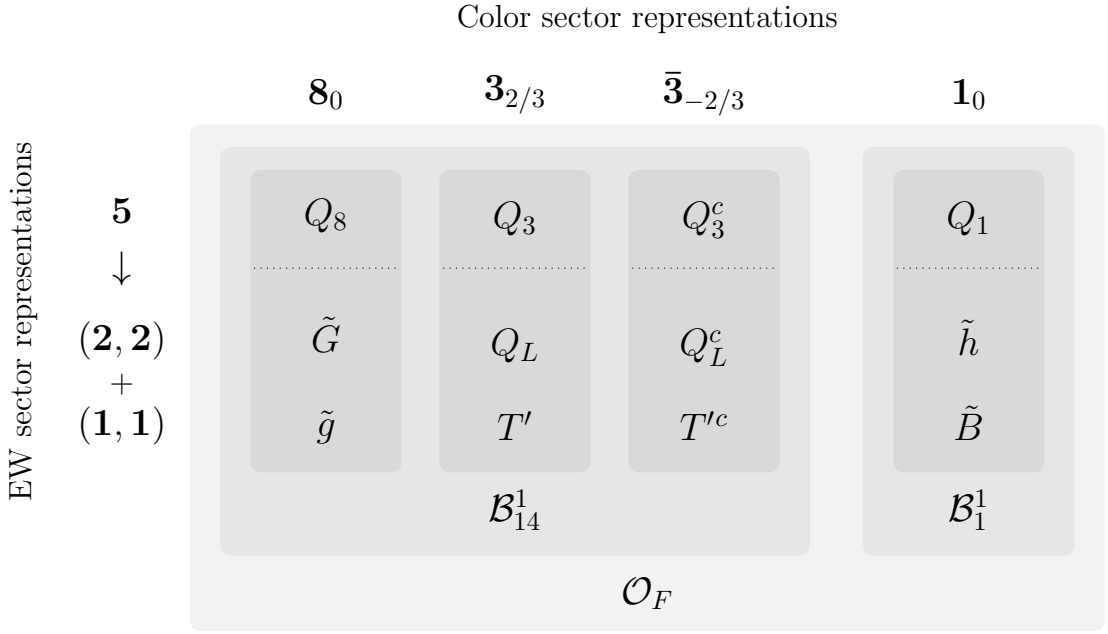

Figure 3.1: Decomposition of the top partners in $\mathcal{O}_F \in (\mathbf{5},\mathbf{15})_{\mathcal{G}}$ under $\mathrm{SU}(3)_c \times \mathrm{U}(1)_X$ (horizontal) and $\mathrm{SO}(5) \to \mathrm{SU}(2)_L \times \mathrm{SU}(2)_R$ (vertical). All fermions are two-component Weyl spinors except for $\tilde{g}$ and $\tilde{B}$, which are Majorana fermions.

of the SM gauge group G_{SM}. By choosing $x = 1/3$, we can identify the last two states as top partners proper. Thus, the top partners originate from the $\mathbf{14}_{\mathrm{Sp}(6)}$, which in turn can come from the antisymmetric $\mathbf{15}_{\mathrm{SU}(6)}$, its conjugate $\overline{\mathbf{15}}_{\mathrm{SU}(6)}$ or the adjoint $\mathbf{35}_{\mathrm{SU}(6)}$. In this thesis, we only consider the case where the top partners are embedded in the $\mathbf{15}$. We denote the operator that contains the top partners by $\mathcal{O}_F \in (\mathbf{5},\mathbf{15})_{\mathcal{G}}$.

Now that the representation of $\mathcal{O}_F$ under $\mathcal{G}$ is fixed, the next step is to work out the physical states in $\mathcal{O}_F$. The decomposition under $\mathrm{SU}(3)_c \times \mathrm{U}(1)_X$ and $\mathrm{SU}(2)_L \times \mathrm{SU}(2)_R$ is shown in Fig. 3.1 along with our notation for the corresponding states. We denote the components of the color octet and singlet bidoublets by

$$\tilde{G} = \left(\begin{pmatrix}\tilde{G}_u^+\\ \tilde{G}_u^0\end{pmatrix}, \begin{pmatrix}\tilde{G}_d^0\\ \tilde{G}_d^-\end{pmatrix}\right), \qquad \tilde{h} = \left(\begin{pmatrix}\tilde{h}_u^+\\ \tilde{h}_u^0\end{pmatrix}, \begin{pmatrix}\tilde{h}_d^0\\ \tilde{h}_d^-\end{pmatrix}\right), \tag{3.37}$$

where the index u/d indicates the hypercharge $Y = \pm 1/2$ of the $\mathrm{SU}(2)_L$ doublet and the superscript is the electric charge after EWSB. For the color (anti)triplets, we set

$$Q_L = \left(\begin{pmatrix}X_{5/3}\\ X_{2/3}\end{pmatrix}, \begin{pmatrix}T\\ B\end{pmatrix}\right), \qquad Q_L^c = \left(\begin{pmatrix}X_{5/3}^c\\ X_{2/3}^c\end{pmatrix}, \begin{pmatrix}T^c\\ B^c\end{pmatrix}\right). \tag{3.38}$$

Since both chiralities appear with the same EW quantum numbers, we refer to these states as vector-like quarks (VLQs).

The doublet $(T,B)^T \in (\mathbf{3},\mathbf{2})_{1/6}$ and the singlet $T'^c \in (\overline{\mathbf{3}},\mathbf{1})_{-2/3}$ mix with the SM quarks q_L, t_R^c. After EWSB, there are actually three states that can mix with the top: Analogous to the EW pNGBs, we can rewrite the VLQs as eigenstates of the custodial $\mathrm{SU}(2)_D$. This leads to a triplet $(X_{5/3}, T_3, B)$ and two singlets T_1, T_2, with

$$T_1 = T', \qquad T_2 = \frac{1}{\sqrt{2}}(X_{2/3} - T), \qquad T_3 = \frac{1}{\sqrt{2}}(X_{2/3} + T). \tag{3.39}$$

The T_i all have electric charge 2/3 and as such can mix with the top quark. While only a few of the states in Tab. 3.1 mix with SM quarks, they all emerge from the same multiplet $(\mathbf{5},\mathbf{15})_{\mathcal{G}}$. We therefore refer to all of them as top partners.

In the next chapter, we work with the top partners in the phase of broken EW symmetry and in terms of four-component spinors. The color octets are then expressed as two Dirac and one Majorana spinor[2],

$$\tilde{G}^+ = \begin{pmatrix} \tilde{G}_u^+ \\ \bar{\tilde{G}}_d^- \end{pmatrix}, \qquad \tilde{G}^0 = \begin{pmatrix} \tilde{G}_u^0 \\ \bar{\tilde{G}}_d^0 \end{pmatrix}, \qquad \tilde{g} = \begin{pmatrix} \tilde{g} \\ \bar{\tilde{g}} \end{pmatrix}, \tag{3.40}$$

where we allow for a notional ambiguity in $\tilde{g}$. Our notation is reminiscent of SUSY, where the fermionic partner of the gluon is a Majorana fermion $\tilde{g}$ called gluino. To highlight this similarity while making it clear that we do not work with a supersymmetric model, we name the color octet fermions *gluonis*. We write Q_8 as a collective symbol for the charged, neutral and Majorana gluonis, $Q_8 = (\tilde{G}^+, \tilde{G}^0, \tilde{g})$. Repeating this for the color singlets, we obtain $Q_1 = (\tilde{h}^+, \tilde{h}^0, \tilde{B})$, which are defined analogously to Eq. (3.40). Their SUSY analogs are the higgsinos and the bino, so we call $\tilde{h}^{+,0}$ the charged and neutral *higgsonis*, and name $\tilde{B}$ the *boni*. Finally, the VLQs can be written as Dirac spinors by

$$X_{5/3} = \begin{pmatrix} X_{5/3} \\ \bar{X}^c_{5/3} \end{pmatrix}, \qquad T_i = \begin{pmatrix} T_i \\ \bar{T}_i^c \end{pmatrix}, \qquad B = \begin{pmatrix} B \\ \bar{B}^c \end{pmatrix}, \tag{3.41}$$

where we again accept an ambiguous notation for readability. For the remainder of this chapter we keep working with two-component spinors.

We now discuss how the top partners described above are embedded in $\mathcal{O}_F$. To this end it is useful to write the flavor indices explicitly: $(\mathcal{O}_F)_{IMN}$ carries one index I in the $\mathbf{5}_{\mathrm{SU}(5)}$ and two indices M, N for the $\mathbf{6}_{\mathrm{SU}(6)}$, with $(\mathcal{O}_F)_{IMN} = -(\mathcal{O}_F)_{INM}$. For the unbroken subgroups we use the same letters but lowercase. We start with the embedding in the color sector. The $\mathbf{14}_{\mathrm{Sp}(6)}$ is embedded in the $\mathbf{15}_{\mathrm{SU}(6)}$ by

$$(\mathcal{B}^1_{14})_{mn} = \begin{pmatrix} -Q_3^c & -\frac{1}{\sqrt{2}} Q_8^a T^a \\ \frac{1}{\sqrt{2}} Q_8^a (T^a)^T & -Q_3 \end{pmatrix}, \tag{3.42}$$

where $Q_3^{(c)}$ are antisymmetric color space matrices, $Q^{(c)}_{3,xy} = \frac{1}{2}\epsilon_{xyz} Q^{(c)}_{3,z}$. For later reference we also give the expression for the embedding in the $\overline{\mathbf{15}}_{\mathrm{SU}(6)}$,

$$(\mathcal{B}^2_{14})_{mn} = \begin{pmatrix} Q_3 & \frac{1}{\sqrt{2}} Q_8^a (T^a)^T \\ -\frac{1}{\sqrt{2}} Q_8^a T^a & Q_3^c \end{pmatrix}. \tag{3.43}$$

To turn the Sp(6) indices into SU(6) ones, we recall that the Goldstone matrix has indices $(U_\chi)_{Mm}$, so the embedding in SU(6) reads

$$(\mathcal{O}_{14})_{MN} = (U_\chi)_{Mm} (U_\chi)_{Nn} (\mathcal{B}^1_{14})_{mn} = U_\chi \mathcal{B}^1_{14} U_\chi^T. \tag{3.44}$$

[2]Technically, we should also express the color octets and singlets as custodial eigenstates. This would result in a field redefinition that has no physical effect on the processes studied in this thesis, as we do not consider couplings to EW pNGBs.

Applying the same procedure to the singlet $\mathbf{1}_{\mathrm{Sp}(6)}$, we obtain

$$\mathcal{B}_1^1 = Q_1 \begin{pmatrix} 0 & -\mathbb{1}_3 \\ \mathbb{1}_3 & 0 \end{pmatrix}, \qquad \mathcal{O}_1 = U_\chi \mathcal{B}_1^1 U_\chi^T. \tag{3.45}$$

The dressed operators $\mathcal{O}_{14}$ and $\mathcal{O}_1$ can be used independently in the construction of the Lagrangian [3]. Note that $(\mathcal{O}_{14,1})_I$ and $(Q_{8,3,1})_I$ still carry a SU(5) index. The VLQs are embedded in the $\mathbf{5}_{\mathrm{SO}(5)}$ by

$$(Q_3')_i = (X_{5/3}, X_{2/3}, T, B, \mathrm{i}T')^T, \tag{3.46a}$$
$$(Q_3^{c\prime})_i = (B^c, -T^c, -X_{2/3}^c, X_{5/3}^c, -\mathrm{i}T'^c)^T. \tag{3.46b}$$

They were chosen to reproduce the correct $\mathrm{SU}(2)_L$ product,

$$Q_3^{c\prime} Q_3' = Q_{3,i}^{c\prime} \tilde{\epsilon}_{ij} Q_{3,j}' = X_{5/3}^c X_{5/3} + X_{2/3}^c X_{2/3} + T^c T + B^c B + T'^c T', \tag{3.47}$$

where

$$\tilde{\epsilon} = \begin{pmatrix} 0 & 0 & 0 & 1 & 0 \\ 0 & 0 & -1 & 0 & 0 \\ 0 & -1 & 0 & 0 & 0 \\ 1 & 0 & 0 & 0 & 0 \\ 0 & 0 & 0 & 0 & 1 \end{pmatrix} = \Sigma_{0,\psi} \tag{3.48}$$

to match the choice of the EW vacuum in Eq. (3.19). The SO(5) index can be transformed to a SU(5) index with the EW Goldstone matrix,

$$Q_3 = U_\psi Q_3', \qquad Q_3^c = U_\psi Q_3^{c\prime}. \tag{3.49}$$

Similarly, the gluonis and higgsonis/boni are embedded by

$$Q_8' = (\tilde{G}_u^+, \tilde{G}_u^0, \tilde{G}_d^0, \tilde{G}_d^-, \mathrm{i}\tilde{g})^T, \qquad Q_8 = U_\psi Q_8', \tag{3.50a}$$
$$Q_1' = (\tilde{h}_u^+, \tilde{h}_u^0, \tilde{h}_d^0, \tilde{h}_d^-, \mathrm{i}\tilde{B})^T, \qquad Q_1 = U_\psi Q_1'. \tag{3.50b}$$

3.2.3 Embeddings of the Standard Model Quarks

For the formulation of the elementary-composite interactions,

$$\mathcal{L}_{\mathrm{mix}} \sim -\lambda_L \mathcal{O}_F \zeta_L - \lambda_R \mathcal{O}_F \zeta_R^c + \mathrm{h.c.}\,, \tag{3.51}$$

we need to determine the embeddings ζ_L, ζ_R^c of the SM quarks q_L, t_R^c in the relevant $\mathcal{G}$ irreps. Since $\mathcal{O}_F \in (\mathbf{5}, \mathbf{15})_{\mathcal{G}}$, we need $\zeta \in (\overline{\mathbf{5}}, \overline{\mathbf{15}})_{\mathcal{G}}$ for Eq. (3.51) to be $\mathcal{G}$ invariant. The color sector embedding for the $\overline{\mathbf{15}}_{\mathrm{SU}(6)}$ is given in Eq. (3.43), from which we read off

$$\zeta_L = \begin{pmatrix} \kappa_L & 0 \\ 0 & 0 \end{pmatrix}, \qquad \kappa_{L,xy} = \frac{1}{2}\epsilon_{xyz}\xi_{L,z}, \tag{3.52a}$$
$$\zeta_R^c = \begin{pmatrix} 0 & 0 \\ 0 & \kappa_R \end{pmatrix}, \qquad \kappa_{R,xy} = \frac{1}{2}\epsilon_{xyz}\xi_{R,z}^c. \tag{3.52b}$$

For the EW sector embedding, Eq. (3.46) yields

$$\xi_L = \big(0, 0, t_L, b_L, 0\big), \qquad \xi_R^c = \big(0, 0, 0, 0, -\mathrm{i}t_R^c\big). \tag{3.53}$$

3.3 Model Lagrangian

In preparation for the phenomenological studies in Chapter 4, we work out parts of the IR Lagrangian of M5 in this section. In particular, we focus on the sectors that lead to decay channels of the gluonis and the colored pNGBs.

The total Lagrangian can be split into the elementary sector (SM minus the Higgs), the composite sector, mixing terms between the two and the anomalous WZW term,

$$\mathcal{L}_{\text{M5}} = \mathcal{L}'_{\text{SM}} + \mathcal{L}_{\text{comp}} + \mathcal{L}_{\text{mix}} + \mathcal{L}_{\text{WZW}}. \tag{3.54}$$

The elementary-composite interactions in Eq. (3.51) are oversimplified, since $\mathcal{O}_{14}$ and $\mathcal{O}_1$ can couple independently to the SM quarks. More correctly,

$$\mathcal{L}_{\text{mix}} = -\lambda_{L,14}\mathcal{O}_{14}\zeta_L - \lambda_{R,14}\mathcal{O}_{14}\zeta^c_R - \lambda_{L,1}\mathcal{O}_1\zeta_L - \lambda_{R,1}\mathcal{O}_1\zeta^c_R + \text{h.c.}\,, \tag{3.55}$$

where the index contractions are implicit. We start the calculation in the color sector. Since we work with a matrix representation, the indices are traced out, e.g.

$$\text{Tr}(\mathcal{O}_{14}\zeta_L) = \text{Tr}\big(U_\chi \mathcal{B}^1_{14} U^T_\chi \zeta_L\big). \tag{3.56}$$

We expand the Goldstone matrix and keep only the leading order in the pNGBs since higher orders are suppressed by $1/f^n_\chi$. Performing the traces yields [54]

$$\begin{aligned}
\mathcal{L}_{\text{mix}} = &- \lambda_{L,14}\left(2Q^c_3\xi_L - \frac{\text{i}}{\sqrt{2}f_\chi}Q^c_3\pi_8\xi_L - \frac{\text{i}}{\sqrt{2}f_\chi}\pi^\dagger_3 Q_8\xi_L + \mathcal{O}(\Pi^2_\chi)\right) && \text{(3.57a)}\\
&- \lambda_{R,14}\left(2Q_3\xi^c_R - \frac{\text{i}}{\sqrt{2}f_\chi}Q_3\pi_8\xi^c_R - \frac{\text{i}}{\sqrt{2}f_\chi}\pi_3 Q_8\xi^c_R + \mathcal{O}(\Pi^2_\chi)\right) && \text{(3.57b)}\\
&- \lambda_{L,1}\left(-\frac{\text{i}}{f_\chi}\pi^\dagger_3 Q_1\xi_L + \mathcal{O}(\Pi^2_\chi)\right) - \lambda_{R,1}\left(-\frac{\text{i}}{f_\chi}\pi_3 Q_1\xi^c_R + \mathcal{O}(\Pi^2_\chi)\right) + \text{h.c.}\,, && \text{(3.57c)}
\end{aligned}$$

where the $\text{SU}(3)_c$ indices are implicit, e.g. $\pi^\dagger_3 Q_8\xi_L = \pi^\dagger_{3,x}Q^a_8 T^a_{xy}\xi_{L,y}$. Next, we expand in the EW sector. Since we are not interested in couplings to the EW pNGBs, we expand $Q = U_\psi Q'$ to zeroth order in Π_ψ, $U_\psi = \mathbb{1}_5 + \mathcal{O}(\Pi_\psi)$. Using $Q'\xi = Q'_i\tilde{\epsilon}_{ij}\xi_j$,

$$\begin{aligned}
= &- \lambda_{L,14}\left(2(T^c t_L + B^c b_L) - \frac{\text{i}}{\sqrt{2}f_\chi}(T^c\pi_8 t_L + B^c\pi_8 b_L) - \frac{\text{i}}{\sqrt{2}f_\chi}\pi^\dagger_3(-\tilde{G}^0_u t_L + \tilde{G}^+_u b_L)\right) && \text{(3.58a)}\\
&- \lambda_{R,14}\left(2T' t^c_R - \frac{\text{i}}{\sqrt{2}f_\chi}T'\pi_8 t^c_R - \frac{\text{i}}{\sqrt{2}f_\chi}\pi_3\tilde{g}t^c_R\right) && \text{(3.58b)}\\
&+ \frac{\text{i}\lambda_{L,1}}{f_\chi}\pi^\dagger_3(-\tilde{h}^0_u t_L + \tilde{h}^+_u b_L) + \frac{\text{i}\lambda_{R,1}}{f_\chi}\pi_3\tilde{B}t^c_R + \mathcal{O}(\Pi_\psi, \Pi^2_\chi) + \text{h.c.}\,. && \text{(3.58c)}
\end{aligned}$$

The first two lines open the decay channel of gluonis into π_3 and a third-generation quark, the third line allows $\pi_3 \to Q_1 q$. After taking into account the mixing induced by the $\mathcal{O}(\Pi^0_\chi)$ contribution, the couplings to π_8 lead to $\pi_8 \to t\bar{t}, b\bar{b}$.

The composite sector Lagrangian $\mathcal{L}_{\text{comp}}$ consists of the generalized kinetic terms of the top partners as in Eq. (2.12) and the series of operators built from the so-called Maurer-Cartan forms d_μ and e_μ defined in Eq. (2.6). Among the latter are the derivative couplings [54, 55]

$$\mathcal{L}_{\text{comp}} \supset \text{i}c_{14}\mathcal{B}^1_{14}\sigma^\mu\bar{\mathcal{B}}^1_{14}d_\mu + \text{i}c_1\mathcal{B}^1_{14}\sigma^\mu\bar{\mathcal{B}}^1_1 d_\mu + \text{h.c.}\,. \tag{3.59}$$

Considering only the color sector $d_\mu \simeq -\frac{1}{2f_\chi}\partial_\mu \Pi_\chi$ and performing the SU(6) traces, we obtain

$$\mathrm{Tr}\big(\mathcal{B}_{14}\sigma^\mu \bar{\mathcal{B}}_1 \partial_\mu \Pi_\chi\big) + \text{h.c.} = \mathrm{Tr}\big(Q_3^c \sigma^\mu \bar{Q}_1 \partial_\mu \kappa - Q_3 \sigma^\mu \bar{Q}_1 \partial_\mu \kappa^\dagger - Q_8 \sigma^\mu \bar{Q}_1 \partial_\mu \pi_8\big) + \text{h.c.} \tag{3.60a}$$

$$= -\frac{1}{2}\left(Q_{3,i}^c \sigma^\mu \bar{Q}_1 \partial_\mu \pi_{3,i} + Q_{3,i} \sigma^\mu \bar{Q}_1 \partial_\mu \pi_{3,i}^\dagger + Q_8^a \sigma^\mu \bar{Q}_1 \partial_\mu \pi_8^a\right) + \text{h.c.}\,. \tag{3.60b}$$

Of those, only the last term opens new decay channels for the gluonis,

$$Q_8^a \sigma^\mu \bar{Q}_1 \partial_\mu \pi_8^a = \left(\tilde{G}_u^{+,a} \sigma^\mu \bar{\tilde{h}}_u^+ + \tilde{G}_u^{0,a} \sigma^\mu \bar{\tilde{h}}_u^0 + \tilde{G}_d^{0,a} \sigma^\mu \bar{\tilde{h}}_d^0 + \tilde{G}_d^{-,a} \sigma^\mu \bar{\tilde{h}}_d^- + \tilde{g} \sigma^\mu \bar{\tilde{B}}\right) \partial_\mu \pi_8^a, \tag{3.61}$$

namely $Q_8 \to \pi_8 Q_1$. The interaction of two 14-plets includes the coupling of gluonis to VLQs and the stop,

$$\mathrm{Tr}\big(\mathcal{B}_{14}\sigma^\mu \bar{\mathcal{B}}_{14} \partial_\mu \Pi_\chi\big) + \text{h.c.} \tag{3.62a}$$

$$= \sqrt{2}\,\mathrm{Tr}\big(Q_3^c \sigma^\mu \bar{Q}_3^c \partial_\mu \pi_8 - Q_3 \sigma^\mu \bar{Q}_3 \partial_\mu \pi_8 - Q_8 \sigma^\mu \bar{Q}_8 \partial_\mu \pi_8 + Q_8 \sigma^\mu \bar{Q}_3 \partial_\mu \kappa + Q_8 \sigma^\mu \bar{Q}_3^c \partial_\mu \kappa^\dagger\big) \tag{3.62b}$$

$$\supset \sqrt{2}\left(\tilde{G}_u^{+,a} \sigma^\mu \bar{X}_{5/3} + \tilde{G}_u^{0,a} \sigma^\mu \bar{X}_{2/3} + \tilde{G}_d^{0,a} \sigma^\mu \bar{T} + \tilde{G}_d^{-,a} \sigma^\mu \bar{B} + \tilde{g}^a \sigma^\mu \bar{T}'\right) t^a \partial_\mu \pi_3. \tag{3.62c}$$

In the next chapter, we will need the form of the WZW term for the pseudo-scalar π_8. In the gauge eigenbasis, it is given by

$$\mathcal{L}_{\mathrm{WZW},\pi_8} = \frac{g_s^2}{16\pi^2 f_\chi}\, d_\chi\, \frac{1}{2} d^{abc}\, \pi_8^a\, \epsilon^{\mu\nu\rho\sigma} G_{\mu\nu}^b G_{\rho\sigma}^c + \frac{g_s g'}{16\pi^2 f_\chi}\, d_\chi Y_\chi\, \pi_8^a\, \epsilon^{\mu\nu\rho\sigma} G_{\mu\nu}^a B_{\rho\sigma}, \tag{3.63}$$

where $d_\chi = 4$ is the dimension of the Sp(4) irrep of the χ and $Y_\chi = 1/3$ is their hypercharge [13]. The first term induces the decay $\pi_8 \to gg$ and the second term couples the sgluon to gZ and $g\gamma$ after EWSB.

As a final remark, we note that the Lagrangian is invariant under an accidental parity,

$$X \to -X: \qquad \pi_3,\, \tilde{G},\, \tilde{g},\, \tilde{h},\, \tilde{B}, \tag{3.64a}$$

$$X \to X: \qquad \text{otherwise}. \tag{3.64b}$$

This means that the lightest of the odd states is stable. We will make use of this fact when we discuss the phenomenology of the model in Section 4.1.

3.4 Calculation of the Scalar Potential

The elementary-composite interactions shown in the previous section explicitly break $\mathcal{G}$. This turns the massless NGBs into pseudo NGBs by generating a potential for them. The scalar potential V fulfills the crucial role of giving a vev to the Higgs field, thereby triggering EWSB. Besides that, it contains the mass terms of the pNGBs and encodes the couplings of the pNGBs among each other, which are phenomenologically important for potential cascade decays.

In this section, we discuss the different contributions to the scalar potential and determine V to $\mathcal{O}(p^2)$ in the chiral expansion. As in Section 3.2.2, we limit the discussion to the case where the top partners come from a single representation $(\mathbf{5}, \mathbf{15})$ of $\mathcal{G}$. The goal of this calculation is to estimate the masses of the colored pNGBs. This allows us to further simplify the calculation by mostly neglecting the contributions of EW pNGBs. However, our analysis can also be used as a starting point for studying the EW sector.

3.4.1 Gauge Terms

The covariant derivative for a generic field from the composite sector reads

$$D_\mu = \partial_\mu - \mathrm{i}\left(g_s G_\mu^a T^a + g' B_\mu T_X\right) - \mathrm{i}\left(g W_\mu^i T_L^i + g' B_\mu T_R^3\right). \tag{3.65}$$

The brackets group the generators that belong to $\mathrm{SU}(3)_c \times \mathrm{U}(1)_X \subset \mathrm{SU}(6)$ and $\mathrm{SU}(2)_L \times \mathrm{SU}(2)_R \subset \mathrm{SU}(5)$, respectively. Since only a subgroup of $\mathcal{G}$ is gauged, Eq. (3.65) explicitly breaks the global symmetry of the composite sector. This allows for gauge boson loops that would have canceled if $\mathcal{G}$ had been fully gauged. The counterterms for these loops contribute to the scalar potential.

To $\mathcal{O}(p^2)$, the EW sector contribution to the potential can be expressed as [56]

$$V_{\text{gauge}}^{\text{EW}} = C_g f_\psi^4 \left(g^2 \operatorname{Tr}\left[T_L^i \Sigma_\psi (T_L^i)^T \Sigma_\psi^\dagger\right] + g'^2 \operatorname{Tr}\left[T_R^3 \Sigma_\psi (T_R^3)^T \Sigma_\psi^\dagger\right]\right). \tag{3.66}$$

Here, C_g is a (typically positive) low-energy constant (LEC) that can be computed on the lattice. Expanding Σ_ψ to first order in the pNGBs[3],

$$V_{\text{gauge}}^{\text{EW}} = C_g f_\psi^4 \left(3g^2 + g'^2\right)\left(-c_\theta^2 + s_{2\theta}\frac{h}{f_\psi}\right) + \mathcal{O}(\Pi_\psi^2), \tag{3.67}$$

we reproduce the result from [53], where the pNGB potential was calculated for a CHM based on SU(5)/SO(5). Eq. (3.66) can straightforwardly be applied to the color sector,

$$V_{\text{gauge}}^{\text{C}} = C_g' f_\chi^4 \left(g_s^2 \operatorname{Tr}\left[T^a \Sigma_\chi (T^a)^T \Sigma_\chi^\dagger\right] + g'^2 \operatorname{Tr}\left[T_X \Sigma_\chi (T_X)^T \Sigma_\chi^\dagger\right]\right) \tag{3.68a}$$

$$= \frac{3}{8} C_g' f_\chi^2 g_s^2 \pi_8^a \pi_8^a + C_g' f_\chi^2 \left(\frac{1}{3} g_s^2 + \frac{2}{9} g'^2\right) \pi_3^\dagger \pi_3 + \mathcal{O}(\Pi_\chi^3) \tag{3.68b}$$

up to a constant offset. The numerical prefactors of the QCD contributions are determined by the quadratic Casimir,

$$(m_R^{\text{QCD}})^2 = C_g' f_\chi^2 g_s^2 \frac{C_2(R)}{4}, \tag{3.69}$$

with $C_2(\mathbf{3}) = 4/3$ and $C_2(\mathbf{8}) = 3$. For the octet, we can compare our result with [57] where the colored pNGBs emerging from SU(6)/SO(6) are studied. We find agreement with Eq. (3.69).

The form of the gauge contributions to V can be understood with the *spurion method* [56]. A spurion is a source of explicit $\mathcal{G}$ breaking that gets formally promoted to a complete representation. For example, the spurion for the gauging of $\mathrm{SU}(3)_c$ is

$$\Xi_\mu \in (\mathbf{1}, \mathbf{35})_{\mathcal{G}}, \qquad \Xi_\mu \to g_\chi \Xi_\mu g_\chi^\dagger, \qquad \Xi_\mu\Big|_{\text{phys}} = g_s T^a G_\mu^a. \tag{3.70}$$

In the following, we leave the restriction of the spurions to their physical values implicit. For the calculation of the potential we define a projector P^a by factoring out the gluon field,

$$\Xi_\mu = P^a G_\mu^a, \qquad P^a \in (\mathbf{1}, \mathbf{35}; \mathbf{8}, \mathbf{1}, 0) \text{ of } \mathcal{G} \times G_{\text{SM}}, \qquad P_{MN}^a = g_s T_{MN}^a. \tag{3.71}$$

Note that the projector carries both global and SM quantum numbers. To find the operators that contribute to V, we have to identify the independent $\mathcal{G} \times G_{\text{SM}}$ invariants that can be

[3]Here and in the following, we evaluate Σ_ψ in the misaligned vacuum, i.e. using $\tilde{\Sigma}_\psi$ from Eq. (3.29).

constructed from the projectors and the Σ matrices to a given order in the chiral expansion, where Σ counts as $\mathcal{O}(p^0)$ and P^a as $\mathcal{O}(p)$. Thus, operators contain two projectors at $\mathcal{O}(p^2)$, and SM invariance forces them to belong to the same gauge field. Using $\Sigma \to g\Sigma g^T$, we find two independent operators for a generic gauge projector P^A,

$$\mathrm{Tr}\big(P^A P^A\big), \quad \mathrm{Tr}\big(P^A \Sigma (P^A)^T \Sigma^\dagger\big). \tag{3.72}$$

Conjugated projectors do not appear because $\overline{\mathbf{Adj}} = \mathbf{Adj}$ and a different order in the second trace is equivalent to the given form due to the cyclic property of the trace. The first operator can be ignored since it only shifts the potential by a constant amount, leaving the traces in Eqs. (3.66) and (3.68) as the only $\mathcal{O}(p^2)$ contributions.

3.4.2 Hyperquark Mass Terms

The global symmetry is also broken explicitly by mass terms for the hyperquarks,

$$\mathcal{L}_{\text{mass}} = -\frac{1}{2}\psi \mathcal{M}_\psi \psi - \frac{1}{2}\chi \mathcal{M}_\chi \chi + \text{h.c.}\,. \tag{3.73}$$

For the ψ, the most general gauge invariant mass matrix reads [53]

$$\mathcal{M}_\psi = \begin{pmatrix} 0 & \mu_d(\mathrm{i}\sigma^2) & 0 \\ -\mu_d(\mathrm{i}\sigma^2) & 0 & 0 \\ 0 & 0 & \mu_s \end{pmatrix}, \qquad \frac{1}{2}\psi \mathcal{M}_\psi \psi = \mu_d \psi_d^+ \psi_d^- + \frac{1}{2}\mu_s \psi_s \psi_s, \tag{3.74}$$

which breaks $\mathrm{SU}(5) \to \mathrm{SO}(4)$ for $\mu_d \neq \mu_s$. For the colored hyperquarks, we choose

$$\mathcal{M}_\chi = \begin{pmatrix} 0 & -\mu_\chi \mathbb{1}_3 \\ \mu_\chi \mathbb{1}_3 & 0 \end{pmatrix} = \mu_\chi \Sigma_{0,\chi}, \qquad \frac{1}{2}\chi \mathcal{M}_\chi \chi = \mu_\chi \chi_{\bar{\mathbf{3}}} \chi_{\mathbf{3}}, \tag{3.75}$$

which breaks $\mathrm{SU}(6) \to \mathrm{Sp}(6)$ [11]. Note that with this mass matrix, we have assumed that the χ are mass degenerate. The spurions associated with the mass terms are given by the mass matrices,

$$\Xi_m^\psi = \mathcal{M}_\psi, \qquad \Xi_m^\chi = \mathcal{M}_\chi, \tag{3.76}$$

and transform in the same irreps as the $\Sigma_{\psi,\chi}$. Since they count as $\mathcal{O}(p^2)$ in the chiral expansion [56], the leading order (LO) operator in the potential contains only one Ξ_m,

$$\mathrm{Tr}\big(\Xi_m \Sigma^\dagger + \Sigma \Xi_m^\dagger\big). \tag{3.77}$$

Thus, the contributions of the hyperquark mass terms to the potential are

$$V_{\text{mass}}^{\text{EW}} = -C_m f_\psi^3 \,\mathrm{Tr}\Big[\mathcal{M}_\psi \Sigma_\psi^\dagger + \Sigma_\psi \mathcal{M}_\psi^\dagger\Big] \tag{3.78a}$$

$$= 2C_m f_\psi^3 \left(-3\mu_d - (\mu_d + \mu_s)c_{2\theta} + 2(\mu_d + \mu_s)s_{2\theta}\frac{h}{f_\psi}\right) + \mathcal{O}(\Pi_\psi^2), \tag{3.78b}$$

$$V_{\text{mass}}^{\text{C}} = -C_m' f_\chi^3 \,\mathrm{Tr}\big[\mathcal{M}_\chi \Sigma_\chi^\dagger + \Sigma_\chi \mathcal{M}_\chi^\dagger\big] \tag{3.78c}$$

$$= \frac{1}{2}C_m' \mu_\chi f_\chi \left(\pi_8^a \pi_8^a + 2\pi_3^* \pi_3\right) + \mathcal{O}(\Pi_\chi^3), \tag{3.78d}$$

with new LECs $C_m^{(\prime)}$. The normalization was chosen to coincide with [53], where the same result was obtained for the EW sector[4]. In $V_{\text{mass}}^{\text{C}}$ we again neglected a constant contribution.

[4]Note that while [53] uses Eq. (3.78a) with $\mathcal{M}_\psi \leftrightarrow \mathcal{M}_\psi^\dagger$, this does not change the result as $\mathcal{M}_\psi$ is hermitian.

3.4.3 Top Couplings

A third source of explicit symmetry breaking are the interactions of the top partners with the elementary quarks, schematically[5]

$$\mathcal{L}_{\text{mix}} \sim -\lambda_L \mathcal{O}_F \zeta_L - \lambda_R \mathcal{O}_F \zeta_R^c + \text{h.c.}\,, \tag{3.79}$$

because the SM quarks are embedded into incomplete multiplets ζ_L, ζ_R^c.

Since $\mathcal{O}_F \in (\mathbf{5}, \mathbf{15})_{\mathcal{G}}$, the spurions $\Xi_{L,R}$ must be in the $(\bar{\mathbf{5}}, \overline{\mathbf{15}})_{\mathcal{G}}$ irrep. As with the gauge spurions, we define a set of projectors by

$$\Xi_L = q^\alpha_{L,i} \mathcal{P}^\alpha_{L,i}, \qquad \Xi_R = t^c_{R,i} \mathcal{P}_{R,i}, \tag{3.80}$$

where α and i are $\text{SU}(2)_L$ and $\text{SU}(3)_c$ indices, respectively. The projectors factorize into an EW ($\hat{P}$) and a colored (P) part,

$$\mathcal{P}_L = \lambda_L \hat{P}_L \otimes P_L \in (\bar{\mathbf{5}}, \overline{\mathbf{15}}; \bar{\mathbf{3}}, \bar{\mathbf{2}}, -\tfrac{1}{6}) \quad \leftrightarrow \quad \mathcal{P}^{\alpha i}_{L,IMN} = \lambda_L \hat{P}^\alpha_{L,I} P^i_{L,MN}, \tag{3.81a}$$

$$\mathcal{P}_R = \lambda_R \hat{P}_R \otimes P_R \in (\bar{\mathbf{5}}, \overline{\mathbf{15}}; \mathbf{3}, \mathbf{1}, \tfrac{2}{3}) \quad \leftrightarrow \quad \mathcal{P}^{i}_{R,IMN} = \lambda_R \hat{P}_{R,I} P^i_{R,MN}, \tag{3.81b}$$

which means that we can construct invariants separately in the EW and color sectors. From Eqs. (3.52) and (3.53) we read off the projectors as

$$\hat{P}_L = \begin{pmatrix} 0 & 0 & 1 & 0 & 0 \\ 0 & 0 & 0 & 1 & 0 \end{pmatrix}, \qquad \hat{P}_R = \begin{pmatrix} 0 & 0 & 0 & 0 & -\text{i} \end{pmatrix} \tag{3.82}$$

and

$$P^i_L = \begin{pmatrix} \kappa_i & 0 \\ 0 & 0 \end{pmatrix}, \qquad P^i_R = \begin{pmatrix} 0 & 0 \\ 0 & \kappa_i \end{pmatrix}, \qquad \kappa_{i,jk} = \frac{1}{2}\epsilon_{ijk}. \tag{3.83}$$

We construct the operators contributing to the pNGB potential by forming singlets out of the $\mathcal{P}_{L,R}$ and the $\Sigma_{\psi,\chi}$. Since the spurions only count as $\mathcal{O}(\sqrt{p})$ in the chiral expansion [56], the operators up to $\mathcal{O}(p^2)$ contain two or four spurions, which allows for a lot more independent operators than for the gauge and mass terms.

EW sector We demonstrate our method for classifying the operators in detail for the EW sector, following the approach of [53, 56]. We start by ignoring the SM quantum numbers and only looking for invariants under the global SU(5). To simplify the notation, we write $\hat{P}_{L/R} \to \hat{P}$, $\Sigma_\psi \to \Sigma$ for now. Under $g \in \text{SU}(5)$,

$$\hat{P} \to g^* \hat{P}, \quad \hat{P}^\dagger \to \hat{P}^\dagger g^T, \quad \Sigma \to g \Sigma g^T, \quad \Sigma^\dagger \to g^* \Sigma^\dagger g^\dagger, \tag{3.84}$$

and we recall that $\Sigma^T = \Sigma$. Now, the idea is to construct operators transforming like an adjoint $X \to g X g^\dagger$ or quasi-adjoint $X \to g^* X g^T$, so that $\text{Tr}(X)$ is invariant under SU(5). To this end, we form Kronecker products of $P^{(*)}$ with $P^{T,\dagger}$ and combine them with $\Sigma^{(\dagger)}$ in Tab. 3.2. There are no further classes like $\Sigma\Sigma PP$ since Σ is unitary. In each class there are two operators transforming like a (quasi-)adjoint. However, using $\text{Tr}(XY) = \text{Tr}(YX) = \text{Tr}\big((XY)^T\big)$, we identify only three algebraically independent operators after taking the trace,

$$O_1 = \text{Tr}\Big(\hat{P}\hat{P}^\dagger\Big) = \hat{P}^\dagger \hat{P}, \qquad O_2 = \text{Tr}\Big(\hat{P}^* \hat{P}^\dagger \Sigma^\dagger\Big), \qquad O_3 = \text{Tr}\Big(\Sigma \hat{P} \hat{P}^T\Big). \tag{3.85}$$

[5] The implications of the separation of $\mathcal{O}_F$ into $\mathcal{O}_{14}$ and $\mathcal{O}_1$ are discussed in Appendix A.

$X \to gXg^\dagger$	$X \to gXg^T$	$X \to g^*Xg^T$	$X \to g^*Xg^\dagger$	Class
$\hat{P}^*\hat{P}^T$	$\hat{P}^*\hat{P}^\dagger$	$\hat{P}\hat{P}^\dagger$	$\hat{P}\hat{P}^T$	PP
$\Sigma\hat{P}\hat{P}^T$	$\Sigma\hat{P}\hat{P}^\dagger$	$\Sigma^\dagger\hat{P}^*\hat{P}^\dagger$	$\Sigma^\dagger\hat{P}^*\hat{P}^T$	ΣPP
$\hat{P}^*\hat{P}^\dagger\Sigma^\dagger$	$\hat{P}^*\hat{P}^T\Sigma$	$\hat{P}\hat{P}^T\Sigma$	$\hat{P}\hat{P}^\dagger\Sigma^\dagger$	$PP\Sigma$
$\Sigma\hat{P}\hat{P}^\dagger\Sigma^\dagger$	$\Sigma\hat{P}\hat{P}^T\Sigma$	$\Sigma^\dagger\hat{P}^*\hat{P}^T\Sigma$	$\Sigma^\dagger P^*P^\dagger\Sigma^\dagger$	$\Sigma PP\Sigma$

Table 3.2: All combinations of two EW spurions $\hat{P}$ in the anti-fundamental representation and the pNGB matrix, as well as their transformation under $g \in \mathrm{SU}(5)$. $\mathrm{Tr}(X)$ is SU(5) invariant for the first and third columns.

The last two are related by complex conjugation,

$$O_2^* = \mathrm{Tr}\Big(\hat{P}^*\hat{P}^\dagger\Sigma^\dagger\Big)^* = \mathrm{Tr}\Big((\hat{P}^*\hat{P}^\dagger\Sigma^\dagger)^\dagger\Big) = \mathrm{Tr}\Big(\Sigma\hat{P}\hat{P}^T\Big) = O_3. \tag{3.86}$$

Next, we construct the operators with four spurions. To simplify the classification, we note that an operator can only be SM invariant if it contains an equal number of $P^{(T)}$ and conjugates $P^{*,\dagger}$. Thus, we already impose this constraint instead of determining all SU(5) invariants first. The unique operator with no Σ insertions is the square of O_1,

$$O_4 = (O_1)^2 = \Big(\hat{P}^\dagger\hat{P}\Big)^2. \tag{3.87}$$

With one Σ, no SM invariants can be built, while there is one operator with two Σ,

$$O_5 = \mathrm{Tr}\Big(\Sigma\hat{P}\hat{P}^\dagger\Sigma^\dagger\hat{P}^*\hat{P}^T\Big). \tag{3.88}$$

By rewriting the trace in index notation,

$$O_5 = \Sigma_{IJ}\hat{P}_J\hat{P}_K^*\Sigma_{KL}^\dagger\hat{P}_L^*\hat{P}_I = \Big(\Sigma_{IJ}\hat{P}_J\hat{P}_I\Big)\Big(\Sigma_{KL}^\dagger\hat{P}_L^*\hat{P}_K^*\Big) \tag{3.89a}$$

$$= \mathrm{Tr}\Big(\Sigma\hat{P}\hat{P}^T\Big)\,\mathrm{Tr}\Big(\hat{P}^*\hat{P}^\dagger\Sigma^\dagger\Big) = O_3O_2, \tag{3.89b}$$

we see that it can also be built out of two-spurion operators.

Now we construct SM invariants from the SU(5) invariant building blocks. We have two projectors, $\hat{P}_L^\alpha \in \bar{\mathbf{2}}_{-1/6}$ and $\hat{P}_R \in \mathbf{1}_{2/3}$, which always have to appear in pairs of the form $\hat{P}_X^*\hat{P}_X$ with $X = L, R$. At $\mathcal{O}(p)$ (i.e. two spurions), there are only two operators,

$$O_L^{\mathrm{EW}} = \hat{P}_L^{\alpha\dagger}\hat{P}_L^\alpha = 2, \qquad O_R^{\mathrm{EW}} = \hat{P}_R^\dagger\hat{P}_R = 1. \tag{3.90}$$

Note that we cannot disregard the constant operators at this stage as they still get multiplied with a color sector operator which might be non-trivial. At $\mathcal{O}(p^2)$, we have O_4 and O_5 with appropriate index contractions. Schematically, the spurions can be chosen as LL, RR and LR, where each letter stands for a pair of spurions. The constant O_4 can be built as

$$O_{LL,1}^{\mathrm{EW}} = \Big(\hat{P}_L^{\alpha\dagger}\hat{P}_L^\alpha\Big)^2 = 4, \quad O_{RR,1}^{\mathrm{EW}} = \Big(\hat{P}_R^\dagger\hat{P}_R\Big)^2 = 1, \quad O_{LR,1}^{\mathrm{EW}} = \hat{P}_L^{\alpha\dagger}\hat{P}_L^\alpha\hat{P}_R^\dagger\hat{P}_R = 2. \tag{3.91}$$

For $O_5 = O_2 O_3$, we find the following hermitian operators,

$$O^{\text{EW}}_{LL,2} = \text{Tr}\Big(\hat{P}^{\alpha *}_L \hat{P}^{\beta\dagger}_L \Sigma^\dagger_\psi\Big)\,\text{Tr}\Big(\Sigma_\psi \hat{P}^{\alpha}_L \hat{P}^{\beta T}_L\Big) = s^4_\theta - 4 s^2_\theta c_\theta \frac{\eta^0_3}{f_\psi} + 4 s^3_\theta c_\theta \frac{h}{f_\psi} + \mathcal{O}(\Pi^2_\psi), \tag{3.92a}$$

$$O^{\text{EW}}_{RR,2} = \text{Tr}\Big(\hat{P}^{*}_R \hat{P}^{\dagger}_R \Sigma^\dagger_\psi\Big)\,\text{Tr}\Big(\Sigma_\psi \hat{P}_R \hat{P}^{T}_R\Big) = c^2_{2\theta} - 2 s_{4\theta} \frac{h}{f_\psi} + \mathcal{O}(\Pi^2_\psi), \tag{3.92b}$$

$$O^{\text{EW}}_{LR,2} = \text{Tr}\Big(P^{\alpha *}_L P^{\dagger}_R \Sigma^\dagger_\psi\Big)\,\text{Tr}\big(\Sigma_\psi P_{L,\alpha} P^T_R\big) = \frac{1}{2} s^2_{2\theta} + 2 s_\theta s_{2\theta} \frac{\eta^0_3}{f_\psi} + s_{4\theta} \frac{h}{f_\psi} + \mathcal{O}(\Pi^2_\psi). \tag{3.92c}$$

This classification is in agreement with [56]. The potentially problematic tadpoles of η^0_3 are addressed in Section 3.4.4.

Color Sector The classification of the color sector operators proceeds analogously to the EW sector. The spurion $P \in \overline{\mathbf{15}}_{\text{SU(6)}}$ and the pNGB matrix $\Sigma \in \mathbf{15}_{\text{SU(6)}}$ are both antisymmetric and transform as

$$P \to g^* P g^\dagger, \quad P^\dagger \to g P^\dagger g^T, \quad \Sigma \to g \Sigma g^T, \quad \Sigma^\dagger \to g^* \Sigma^\dagger g^\dagger \tag{3.93}$$

with $g \in \text{SU(6)}$. There are six building blocks,

$$X \to g^* X g^T: \qquad P P^\dagger, \quad P\Sigma, \quad \Sigma^\dagger P^\dagger, \tag{3.94a}$$

$$X \to g X g^\dagger: \qquad P^\dagger P, \quad P^\dagger \Sigma^\dagger, \quad \Sigma P, \tag{3.94b}$$

out of which we construct the SU(6) invariant traces in Tab. 3.3. Turning to SM invariance, there are four color singlet combinations of the spurions $P_L \in \overline{\mathbf{3}}$ and $P_R \in \mathbf{3}$,

$$P^i_L P^{i\dagger}_L, \quad P^i_R P^{i\dagger}_R, \quad P^i_L P^i_R, \quad P^{i\dagger}_L P^{i\dagger}_R. \tag{3.95}$$

However, each operator must have an even number of left- and right-handed spurions. Otherwise the corresponding EW operator would be in the $\mathbf{2}\times\mathbf{2}\times\mathbf{2}\times\mathbf{1}$ or $\mathbf{2}\times\mathbf{1}\times\mathbf{1}\times\mathbf{1}$ of SU(2)_L, neither of which contain a singlet. Thus, contractions of the form $P^i_L P^{i\dagger}_L P^j_L P^j_R$ are not possible even though they are color singlets. Furthermore, to match the EW operators, the projectors must occur in pairs $P^*_X P_X$ with $X = L, R$. Still, there is a large number of color sector operators at $\mathcal{O}(p^2)$, many of which do not contribute to the pNGB masses. We therefore relegate the complete list of operators to Appendix A, where we also argue the completeness of the classification, and show only those with a $\mathcal{O}(\Pi^2_\chi)$ contribution in Tab. 3.4.

Number of spurions	Traces
$1P$	$\text{Tr}(P\Sigma)$, $\text{Tr}\big(P^\dagger\Sigma^\dagger\big)$
$2P$	$\text{Tr}\big(P^\dagger P\big)$, $\text{Tr}(P\Sigma P\Sigma)$, $\text{Tr}\big(P^\dagger\Sigma^\dagger P^\dagger\Sigma^\dagger\big)$
$3P$	$\text{Tr}\big(PP^\dagger P\Sigma\big)$, $\text{Tr}\big(PP^\dagger\Sigma^\dagger P^\dagger\big)$
$4P$	$\text{Tr}\big(PP^\dagger PP^\dagger\big)$, $\text{Tr}\big(PP^\dagger P\Sigma P\Sigma\big)$, $\text{Tr}\big(PP^\dagger\Sigma^\dagger P^\dagger\Sigma^\dagger P^\dagger\big)$, $\text{Tr}\big(PP^\dagger\Sigma^\dagger P^\dagger P\Sigma\big)$

Table 3.3: SU(6) invariants with up to four spurions P in the antisymmetric $\overline{\mathbf{15}}$.

Name	Operator	Contribution to pNGB mass
$O^{\mathrm{C}}_{L,1}$	$\mathrm{Tr}(P^i_L\Sigma_\chi)\,\mathrm{Tr}\Big(P^{i\dagger}_L\Sigma^\dagger_\chi\Big)$	$\pi_3^\dagger\pi_3/(4f_\chi^2)$
$O^{\mathrm{C}}_{R,1}$	$\mathrm{Tr}(P^i_R\Sigma_\chi)\,\mathrm{Tr}\Big(P^{i\dagger}_R\Sigma^\dagger_\chi\Big)$	$\pi_3^\dagger\pi_3/(4f_\chi^2)$
$O^{\mathrm{C}}_{LL,2}$	$\mathrm{Tr}(P^i_L\Sigma_\chi)\,\mathrm{Tr}\Big(P^{i\dagger}_L\Sigma^\dagger_\chi\Big)\,\mathrm{Tr}\Big(P^{j\dagger}_L P^j_L\Big)$	$3\pi_3^\dagger\pi_3/(8f_\chi^2)$
$O^{\mathrm{C}}_{LL,3}$	$\mathrm{Tr}(P^i_L\Sigma_\chi)\,\mathrm{Tr}\Big(P^{j\dagger}_L\Sigma^\dagger_\chi\Big)\,\mathrm{Tr}\Big(P^{j\dagger}_L P^i_L\Big)+\mathrm{h.c.}$	$\pi_3^\dagger\pi_3/(8f_\chi^2)$
$O^{\mathrm{C}}_{LL,8}$	$\mathrm{Tr}(P^i_L\Sigma_\chi)\,\mathrm{Tr}\Big(P^j_L P^{j\dagger}_L\Sigma^\dagger_\chi P^{i\dagger}_L\Big)+\mathrm{h.c.}$	$\pi_3^\dagger\pi_3/(8f_\chi^2)$
$O^{\mathrm{C}}_{LL,10}$	$\mathrm{Tr}\Big(P^i_L P^{i\dagger}_L\Sigma^\dagger_\chi P^{j\dagger}_L P^j_L\Sigma_\chi\Big)$	$\pi_3^\dagger\pi_3/(8f_\chi^2)$
$O^{\mathrm{C}}_{LR,3}$	$\mathrm{Tr}(P^i_L\Sigma_\chi)\,\mathrm{Tr}\Big(P^{i\dagger}_L\Sigma^\dagger_\chi\Big)\,\mathrm{Tr}\Big(P^{j\dagger}_R P^j_R\Big)$	$3\pi_3^\dagger\pi_3/(8f_\chi^2)$
$O^{\mathrm{C}}_{LR,4}$	$\mathrm{Tr}(P^i_R\Sigma_\chi)\,\mathrm{Tr}\Big(P^{i\dagger}_R\Sigma^\dagger_\chi\Big)\,\mathrm{Tr}\Big(P^{j\dagger}_L P^j_L\Big)$	$3\pi_3^\dagger\pi_3/(8f_\chi^2)$
$O^{\mathrm{C}}_{LR,7}$	$\mathrm{Tr}(P^i_L\Sigma_\chi)\,\mathrm{Tr}(P^i_R\Sigma_\chi)\,\mathrm{Tr}\Big(P^{j\dagger}_L\Sigma^\dagger_\chi P^{j\dagger}_R\Sigma^\dagger_\chi\Big)+\mathrm{h.c.}$	$-3\pi_3^\dagger\pi_3/(8f_\chi^2)$
$O^{\mathrm{C}}_{LR,8}$	$\mathrm{Tr}(P^i_L\Sigma_\chi)\,\mathrm{Tr}\big(P^j_R\Sigma_\chi\big)\,\mathrm{Tr}\Big(P^{i\dagger}_L\Sigma^\dagger_\chi P^{j\dagger}_R\Sigma^\dagger_\chi\Big)+\mathrm{h.c.}$	$-\pi_3^\dagger\pi_3/(8f_\chi^2)$
$O^{\mathrm{C}}_{LR,13}$	$\mathrm{Tr}(P^i_L\Sigma P^i_R\Sigma)\,\mathrm{Tr}\Big(P^{j\dagger}_L\Sigma^\dagger_\chi P^{j\dagger}_R\Sigma^\dagger_\chi\Big)$	$-(3\pi_8^a\pi_8^a+12\pi_3^\dagger\pi_3)/(16f_\chi^2)$
$O^{\mathrm{C}}_{LR,14}$	$\mathrm{Tr}\big(P^i_L\Sigma P^j_R\Sigma\big)\,\mathrm{Tr}\Big(P^{i\dagger}_L\Sigma^\dagger_\chi P^{j\dagger}_R\Sigma^\dagger_\chi\Big)$	$-\pi_3^\dagger\pi_3/(4f_\chi^2)$
$O^{\mathrm{C}}_{LR,21}$	$\mathrm{Tr}\Big(P^i_L P^{i\dagger}_L\Sigma^\dagger_\chi P^{j\dagger}_R P^j_R\Sigma_\chi\Big)$	$-\pi_3^\dagger\pi_3/(8f_\chi^2)$
$O^{\mathrm{C}}_{LR,22}$	$\mathrm{Tr}\Big(P^i_L P^{j\dagger}_L\Sigma^\dagger_\chi P^{j\dagger}_R P^i_R\Sigma_\chi\Big)$	$-(3\pi_8^a\pi_8^a+8\pi_3^\dagger\pi_3)/(64f_\chi^2)$

Table 3.4: Color singlet operators with up to four spurions $P_L \in \bar{\mathbf{3}}$ or $P_R \in \mathbf{3}$. We show only those operators that contribute to the masses of the colored pNGBs. Additionally, there are RR operators identical to the second panel with $L \to R$.

Combination The operators in the pNGB potential are built from $\mathcal{P}_{L,R}$ and can schematically be written as

$$\mathcal{O}_L = \mathcal{P}_L^\dagger\mathcal{P}_L = \lambda_L^2(\hat{P}_L^\dagger\hat{P}_L)(P_L^\dagger P_L) = \lambda_L^2 O_L^{\mathrm{EW}} O_L^{\mathrm{C}}, \tag{3.96a}$$

$$\mathcal{O}_{LL} = \mathcal{P}_L^\dagger\mathcal{P}_L\mathcal{P}_L^\dagger\mathcal{P}_L = \lambda_L^4(\hat{P}_L^\dagger\hat{P}_L\hat{P}_L^\dagger\hat{P}_L)(P_L^\dagger P_L P_L^\dagger P_L) = \lambda_L^4 O_{LL}^{\mathrm{EW}} O_{LL}^{\mathrm{C}}, \tag{3.96b}$$

$$\mathcal{O}_{LR} = \mathcal{P}_L^\dagger\mathcal{P}_L\mathcal{P}_R^\dagger\mathcal{P}_R = \lambda_L^2\lambda_R^2(\hat{P}_L^\dagger\hat{P}_L\hat{P}_R^\dagger\hat{P}_R)(P_L^\dagger P_L P_R^\dagger P_R) = \lambda_L^2\lambda_R^2 O_{LR}^{\mathrm{EW}} O_{LR}^{\mathrm{C}}, \tag{3.96c}$$

with analogous expressions for $\mathcal{O}_R, \mathcal{O}_{RR}$. The parentheses represent appropriate index contractions and potential insertions of $\Sigma_{\psi,\chi}$. We have to take into account all combinations of EW and color sector operators. At $\mathcal{O}(p)$, there are only two non-trivial operators,

$$\mathcal{O}_L = \lambda_L^2 O_L^{\mathrm{EW}} O_{L,1}^{\mathrm{C}} = 2\lambda_L^2\frac{\pi_3^\dagger\pi_3}{f_\chi^2} + \mathcal{O}(\Pi_\chi^3), \qquad \mathcal{O}_R = \lambda_R^2 O_R^{\mathrm{EW}} O_{R,1}^{\mathrm{C}} = \lambda_R^2\frac{\pi_3^\dagger\pi_3}{f_\chi^2} + \mathcal{O}(\Pi_\chi^3). \tag{3.97}$$

For the four-spurion operators however, 8 LL, 8 RR and 16 LR combinations can be built from Eqs. (3.91), (3.92) and Tab. 3.4. In general form, the top contribution to the pNGB potential

reads [53]

$$V_{\text{top}} = \frac{f_\chi^4}{4\pi}(C_L\mathcal{O}_L + C_R\mathcal{O}_R) + \frac{f_\chi^4}{(4\pi)^2}\sum_n (C_{LL,n}\mathcal{O}_{LL,n} + C_{RR,n}\mathcal{O}_{RR,n}) + \frac{f_\chi^4}{(4\pi)^2}\sum_n C_{LR,n}\mathcal{O}_{LR,n}, \tag{3.98}$$

where the inclusion of the hermitian conjugate for complex operators is understood and the factors of 4π follow from naive dimensional analysis [58, 59].

3.4.4 Discussion

The masses of the colored pNGBs can now be read off from $V^{\text{C}}_{\text{gauge}}$, $V^{\text{C}}_{\text{mass}}$ and V_{top}. First, we can slightly reduce the complexity of V_{top} by using $\theta \ll 1$, which means that $O^{\text{EW}}_{LL,2}$ and $O^{\text{EW}}_{LR,2}$ can safely be ignored and we may set $c^2_{2\theta} \approx 1$ in $O^{\text{EW}}_{RR,2}$. This leaves four low-energy constants in the mass of π_8,

$$m^2_{\pi_8} = \frac{3}{4}C'_g f_\chi^2 g_s^2 + C'_m \mu_\chi f_\chi - \frac{\lambda_L^2\lambda_R^2 f_\chi^2}{(4\pi)^2}\left(\frac{3}{4}C^{1,13}_{LR} + \frac{3}{16}C^{1,22}_{LR}\right). \tag{3.99}$$

Here, we label the coefficients in V_{top} with the indices of the EW and color sector operators, e.g. $C^{1,13}_{LR}$ is the coefficient of $\lambda_L^2\lambda_R^2 O^{\text{EW}}_{LR,1}O^{\text{C}}_{LR,13}$. The triplet mass is given by

$$\begin{aligned} m^2_{\pi_3} = {} & C'_g f_\chi^2\left(\frac{1}{3}g_s^2 + \frac{2}{9}g'^2\right) + C'_m\mu_\chi f_\chi + \frac{f_\chi^2}{4\pi}\left(\frac{1}{2}\lambda_L^2 C_L + \frac{1}{4}\lambda_R^2 C_R\right) \\ & + \frac{\lambda_L^4 f_\chi^2}{(4\pi)^2}\left(\frac{3}{2}C^{1,2}_{LL} + C^{1,3}_{LL} + C^{1,8}_{LL} + \frac{1}{2}C^{1,10}_{LL}\right) \\ & + \frac{\lambda_R^4 f_\chi^2}{(4\pi)^2}\left(\frac{3}{8}C^{1,2}_{RR} + \frac{1}{4}C^{1,3}_{RR} + \frac{1}{4}C^{1,8}_{RR} + \frac{1}{8}C^{1,10}_{RR} + \frac{3}{8}C^{2,2}_{RR} + \frac{1}{4}C^{2,3}_{RR} + \frac{1}{4}C^{2,8}_{RR} + \frac{1}{8}C^{2,10}_{RR}\right) \\ & + \frac{\lambda_L^2\lambda_R^2 f_\chi^2}{(4\pi)^2}\left(\frac{3}{4}C^{1,3}_{LR} + \frac{3}{4}C^{1,4}_{LR} - \frac{3}{2}C^{1,7}_{LR} - \frac{1}{2}C^{1,8}_{LR} - \frac{3}{2}C^{1,13}_{LR} - \frac{1}{2}C^{1,14}_{LR} - \frac{1}{4}C^{1,21}_{LR} - \frac{1}{4}C^{1,22}_{LR}\right). \end{aligned} \tag{3.100}$$

Note that the contributions from complex operators receive a factor of 2 from the hermitian conjugate since the coefficients are real. The overall mass scale is set by the condensation scale f_χ and the mass of the hyperquarks μ_χ.

Our goal with this calculation was to gain insight into the mass hierarchy of π_8 and π_3. Unfortunately, this is not possible with such a large number of unknown coefficients. One might argue that the next-to-leading order (NLO) operators from the top sector can be neglected since they are suppressed by $\lambda^2_{L,R}/4\pi$ compared to the LO term. In this case, the mass splitting is

$$m^2_{\pi_3} - m^2_{\pi_8} \simeq C'_g f_\chi^2\left(-\frac{5}{12}g_s^2 + \frac{2}{9}g'^2\right) + \frac{f_\chi^2}{4\pi}\left(\frac{1}{2}\lambda_L^2 C_L + \frac{1}{4}\lambda_R^2 C_R\right). \tag{3.101}$$

The gauge terms on their own imply a heavier π_8. All in all however, the hierarchy depends on the relative sizes of the gauge and top contribution, as well as the signs of $C_{L,R}$, which are a priori unknown. This last fact also poses a problem for the approximation in Eq. (3.101): It implicitly assumes that the signs of the NLO coefficients are roughly evenly distributed. But if

they instead mostly align, the sheer number of NLO operators can be enough to overcome the suppression, making them a relevant contribution again. To summarize, without lattice data on the LECs we cannot determine whether π_8 or π_3 are heavier.

Our classification can be used as a starting point for an analysis of the scalar potential of the EW pNGBs. Firstly, their masses can be calculated analogously to the Π_χ. To this end, the $\mathcal{O}(\Pi_\psi^2)$ contribution to the EW sector operators has to be determined. Apart from that, the results of Section 3.4.3 can be straightforwardly applied. The lower number of EW sector operators significantly reduces the number of independent parameters for the masses. Furthermore, by minimizing $V(\theta)$ with the pNGBs set to 0, the misalignment angle θ can be expressed in terms of LECs. Finally, the linear order of two EW operators in Eq. (3.92) includes tadpoles of η_3^0. These are problematic as they induce a vev for the η_3 triplet that breaks the custodial symmetry [53]. The coefficients of the potential must therefore be chosen to cancel these tadpoles. By imposing the mass relations, the minimization of the potential and the vanishing tadpoles, the freedom in the parameter space of the EW potential may be significantly reduced.

4 | LHC Phenomenology of Gluonis

Due to its large particle content, the model M5 offers a rich phenomenology. Besides the partners for the third generation quarks required for a partially composite top quark, there are additional fermionic resonances in the **8** (gluonis) and the **1** (higgsonis and boni) of $\mathrm{SU}(3)_c$, which are named in analogy to supersymmetric particles with the same quantum numbers. In this chapter we explore the phenomenology of these exotic top partners, focusing on the gluonis as they have the largest production cross section at the LHC, and investigate to which extent current LHC data constrains the parameter space. After determining the possible decay channels for the BSM particles we formulate simplified models for different scenarios. We then implement these in the Universal FeynRules Output (UFO) format [60] to simulate events with a Monte Carlo generator. By comparing the simulation results with recasted ATLAS and CMS searches, we derive bounds on the masses of the new particles.

4.1 Phenomenological Considerations

We start by discussing how gluonis can be produced at the LHC. Then we derive their decay channels and formulate appropriate simplified models.

4.1.1 Gluoni Pair Production

The cross section for pair production of gluonis at the LHC is dominated by QCD pair production. At tree level, the hard scattering processes are

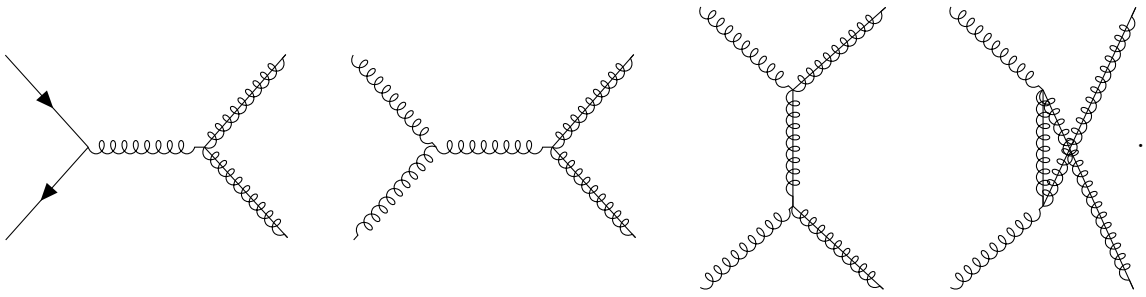

. (4.1)

From the partonic processes, the total production cross section is obtained by convolving the hard cross section $\hat{\sigma}$ with the corresponding parton distribution functions (PDFs),

$$\sigma(pp \to Q_8 Q_8) = \sum_i \int \mathrm{d}x_1 \mathrm{d}x_2 \, f_{i/p}(x_1, \mu_F^2) f_{\bar{i}/p}(x_2, \mu_F^2) \hat{\sigma}(i\bar{i} \to Q_8 Q_8; x_1 x_2 s), \tag{4.2}$$

where we write Q_8 as a collective symbol for the Dirac gluonis $\tilde{G}^{\pm,0}$ and the Majorana $\tilde{g}$, i runs over the partons and $f_{i/p}(x, \mu_F^2)$ is the PDF of i in the proton with momentum fraction x and

factorization scale μ_F. In practice, the pair production is dominated by gg because the LHC is "essentially a gluon-gluon collider" [61] in the sense that the large gluon PDF dominates the production cross section.

The Dirac gluonis $\tilde{G}^{\pm,0}$ originate from a $\mathrm{SU}(2)_L$ doublet, so they couple to EW gauge bosons. Thus, EW production via Drell-Yan is also possible,

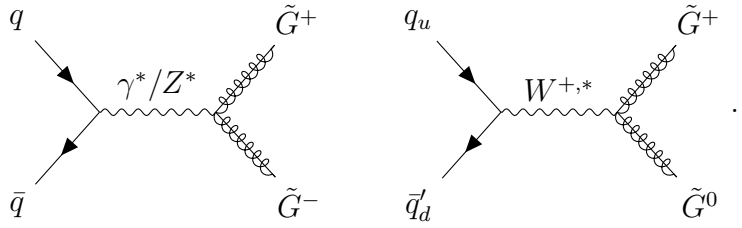

. (4.3)

However, for most of the phase space the EW production represents only a small correction to the QCD production, which is dominant because of the larger coupling constant α_s and the presence of color factors. Therefore, we only consider QCD pair production in the following.

We finally comment on the expected size of the cross section. The production cross section of color octets is enhanced by large color factors. For example,

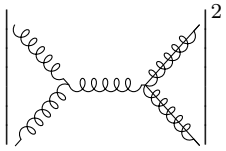
$$\propto (f^{aa'c}f^{bb'c})(f^{aa'd}f^{bb'd})^* = N_c^2(N_c^2-1) = 72, \tag{4.4}$$

whereas for a color triplet top partner,

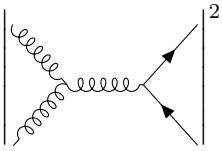
$$\propto (f^{aa'c}T^c_{ij})(f^{aa'd}T^d_{ij})^* = \frac{1}{2}N_c(N_c^2-1) = 12. \tag{4.5}$$

This remains qualitatively true when higher orders are taken into account: At $\sqrt{s} = 13$ TeV and $m = 1.5$ TeV, for example,

$$\sigma(pp \to \tilde{g}\tilde{g}) = (15.7 \pm 2.4)\ \text{fb}, \qquad \sigma(pp \to T\bar{T}) = (2.0 \pm 0.2)\ \text{fb}, \tag{4.6}$$

where the calculation was performed to $\mathrm{NNLO}_{\mathrm{approx}}$+NNLL for the gluoni [62] and to NNLO for the triplet top partner [63, 64]. The fact that such detailed calculations are available for gluonis is thanks to their similarity to the gluino in SUSY. The LHC SUSY Cross Section Working Group has published cross sections for gluino pair production at the LHC with squarks decoupled [62, 65], which is the same process as pair production of the Majorana gluonis in M5. For $\tilde{G}^{\pm,0}$, we have to take into account the Dirac nature, $\sigma_{\tilde{G}} = 2\sigma_{\tilde{g}}$. This neglects EW contributions, but they are small corrections as explained above.

4.1.2 Decay Channels

We now derive the decay channels of the gluonis. As a first step, we reduce the number of free parameters by defining a few common mass scales. As we have seen in Section 3.4, the colored pNGBs are in general not mass degenerate, $m_{\pi_8} \neq m_{\pi_3}$. However, we take the top partners within the same color representation to be degenerate with masses m_8, m_3 and m_1 for

the color octets, triplets and singlets, respectively. In fact, as they both emerge from $\mathbf{14}_{\mathrm{Sp}(6)}$, we can expect $m_8 \approx m_3$. To allow for on-shell decays, we assume that the gluonis are the heaviest particles in the model. Also, we require the decays to respect the parity identified in Eq. (3.64), so the lightest of the odd particles is stable. An AdS/QCD study suggests that the color singlets might be the lightest BSM particles [26, 66]. In the following, we assume that this is the case. The phenomenology depends strongly on this assumption. In Chapter 5, we discuss how the results would change if the pNGBs were the lightest particles instead.

Next, we determine which couplings are allowed by symmetry, considering only two-body decays. Starting with $\mathrm{SU}(3)_c$, there are three combinations of color representations with at least one octet that can occur in the Lagrangian,

$$\mathbf{8} \times \mathbf{8} \times \mathbf{8} \ni \mathbf{1}, \qquad \mathbf{8} \times \mathbf{8} \times \mathbf{1} \ni \mathbf{1}, \qquad \mathbf{8} \times \mathbf{3} \times \bar{\mathbf{3}} \ni \mathbf{1}. \tag{4.7}$$

To satisfy Lorentz invariance, the gluoni has to decay into one fermion and either a scalar or a vector. This rules out the three-octet vertex and fixes the second $\mathbf{8}$ in $\mathbf{8} \times \mathbf{8} \times \mathbf{1}$ to be the sgluon or gluon, since all octet fermions have the same mass. Matching the electric charges leaves the following decay channels,

$$\tilde{G}^+ \to \pi_8 \tilde{h}^+,\ \pi_8 l^+,\ g\tilde{h}^+,\ \pi_3^* X_{5/3},\ \pi_3 \bar{B},\ \pi_3 \bar{q}_d, \tag{4.8a}$$

$$\tilde{G}^0, \tilde{g} \to \pi_8 \tilde{h}^0,\ \pi_8 \tilde{B},\ \pi_8 \nu,\ g\tilde{h}^0,\ g\tilde{B},\ \pi_3 \bar{T}_i,\ \pi_3 \bar{q}_u, \tag{4.8b}$$

and it is understood that the charge conjugate decays of the Majorana gluonis are also allowed. We should also take into account the $\mathrm{SU}(2)_L$ representations before EWSB. $\tilde{G}^0$ and $\tilde{h}^0$ emerge from doublets, while the Majoranas $\tilde{g}$ and $\tilde{B}$ are EW singlets. Thus, only $\tilde{G}^0$ decays to a higgsoni and only $\tilde{g}$ to a boni. More precisely, the mass eigenstates are actually linear combinations of the neutral states, which also allows for $\tilde{G}^0 \to \pi_8 \tilde{B}$ and $\tilde{g} \to \pi_8 \tilde{h}^0$. But these interactions are proportional to a mixing angle $\sin 2\alpha$, which we assume to be small. The decays into π_8 and l^+, ν do not occur as they are forbidden by the parity Eq. (3.64).

This is as far as symmetry arguments will lead us and we turn to the Lagrangian to see if the remaining couplings actually occur. The elementary-composite interactions in Eq. (3.58) include couplings of the gluonis to the stop and only third generation quarks, so we can neglect the first two generations. The gluonis do couple to the sgluon and the higgsonis/boni in the derivative couplings in Eq. (3.60). In Eq. (3.62), gluonis also couple to π_3 and VLQs. However, since $m_8 \approx m_3$, the decays to top partners are likely to be kinematically forbidden, so we ignore them in the following. We also neglect the decays to a gluon and color singlet as they are loop-suppressed. This leaves

$$\tilde{G}^+ \to \pi_8 \tilde{h}^+,\ \pi_3 \bar{b}, \tag{4.9a}$$

$$\tilde{G}^0 \to \pi_8 \tilde{h}^0,\ \pi_3 \bar{t}, \tag{4.9b}$$

$$\tilde{g} \to \pi_8 \tilde{B},\ \pi_3 \bar{t},\ \pi_3^* t \tag{4.9c}$$

as the possible decay channels for the gluonis.

Since we assumed that $m_1 < m_{8,3,\pi_3,\pi_8}$, the higgsonis and the boni are stable, which opens the interesting possibility to interpret them as dark matter (DM). However, *dark* matter cannot interact with photons, ruling out $\tilde{h}^+$ as a DM candidate. We can easily fix this by assuming a small mass splitting between $\tilde{h}^+$ and $\tilde{h}^0$, $m_{\tilde{h}^+} = m_{\tilde{h}^0} + \delta m$ with $\delta m \sim 150$ MeV. This allows

$\tilde{h}^+$ to decay to $\tilde{h}^0$ and a pion or two leptons,

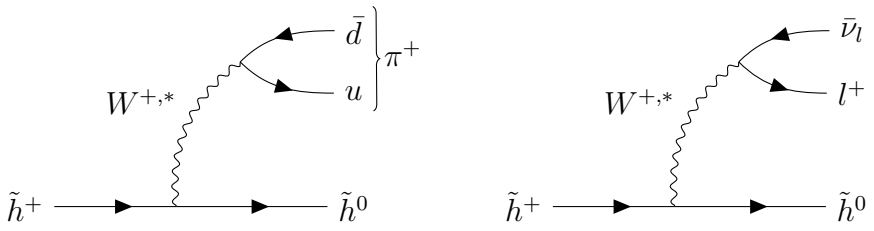

(4.10)

where $l = e, \mu$. Of those, the decay to leptons is phase space suppressed, being a three-body decay, whereas $\tilde{h}^+ \to \tilde{h}^0\pi^+$ is an effective two-body decay. We further take $m_{\tilde{h}^0} = m_{\tilde{B}} + \delta m$, so that $\tilde{h}^0 \to \pi^0\tilde{B}$, leaving us with $\tilde{B}$ as the only DM candidate. The boni does not leave a signature in particle detectors and can only be indirectly observed as missing transverse energy (missing E_T, MET). The pions from the higgsoni decays are very soft, i.e. they have very little kinetic energy. Since the triggers of particle detectors apply cuts on the transverse momentum p_T of at least order GeV, very soft particles are essentially invisible to the detector.

We now turn to the decay channels of the pNGBs, starting with the stop. QCD and charge conservation allow

$$\pi_3 \to \bar{q}_d\bar{q}'_d,\ q_u\nu,\ \tilde{h}^+q_d,\ \tilde{h}^0q_u,\ \tilde{B}q_u. \tag{4.11}$$

We do not consider the first two decays since they violate the parity Eq. (3.64). The couplings to $Q_1 q$ are present for third generation quarks in Eq. (3.58),

$$\pi_3 \to \tilde{h}^+b,\ \tilde{h}^0t,\ t\tilde{B}. \tag{4.12}$$

To simplify the topology of the final states, we assume in the following that $\pi_3 \to t\tilde{B}$ dominates. That is, we assume $\lambda_{R,1} \gg \lambda_{L,1}$ in Eq. (3.55). In practice, this does not require a huge tuning, a relative factor of about 3 is sufficient to ensure that the right-handed coupling dominates.

The sgluon can decay to gg, $g\gamma$ and gZ through the anomalous WZW term Eq. (3.63). The branching ratios are related by

$$\frac{\mathrm{Br}(\pi_8 \to g\gamma)}{\mathrm{Br}(\pi_8 \to gg)} = 0.048, \qquad \frac{\mathrm{Br}(\pi_8 \to gZ)}{\mathrm{Br}(\pi_8 \to gg)} = 0.014, \tag{4.13}$$

with a mass and renormalization scale of the couplings of 1 TeV [13]. Thus, the dominant diboson decay is into gg and we neglect the $g\gamma$ and gZ decays in the following. Another decay channel can be found in the following terms of the elementary-composite interactions Eq. (3.58),

$$\mathcal{L}_{\mathrm{mix}} \supset \frac{\mathrm{i}\lambda_{L,14}}{\sqrt{2}f_\chi}(T^c\pi_8 t_L + B^c\pi_8 b_L) + \frac{\mathrm{i}\lambda_{R,14}}{\sqrt{2}f_\chi}T'\pi_8 t^c_R + \mathrm{h.c.}\,. \tag{4.14}$$

When transforming to the mass eigenbasis, the VLQs mix with the top and bottom. This allows π_8 to decay into $t\bar{t}$ and $b\bar{b}$. To summarize, the sgluon can decay as

$$\pi_8 \to gg,\ t\bar{t},\ b\bar{b}. \tag{4.15}$$

The branching ratios depend strongly on the coupling constants and the octet mass [13]. However, having two free branching ratios significantly increases the number of scenarios that have to be simulated. Therefore, we assume that the decay $\pi_8 \to b\bar{b}$ is negligible. This is generically not the case, but our results remain quite general, since Eq. (4.15) can be roughly divided into final states with heavy jets ($t\bar{t}$) and light jets (gg, $b\bar{b}$). That is, we can expect the results for $\pi_8 \to b\bar{b}$ to be similar to $\pi_8 \to gg$.

4.1.3 Simplified Models

Based on the phenomenology described in the previous section, we now formulate simplified models as the basis for the simulations, following the guidelines laid out in [67,68]. A simplified model is an extension of the SM by only a few particles and parameters. They are used by experimental collaborations to set limits on processes that occur in various BSM models. A simplified model can be defined by its Lagrangian, or equivalently by listing production cross sections, masses and branching ratios needed to fully characterize it. In the following, we do not show the kinetic terms.

We start with the pNGBs, which only occur as intermediate particles in the gluoni decays,

$$\mathcal{L}_{\text{pNGB}} = \left(\lambda_{\pi_3} \pi_3^\dagger \overline{\tilde{B}} P_R t + \text{h.c.}\right) + \lambda_{tt}\, \text{i}\, \bar{t} \pi_8 \gamma_5 t + \lambda_{gg}\, d^{abc} \epsilon^{\mu\nu\rho\sigma} \pi_8^a G^b_{\mu\nu} G^c_{\rho\sigma}. \tag{4.16}$$

The stop decays to $t\tilde{B}$ with a branching ratio of 100% independent of λ_{π_3}. The coupling is to the right-handed top since $\tilde{B}$ is a $\text{SU}(2)_L$ singlet. The terms for the (pseudo-scalar) sgluon, adapted from [13], leave one free branching ratio $\text{Br}(\pi_8 \to t\bar{t}) = 1 - \text{Br}(\pi_8 \to gg)$. Next, we formulate the decays of higgsonis to the boni,

$$\mathcal{L}_{Q_1} = \lambda_{\tilde{h}W} \overline{\tilde{h}}^+ \not{W}^+ \tilde{h}^0 + \lambda_{\tilde{h}Z} \overline{\tilde{h}}^0 \not{Z} \tilde{B} + \text{h.c.}\,, \tag{4.17}$$

where the off-shell gauge bosons mediate the decays $\tilde{h}^+ \to \tilde{h}^0 + \text{soft}$ and $\tilde{h}^0 \to \tilde{B} + \text{soft}$ with soft pions or leptons. Finally, the underlying Lagrangian of the gluonis can be expressed as

$$\mathcal{L}_{\tilde{g}} = \left(\lambda_1\, \pi_3^\dagger\, \overline{\tilde{g}} P_R t + \lambda_2\, \text{i}\, \overline{\tilde{g}} \pi_8 \gamma_5 \tilde{B} + \text{h.c.}\right) + \mathcal{L}_{\text{pNGB}}, \tag{4.18a}$$

$$\mathcal{L}_{\tilde{G}^+} = \left(\lambda_1\, \pi_3^\dagger\, \overline{\tilde{G}}^{+c} P_L b + \lambda_2\, \text{i}\, \overline{\tilde{G}}^+ \pi_8 \gamma_5 \tilde{h}^+ + \text{h.c.}\right) + \mathcal{L}_{\text{pNGB}} + \mathcal{L}_{Q_1}, \tag{4.18b}$$

$$\mathcal{L}_{\tilde{G}^0} = \left(\lambda_1\, \pi_3^\dagger\, \overline{\tilde{G}}^{0c} P_L t + \lambda_2\, \text{i}\, \overline{\tilde{G}}^0 \pi_8 \gamma_5 \tilde{h}^0 + \text{h.c.}\right) + \mathcal{L}_{\text{pNGB}} + \mathcal{L}_{Q_1}, \tag{4.18c}$$

where ψ^c denotes the charge conjugate of a fermion ψ. The gluonis are characterized by $\text{Br}(Q_8 \to \pi_3 \bar{q}) = 1 - \text{Br}(Q_8 \to \pi_8 Q_1)$.

Note that we wrote the scalar-fermion-fermion couplings as dimension-four operators even though some of them occur as dimension-five derivative couplings in the composite sector Lagrangian. This is only to simplify the notation and does not have any physical effect: In a two-body decay, the momenta of the particles can be expressed in terms of their masses. So while the Feynman rule corresponding to $\lambda \overline{\psi} \gamma^\mu \psi (\partial_\mu \phi)$ depends on the scalar momentum, this can be absorbed into λ for the case of two-body decays.

4.2 Simulation Tools

In this section, we discuss the tools that were used for simulating the production and decays of gluonis as well as determining bounds on the mass scales in the model. The first step was to translate the simplified models from the previous section into a computer-readable form. One possibility is to implement one's model in FeynRules [14] and produce a Universal FeynRules Output (UFO) [60], a collection of Python files that define the particles, parameters and vertices of a model. The UFO is compatible with all common Monte Carlo (MC) event generators.

We did not write a new model from scratch but built on the `eVLQ` implementation [69], which extends the SM [70] by vector-like quarks (VLQs) of charge $5/3, 2/3, -1/3, -4/3$ [71] and color singlet scalars of charge 1 and 0. The implementation is completely general, including all gauge invariant interactions, so that it can be used for many different models by setting the coupling constants of the superfluous vertices to zero. In our implementation, `CHM5`, we extended `eVLQ` to be able to describe our model. To this end, we created copies of existing files where multiple particles have the same quantum numbers (e.g. neutral color singlet scalars $a, \eta, \eta^0_{1,3,5}$) and implemented the particles that were not yet covered: the doubly charged scalar η_5^{++}, the colored scalars π_8 and π_3 and the color singlet and octet top partners. The new files include all interactions with particles in `eVLQ` and can thus be used as a modular expansion. Due to the large number of particles we did not implement all BSM-BSM-SM or BSM-BSM-BSM vertices of the new BSM particles, but only those in the simplified models in Section 4.1.3. The `CHM5` implementation is documented in Appendix B.

We then simulated events with gluonis using the MC generator MadGraph5_aMC@NLO (MG) [15]. MG considers the pair production and the subsequent decay of gluonis separately, using the narrow-width approximation: If an unstable particle's width is small compared to its mass, then the total cross section can be factorized into the production cross section and the branching ratio for a given decay [72],

$$\sigma(pp \to X \to Y) = \sigma_{\text{prod}}(X) \left(\frac{\Gamma_{X\to Y}}{\Gamma_X} + \mathcal{O}\left(\frac{\Gamma_X}{m_X}\right)\right) \simeq \sigma_{\text{prod}}(X)\,\text{Br}(X \to Y). \tag{4.19}$$

Since we expect $m_8 > 1$ TeV and the couplings facilitating the decays scale with $1/f_\chi$, we can be sure that $\Gamma_{Q_8} \ll m_8$. We used MG in LO mode, so the gluonis were pair produced as in Eq. (4.1). The center of mass energy was set to $\sqrt{s} = 13$ TeV to allow for a comparison with recent LHC data. The hard scattering events were convolved with the `NNPDF23_lo_as_0130_qed` PDF set [73] included in the `LHAPDF6` library [74]. The renormalization and factorization scales were set to $\mu_R = \mu_F = m_8$. For the decays, we used MadWidth [75] to compute the widths. We then decayed the gluonis and the pNGBs with MadSpin[1] [76]. Finally, the events were showered with Pythia 8 [77] and saved in the HepMC format [78]. For the further analysis detailed below we used the LO events but scaled up the cross section to $\text{NNLO}_{\text{approx}}$+NNLL.

Before we discuss how to obtain bounds on the masses from the simulated events, we review how the experimental collaborations go about it. ATLAS and CMS regularly publish searches for evidence of new physics in the LHC data, using the following analysis. First, the events are reconstructed from the detector signatures and jets are identified using the anti-k_T jet clustering algorithm [79, 80]. Depending on which signatures are searched for, the events are then required to satisfy several conditions such a minimal or maximal number of jets, bounds on the transverse momenta or other kinematic observables, etc. Events that do not satisfy these are not considered signal candidates and are discarded, while the remaining events are sorted into signal regions (SRs). The results of the search are then the observed number of events in each SR. By comparing the observed event yield with the number of events expected from the SM, limits on the masses, production cross sections and branching ratios of BSM particles can be obtained using the CL_s method [81].

[1] For the decays of the sgluon, MadSpin was not able to deal with the color structures. In this case, we used MadGraph's decay chain syntax.

The experimental collaborations set limits in the context of simplified models for standard scenarios. Naturally, not every model that is discussed in the theory literature can be taken into account. However, the cuts and signal regions of a given search can be implemented and then applied to MC generated events. This way, searches can be *recasted* and limits can be obtained for an arbitrary model. Two popular tools for this purpose are MadAnalysis5 (MA) [16–19] and CheckMATE (CM) [20, 21]. Both accept a HepMC file and perform a detector simulation using Delphes [82]. The reconstructed events are then sorted in the SRs and the MC event yield is compared with the number of events observed in the experiment. To this end, the cross section of the process has to be supplied to correctly scale the event yields. For this we used the $\text{NNLO}_{\text{approx}}$+NNLL gluino production cross section [62, 65] as explained in Section 4.1.1. Finally, the exclusion level is computed with the CL_s method. CM calculates an expected and observed CL_s, of which we use the latter. We chose to use both MA and CM, since different searches have been recasted. While the CM database contains mostly ATLAS searches at 13 TeV [83], the MA Public Analysis Database [84] has about the same number of ATLAS and CMS searches implemented.

To determine the mass bounds, we simulate a given process on a grid in the m_8-m_1 mass plane. Using a Python script, we then triangulate the grid, linearly interpolate the CL_s values with the `LinearTriInterpolator` of the `matplotlib` library [85] and plot the contours of the 95% CL and sometimes also 68% CL exclusions.

4.3 Simulated Scenarios

We consider three different scenarios for the decays of the gluonis:

(S1) Decay exclusively via π_3, e.g.

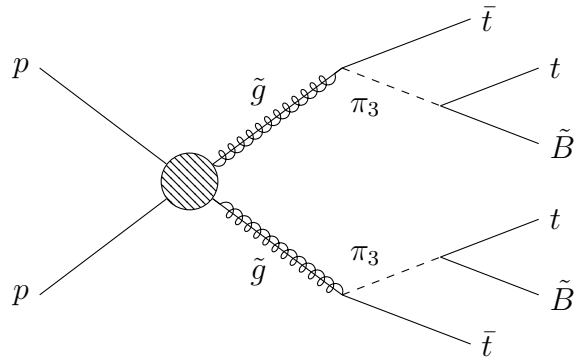

(4.20)

where the blob indicates QCD pair production. The Majorana gluoni can decay to $\pi_3\bar{t}$ or $\pi_3^* t$, while the pair of Dirac gluonis $\tilde{G}^+\tilde{G}^-$ or $\tilde{G}^0\bar{\tilde{G}}^0$ always decays to $\pi_3\bar{q}\pi_3^* q$ with $q = b, t$. In this class we simulate pair production of

(S1a) only the Majorana gluoni $\tilde{g}$. The final state consists of four top quarks and two undetectable bonis, $4t$+MET. This process is also present in SUSY models as a decay channel of the gluino, $\tilde{g} \to \bar{t}\tilde{t} \to \bar{t}t\tilde{\chi}_1^0$, where $\tilde{t}$ is the scalar partner of the top quark and $\tilde{\chi}_1^0$ the lightest neutralino. The SUSY process has been extensively searched for, e.g. [86, 87]. It can therefore be used as a benchmark for testing our simulation setup by checking if we can reproduce the limits obtained by ATLAS and CMS.

(S1b) only the charged gluoni $\tilde{G}^+$ with final state $2b2t$+MET. Due to the Dirac nature of $\tilde{G}^+$, this process has a larger cross section than (S1a), $\sigma_{\tilde{G}^+} = 2\sigma_{\tilde{g}}$.

(S1c) the whole octet multiplet Q_8 with combined cross section $\sigma_{Q_8} = 5\sigma_{\tilde{g}}$.

(S2) Decay exclusively via π_8, e.g.

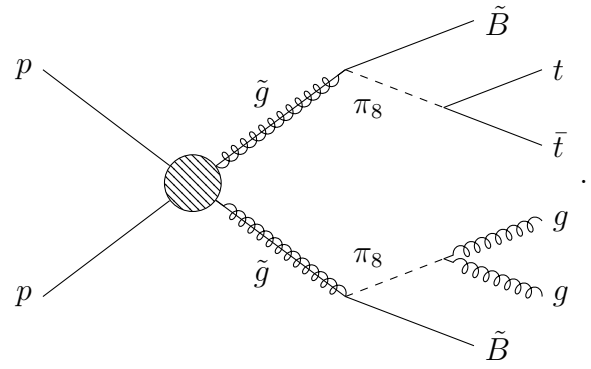

(4.21)

Since we do not know the branching ratios of π_8, we consider the three cases where $\mathrm{Br}(\pi_8 \to t\bar{t}) = 100\%$, $\mathrm{Br}(\pi_8 \to gg) = 100\%$ and $\mathrm{Br}(\pi_8 \to t\bar{t}) = \mathrm{Br}(\pi_8 \to gg) = 50\%$. The resulting final states are $4t$+MET, $4j$+MET and $2t2j$+MET, plus soft pions or leptons in case of Dirac gluonis. For purely $\pi_8 \to t\bar{t}$, the final state is the same as for (S1a) but with different kinematics. We simulate the three scenarios for π_8 with

(S2a) only $\tilde{g}$,

(S2b) the whole multiplet.

(S3) Decay via π_3 and π_8 with $\mathrm{Br}(Q_8 \to \pi_3\bar{q}) = \mathrm{Br}(Q_8 \to \pi_8 Q_1) = 50\%$, e.g.

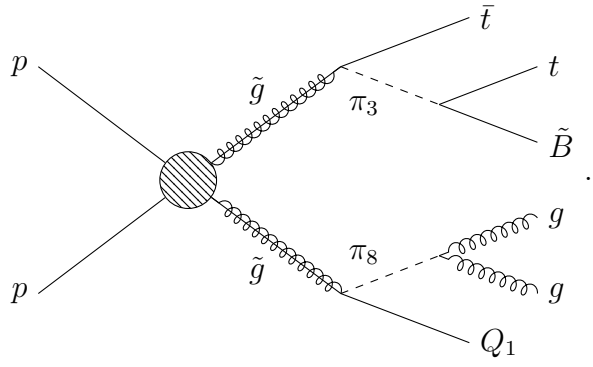

(4.22)

In this combined analysis we consider only the mixed case $\mathrm{Br}(\pi_8 \to gg) = \mathrm{Br}(\pi_8 \to t\bar{t}) = 50\%$ since we found the bounds for (S2) to be mostly independent of the decay of π_8, as we will see in the discussion of Fig. 4.6. We derive the bounds for pair production of

(S3a) only $\tilde{g}$,

(S3b) only $\tilde{G}^+$,

(S3c) the whole multiplet.

4.4 Recasted Searches and Consistency Checks

In this section, we highlight the recasted searches that are most sensitive to the gluoni decays. To this end, we show the mass bounds for the scenarios (S1c) and (S2b) separately for each search in Fig. 4.1. Here, the gray dots are the simulated points. The coarse structures in the contour lines are due to the limited resolution of the grid and could be improved if a more precise knowledge of the bounds is required. Fig. 4.1 shows that the bounds are dominated by only a few searches.

- **CMS-SUS-19-006** [87]: This is a search for gluino and squark pair production with multiple jets and large MET in the final state using 137 fb^{-1} of data. The results are interpreted within multiple simplified models, including the $4t$+MET, $4b$+MET, $4q$+MET and $4q2V$+MET final states from gluinos, where $q = u, d, s, c$ are light quarks and $V = W, Z$. The signal candidates are divided into 174 orthogonal SRs, and covariance and correlation matrices for the SRs are provided. These are used by the recast implemented in MA [89] to perform a statistical combination of the SRs. This explains why this search gives the strongest bound for most scenarios. The optimization for both $4t$ and $4j$ final states makes the recast competitive both for $\pi_8 \to t\bar{t}$ and $\pi_8 \to gg$.

- **ATLAS-CONF-2019-040** [88]: This search looks for gluinos and squarks in final states containing jets and MET but no charged leptons. It uses the full Run 2 dataset of 139 fb^{-1}. The simplified model for the gluinos assumes $\tilde{g} \to qq\tilde{\chi}_1^0$ or $\tilde{g} \to q'qW\tilde{\chi}_1^0$, where $q^{(\prime)}$ are light quarks. We therefore expect the recast to be very sensitive to final states with multiple light jets, such as those from $\pi_8 \to gg$. This is confirmed by comparing Figs. 4.1c-e. For the final states dominated with top quarks, however, this search is subdominant. Note that it is implemented in both MA and CM.

- **ATLAS-CONF-2018-041** [86]: This is a search for gluino pair production with decays to third generation quarks and neutralinos using 79.8 fb^{-1} of data. The search looks for b-tagged jets and MET, and considers both hadronic and leptonic decays of the W. It is implemented in CM, but the recast can rarely keep up with the strong bounds from CMS-SUS-19-006.

Fig. 4.1 also shows the mass bounds from several other searches, which however are less sensitive to our signatures. We briefly summarize those: ATLAS-1908-03122 [90] searches for bottom-squark production with Higgs bosons in the final state. ATLAS-SUSY-2016-07 [91] is a search for gluinos and squarks in final states with light quarks and no leptons. It is implemented in both MA and CM. CMS-SUS-16-033 [92] searches for pair production of gluinos and stops decaying to light or third-generation quarks, similarly to CMS-SUS-19-006 but using only 35.9 fb^{-1}. Finally, ATLAS-2101-01629 [93] searches for pair production and chain decays of gluinos $\tilde{g} \to q\bar{q}'\tilde{\chi}_1^\pm$ and squarks $\tilde{q} \to q'\tilde{\chi}_1^\pm$ with $\tilde{\chi}_1^\pm \to W^\pm\tilde{\chi}_1^0$.

We took several steps to test our FeynRules implementation and simulation setup. We should be able to reproduce the mass bounds from SUSY searches for gluino pair production with $\tilde{g} \to \bar{t}\tilde{t} \to \bar{t}t\tilde{\chi}_1^0$ from the scenario (S1a). To this end, we focus on ATLAS-CONF-2018-041 and CMS-SUS-19-006, which both search – among other SUSY processes – for gluinos in this channel, as discussed above. In both searches, the stop was actually taken off-shell, i.e. the gluino had a three-body decay $\tilde{g} \to \bar{t}t\tilde{\chi}_1^0$, which slightly changes the kinematics.

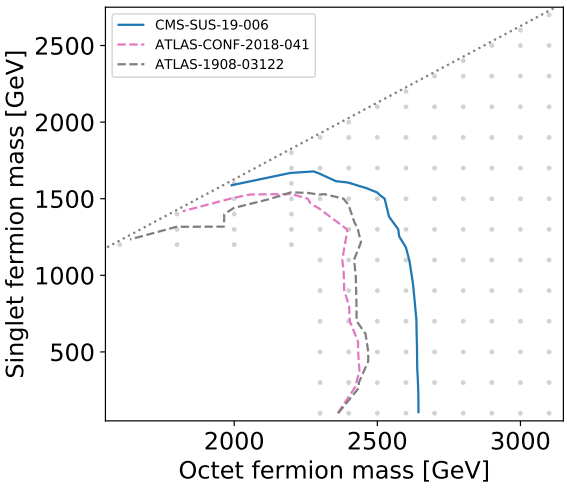

(a) Scenario (S1c) with $m_{\pi_3} = m_8 - 200$ GeV

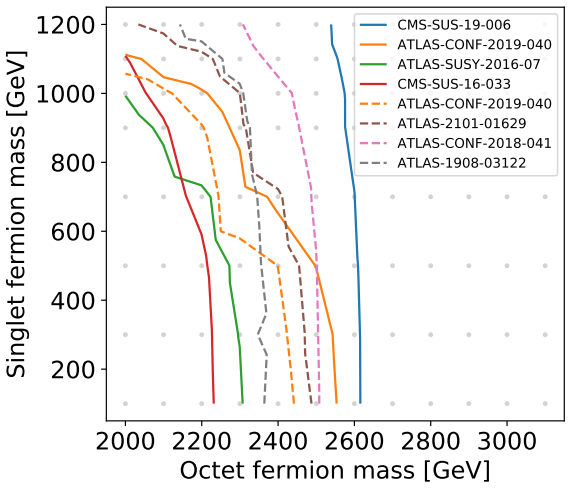

(b) Scenario (S1c) with $m_{\pi_3} = 1.4$ TeV

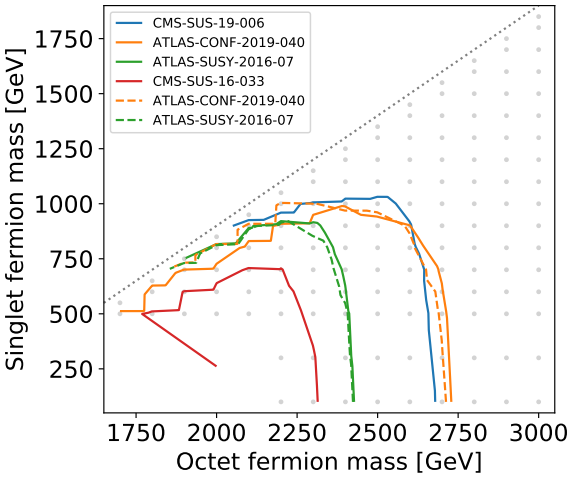

(c) Scenario (S2b) with $\pi_8 \to gg$

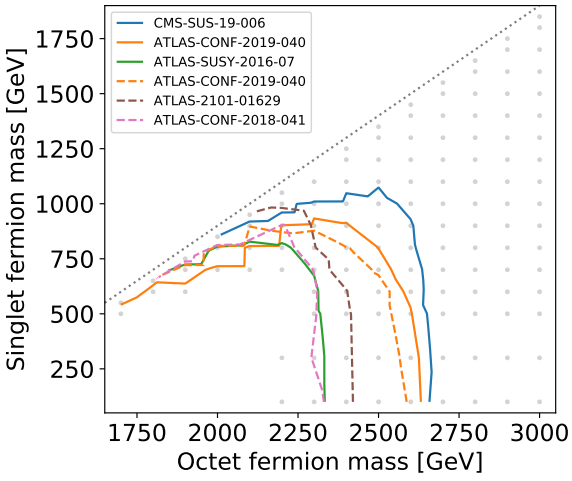

(d) Scenario (S2b) with $\pi_8 \to gg, tt$

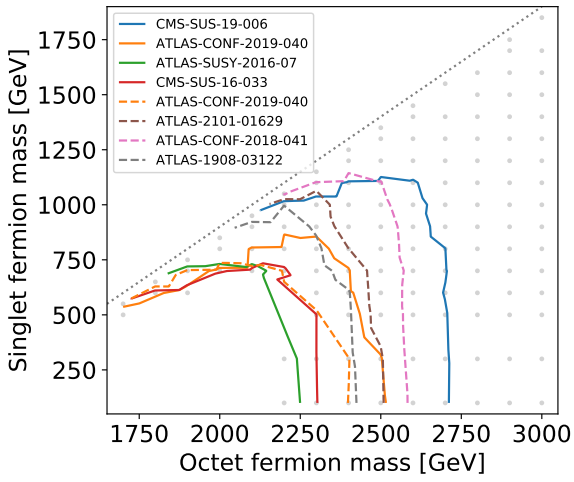

(e) Scenario (S2b) with $\pi_8 \to tt$

Figure 4.1: Comparison of the bounds at 95% CL obtained from different searches implemented in MA (solid lines) and CM (dashed lines) for scenario (S1c) in (a)-(b) and scenario (S2b) with $m_{\pi_8} = 1.1$ TeV in (c)-(e). The dotted lines indicate the kinematically forbidden regions, the gray dots are the simulated points. The coarse features of the contour lines are due to the limited grid resolution.

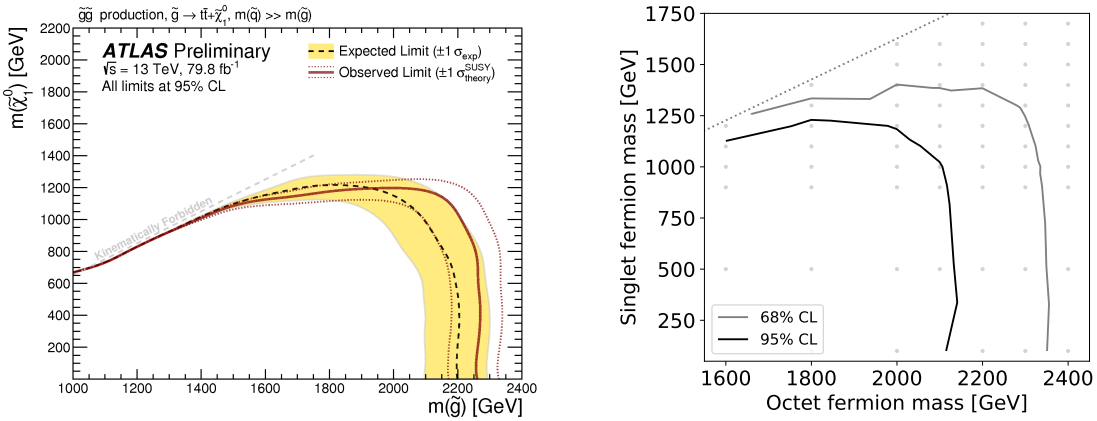

Figure 4.2: Comparison of the mass bounds in ATLAS-CONF-2018-041 [86] (left) with the recast implemented in CM (right) for the SUSY scenario (S1a) with stop mass $m_{\pi_3} = m_8 - 200$ GeV.

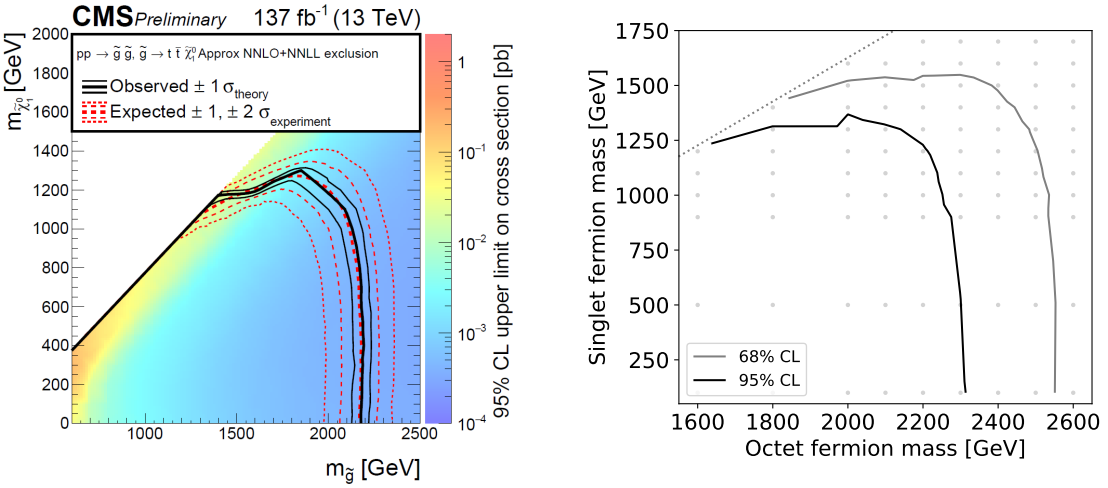

Figure 4.3: Comparison of the mass bounds in CMS-SUS-19-006 [87] (left) with the recast implemented in MA (right) for the SUSY scenario (S1a) with stop mass $m_{\pi_3} = m_8 - 200$ GeV.

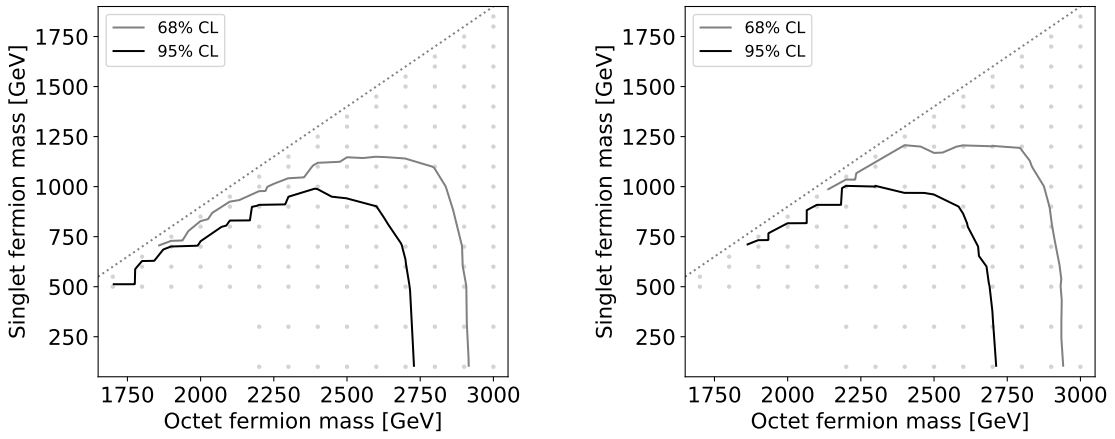

Figure 4.4: Comparison of the mass bounds obtained from the recast of ATLAS-CONF-2019-040 [88] implemented in MA (left) and CM (right) for the scenario (S2b) with $\pi_8 \to gg$. The sgluon mass was fixed to $m_{\pi_8} = 1.1$ TeV.

For the comparison, we simulated (S1a) with $m_{\pi_3} = m_8 - 200$ GeV. The results obtained from the recasts of the ATLAS and CMS SUSY searches are shown in Figs. 4.2 and 4.3 respectively, along with the experimentally determined mass bounds. ATLAS finds an observed bound of 2.25 TeV on the gluino mass for vanishing neutralino mass, and a maximum bound on $m_{\tilde{\chi}_1^0}$ of about 1.2 TeV. The bound from the recast[2] reaches up to 2.15 TeV for m_8 and 1.2 TeV for m_1. The bounds from recasts are expected to be lower than from the experiment, since correlations among the signal regions are usually neglected for the recasts. Therefore, a deviation of 100 GeV is well within the acceptable range. The recast of CMS-SUS-19-006 overshoots the maximum bounds of about 2.2 TeV on m_8 and 1.3 TeV on m_1 by ∼100 GeV each. This can be explained by the statistical combination of SRs mentioned above. In light of this and the different kinematics, we find a bound that is too large by 100 GeV acceptable.

A further opportunity to test our setup is provided by analyses that are implemented in both MA and CM. In Fig. 4.4, we compare the two recasts of ATLAS-CONF-2019-040 for the scenario they are most sensitive to, (S2b) with $\pi_8 \to gg$. We find good agreement between the two tools.

4.5 Mass Bounds

Having established that our simulation setup is reliable, we can finally discuss the results, starting with the decay via the stop, scenario (S1). The bounds on the gluoni and boni masses are shown in Fig. 4.5. We considered two cases for the stop mass: In the first row, m_{π_3} is variable and close to the gluoni mass, $m_{\pi_3} = m_8 - 200$ GeV. Here, the dashed line indicates the region where the π_3 is off-shell, $m_{\pi_3} < m_1 + m_t$. From SUSY searches for pair production of a stop with subsequent decay $\tilde{t} \to t\tilde{\chi}_1^0$, bounds on m_{π_3} have been established up to 1250 GeV by ATLAS [94] and 1310 GeV by CMS [95]. When fixing the stop mass in the second row of Fig. 4.5, we therefore chose $m_{\pi_3} = 1.4$ TeV to lie just above the current bounds. For vanishing boni mass, $\tilde{g}$, $\tilde{G}^+$ and the full multiplet are excluded up to 2.3 TeV, 2.4 TeV and 2.6 TeV, respectively, independently of the stop mass. The 68% CL exclusion lies 200-300 GeV higher. The hierachy of the bounds is as expected, as the $\tilde{G}^+$ is produced with double the cross section of $\tilde{g}$, and the full multiplet even with $\sigma_{Q_8} = 5\sigma_{\tilde{g}}$. For Q_8, the bounds on m_1 reach almost up to 1.7 TeV. In Fig. 4.5d-e, the bounds for $\tilde{g}$ and $\tilde{G}^+$ decrease with increasing boni mass, whereas they remain approximately constant for Q_8 due to the larger cross section.

Next, we studied the decay via the sgluon in scenario (S2). To avoid the current bounds on the sgluon mass [96], we fixed $m_{\pi_8} = 1.1$ TeV. In Fig. 4.6, we show the bounds for the sgluon decaying to gg, to $t\bar{t}$ and to both for the Majorana gluoni (first row) and the full multiplet (second row). Recalling that the higgsonis decay to a boni and undetectably soft particles, we notice that the three gluonis are identical for this process apart from the larger cross section for the Dirac gluonis. We were therefore able to simplify the simulation setup for Q_8 by generating the events only with $\tilde{g}$ and then performing the analysis with a cross section of $5\sigma_{\tilde{g}}$. For $\tilde{g}$, the bounds on m_8 at $m_1 \to 0$ lie between 2.3 TeV and 2.4 TeV, while the full multiplet is excluded at about 2.7 TeV. The bounds on m_1 reach as high as 750 GeV for $\tilde{g}$ and just above 1.1 TeV

[2]The exclusion levels are linearly interpolated between the simulated points, but in reality they fall off non-linearly towards larger masses. The contours should therefore be treated with care between grid points. We read off bounds only with a precision of 50 GeV.

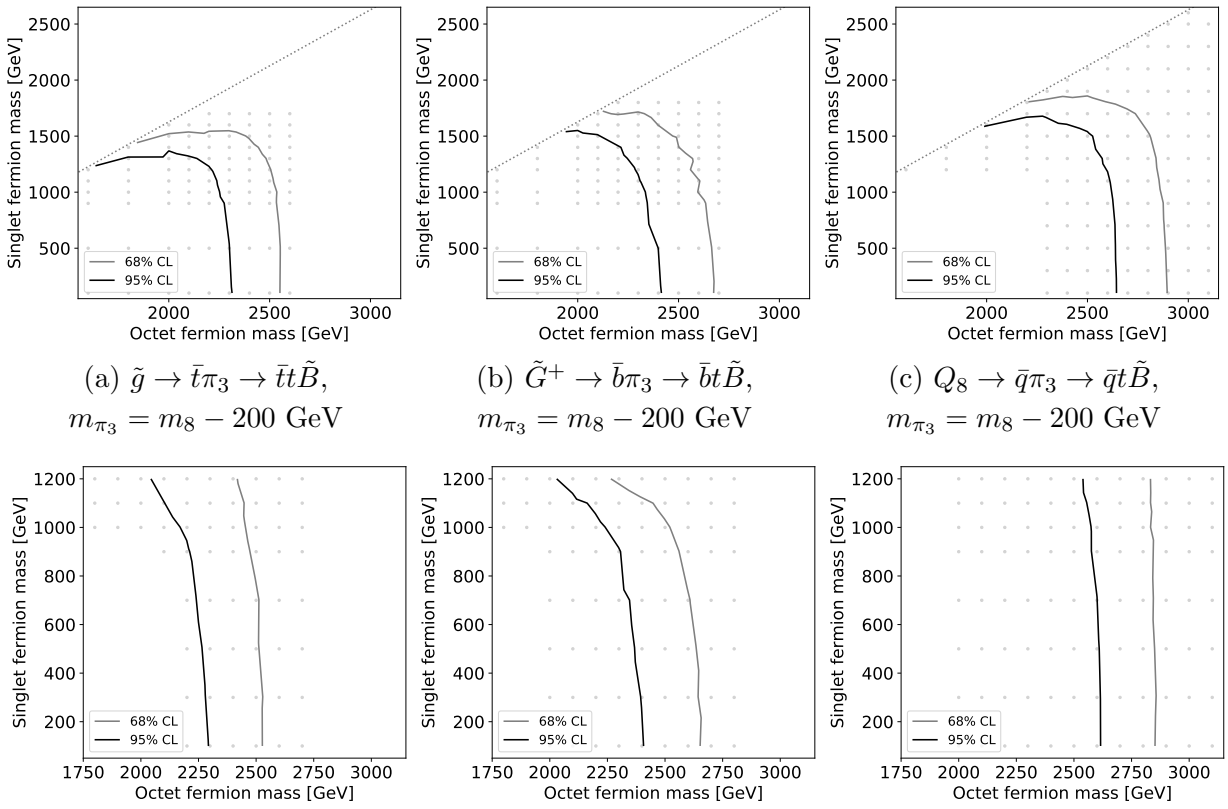

(a) $\tilde{g} \to \bar{t}\pi_3 \to \bar{t}t\tilde{B}$, $m_{\pi_3} = m_8 - 200$ GeV

(b) $\tilde{G}^+ \to \bar{b}\pi_3 \to \bar{b}t\tilde{B}$, $m_{\pi_3} = m_8 - 200$ GeV

(c) $Q_8 \to \bar{q}\pi_3 \to \bar{q}t\tilde{B}$, $m_{\pi_3} = m_8 - 200$ GeV

(d) $\tilde{g} \to \bar{t}\pi_3 \to \bar{t}t\tilde{B}$, $m_{\pi_3} = 1.4$ TeV

(e) $\tilde{G}^+ \to \bar{b}\pi_3 \to \bar{b}t\tilde{B}$, $m_{\pi_3} = 1.4$ TeV

(f) $Q_8 \to \bar{q}\pi_3 \to \bar{q}t\tilde{B}$, $m_{\pi_3} = 1.4$ TeV

Figure 4.5: Bounds on the fermion masses for scenario (S1), pair production of a gluoni Q_8 with subsequent decay to a SM quark q and a stop π_3. In the first row the stop mass is 200 GeV below the octet mass, in the second row it is fixed to 1.4 TeV. We include only the $\tilde{g}$ in the first and $\tilde{G}^+$ in the second column. The third column shows the bounds for the full octet multiplet, assuming it is mass degenerate. The boni $\tilde{B}$ is stable.

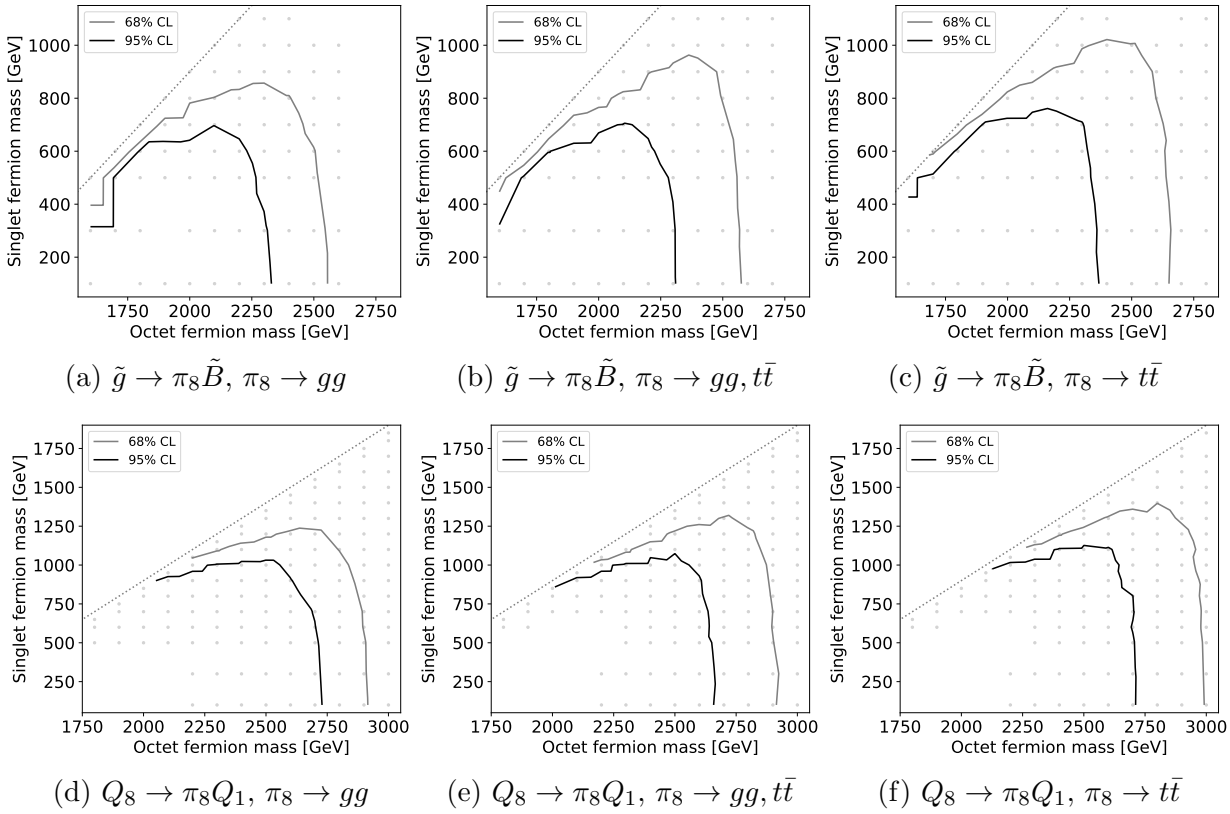

(a) $\tilde{g} \to \pi_8 \tilde{B}$, $\pi_8 \to gg$ (b) $\tilde{g} \to \pi_8 \tilde{B}$, $\pi_8 \to gg, t\bar{t}$ (c) $\tilde{g} \to \pi_8 \tilde{B}$, $\pi_8 \to t\bar{t}$

(d) $Q_8 \to \pi_8 Q_1$, $\pi_8 \to gg$ (e) $Q_8 \to \pi_8 Q_1$, $\pi_8 \to gg, t\bar{t}$ (f) $Q_8 \to \pi_8 Q_1$, $\pi_8 \to t\bar{t}$

Figure 4.6: Bounds on the fermion masses for scenario (S2), pair production of a gluoni Q_8 with subsequent decay to a singlet fermion Q_1 and a sgluon π_8. The sgluon mass is fixed to $m_{\pi_8} = 1.1$ TeV. In the first row only the Majorana gluoni is considered, which decays to a sgluon and a boni. In the second row the full multiplets are taken into account, assuming that they are each mass degenerate apart from a very small mass splitting in Q_1. The boni is stable, for the sgluon we consider the decays to gg (left column), to $t\bar{t}$ (right column) or to either with $\mathrm{Br}(\pi_8 \to gg) = \mathrm{Br}(\pi_8 \to t\bar{t}) = 50\%$ (middle column).

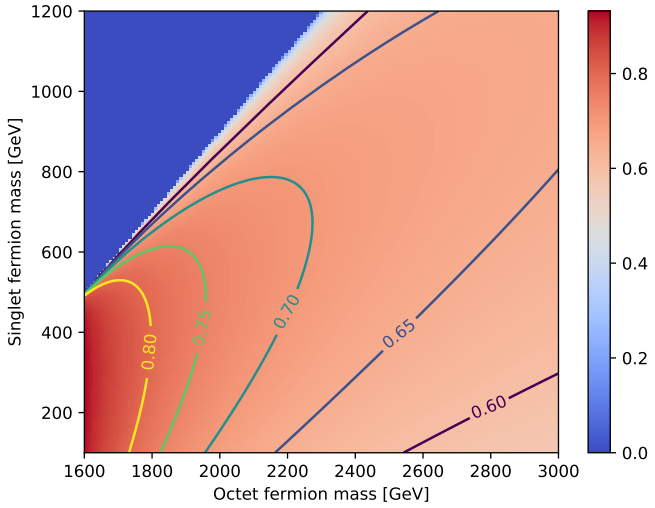

Figure 4.7: Branching ratio of $Q_8 \to \pi_8 Q_1$ for $m_{\pi_8} = 1.1$ TeV and $m_{\pi_3} = 1.4$ TeV. For very heavy gluonis, $m_8 \to \infty$, the branching ratio tends to 50%. For $m_8 \to 0$, the decay via π_8 dominates, whereas it is kinematically forbidden in the top left.

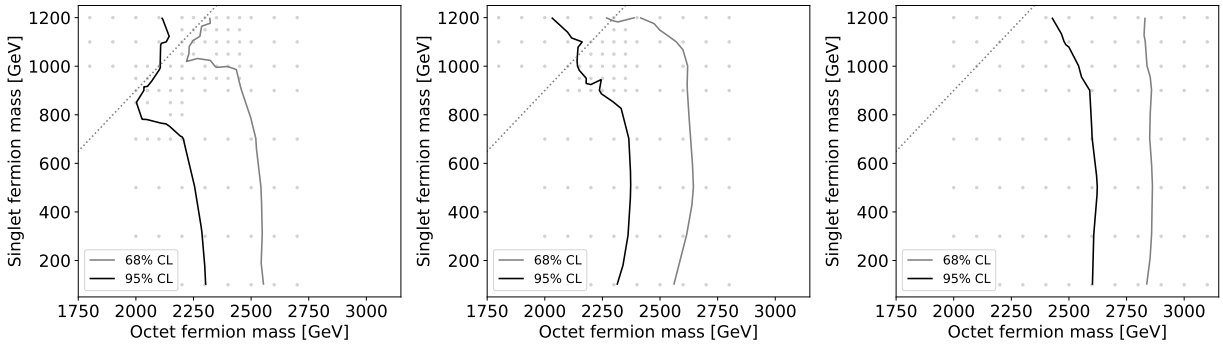

(a) $\tilde{g} \to \bar{t}\pi_3$ or $\tilde{g} \to \pi_8 \tilde{B}$ (b) $\tilde{G}^+ \to \bar{b}\pi_3$ or $\tilde{G}^+ \to \pi_8 \tilde{h}^+$ (c) $\tilde{Q}_8 \to \bar{q}\pi_3$ or $\tilde{Q}_8 \to \pi_8 Q_1$

Figure 4.8: Bounds on the fermion masses for scenario (S3), pair production of a gluoni Q_8 with subsequent decay via a stop or sgluon with $\mathrm{Br}(Q_8 \to \bar{q}\pi_3) = \mathrm{Br}(Q_8 \to \pi_8 Q_1) = 50\%$ in the limit $m_8 \to \infty$. The scalar masses are fixed to $m_{\pi_3} = 1.4$ TeV and $m_{\pi_8} = 1.1$ TeV. Above the dotted line, $\mathrm{Br}(Q_8 \to \pi_8 Q_1) = 0$. For the sgluon, we consider only $\mathrm{Br}(\pi_8 \to gg) = \mathrm{Br}(\pi_8 \to t\bar{t}) = 50\%$.

for Q_8, both for $\pi_8 \to t\bar{t}$. All in all, the bounds are similar for all decays of π_8. We further note that despite the different kinematics, the bounds on m_8 for (S2) are of the same order of magnitude as those for (S1).

For the final simulations, we let the gluonis decay via either π_3 or π_8. The description of (S3) given in Section 4.3 is oversimplified: To keep the branching ratios fixed to $\mathrm{Br}(Q_8 \to \pi_3 \bar{q}) = \mathrm{Br}(Q_8 \to \pi_8 Q_1) = 50\%$ over the whole m_8-m_1 plane, we would have to redefine the couplings at each point to account for the varying phase space factors. As this is very tedious, we instead adopted the following procedure. We fixed the couplings so that the decay occurs with equal branching ratio for $m_8 \to \infty$. For finite mass,

$$\mathrm{Br}(\tilde{g} \to \pi_8 \tilde{B}) = \frac{(m_8^2 + 2m_8 m_1 + m_1^2 - m_{\pi_8}^2)\lambda_{\pi_8}^{1/2}}{(m_8^2 + 2m_8 m_1 + m_1^2 - m_{\pi_8}^2)\lambda_{\pi_8}^{1/2} + (m_8^2 - m_{\pi_3}^2 + m_t^2)\lambda_{\pi_3}^{1/2}}, \tag{4.23}$$

where $\lambda_{\pi_8} = \lambda(m_8^2, m_{\pi_8}^2, m_1^2)$ and $\lambda_{\pi_3} = \lambda(m_8^2, m_{\pi_3}^2, m_t^2)$ with the Källén function $\lambda(x, y, z) = x^2 + y^2 + z^2 - 2xy - 2yz - 2xz$. We show the branching ratio for the relevant part of parameter space in Fig. 4.7, where we set the scalar masses to $m_{\pi_8} = 1.1$ TeV and $m_{\pi_3} = 1.4$ TeV. The resulting bounds are presented in Fig. 4.8. Above the dotted line $m_8 = m_{\pi_8} + m_1$, the decay via π_8 is kinematically forbidden.

The behavior of the bounds for the Majorana gluoni in Fig. 4.8a can be understood as follows. For small m_1, the bounds behave like in Figs. 4.5d and 4.6b since both scenarios give very similar bounds. Above $m_1 = 700$ GeV, the exclusion plateaus as in Fig. 4.6b as (S2) makes up more than 70% of the decays in this region. As we near the kinematic line, the stronger bounds from (S1) become more relevant again. Finally, above the dotted line we are completely in scenario (S1) with fixed stop mass, so the bounds are close to Fig. 4.5d, reaching $m_8 = 2.1$ TeV for $m_1 = 1.2$ TeV.

The bounds for the charged gluoni[3], shown in Fig. 4.8b, behave analogously. In this case, we reused the simulated points from Fig. 4.5e for the region where the channel $\tilde{G}^+ \to \pi_8 \tilde{h}^+$ is

[3]For technical reasons, we slightly modified the scenario: We had difficulties with the soft pions in MG. To simplify the simulation setup, we therefore used $\tilde{h}^+ \to \phi^+ \tilde{B} \to e^+ \nu_e \tilde{B}$ with $m_{\tilde{h}^+} - m_{\tilde{B}} = 5$ GeV. The auxiliary scalar ϕ^+ has a mass of 2 GeV. We treated $\tilde{h}^0$ as stable as well. This does not have physical effects since both the pions and leptons are too soft to be detected anyways.

forbidden due to technical difficulties with the combined process in MG. This is possible since this region is physically identical to scenario (S1b). In Fig. 4.8c, we consider the full multiplet. The bounds on m_8 are constant at 2.6 TeV for $m_1 < 900$ TeV, above which they decrease significantly more than in Fig. 4.5f. This is due to the plateau of the bounds from (S2) in Fig. 4.6e, which reduces the combined bounds in (S3). In the case of the full multiplet, the bounds do not reach the region where the channel $Q_8 \to \pi_8 Q_1$ is forbidden.

In this chapter we have derived bounds on the gluoni masses in the model M5. However, as mentioned above, we expect the gluonis to have similar masses to the VLQs, $m_8 \approx m_3$. More precisely, since they only differ in their color representation,

$$\frac{|m_8 - m_3|}{m_8} = \mathcal{O}(\alpha_s) \sim 10\%. \tag{4.24}$$

This allows us to translate bounds on m_8 into realistic ranges for m_3. For a light boni, m_8 is excluded up to ~ 2.7 TeV, so we expect the VLQ mass to be at least 2.4 TeV. Current experimental searches for VLQs focus on the decay channels $T \to bW^+, tZ, th$ for the top-like, $B \to tW^-, bZ, bh$ for the bottom-like and $X_{5/3} \to tW^+$ for the charge-5/3 VLQ. The strongest bounds obtained from VLQ pair production are $m_T > 1.60$ TeV by ATLAS [97] and $m_T > 1.37$ TeV by CMS [98], $m_B > 1.42$ TeV by ATLAS [97] and $m_B > 1.57$ TeV by CMS [99], as well as $m_{X_{5/3}} > 1.33$ TeV by CMS [100]. Therefore, setting bounds on m_3 by recasting VLQ searches is redundant as they are subdominant to the bounds from the gluonis.

5 | Conclusion and Outlook

In this work we studied a composite Higgs model with an underlying fermionic UV completion based on the coset $\mathrm{SU}(5) \times \mathrm{SU}(6) \times \mathrm{U}(1)/\mathrm{SO}(5) \times \mathrm{Sp}(6)$. We derived the SM quantum numbers of the pNGBs and the top partners, which we embedded in the $(\mathbf{5}, \mathbf{15})$ of $\mathrm{SU}(5) \times \mathrm{SU}(6)$. The colored pNGBs are the stop π_3 and the sgluon π_8, the top partners include among others color octet Q_8 ("gluonis") and color singlet Q_1 ("higgsonis" and "boni") multiplets, where the naming is reminiscent of the conventions in the SUSY literature. We then calculated parts of the Lagrangian of the model and investigated the scalar potential V of the colored pNGBs Π_χ in detail with the aim of gaining insights into the mass hierarchy. To this end, we classified the operators that contribute to V up to $\mathcal{O}(p^2)$ in the chiral expansion and expanded them to second order in Π_χ. The scalar potential is generated by explicit breaking of the global symmetry, such as the gauging of the SM subgroup of $\mathrm{SO}(5) \times \mathrm{Sp}(6)$, mass terms for the hyperquarks and the mixing terms of the top partners with the third-generation quarks. In particular the latter sector contributes a large number of independent operators to V. The scalar masses are therefore dependent on too many unknown coefficients to determine whether π_3 or π_8 are heavier.

The remainder of this thesis was dedicated to studying the LHC phenomenology of the model. Here, we focused on the gluonis as they have the largest production cross section, and since to our knowledge, charged color octet fermions have not been considered so far. We derived the possible decay channels of the gluonis, leading to $Q_8 \to \bar{q}\pi_3$ and $Q_8 \to \pi_8 Q_1$, where $\pi_3 \to t\tilde{B}$, $\pi_8 \to gg, t\bar{t}$ and the lightest color singlet $\tilde{B}$ is stable, making it a dark matter candidate. We then formulated simplified models for these decays and implemented them in FeynRules. This allowed us to simulate the gluoni pair production using MadGraph5_aMC@NLO and compare the results with experimental searches recasted in MadAnalysis5 and CheckMATE. This way we derived exclusion bounds on the masses of the gluonis and the boni. After ensuring that our simulation setup was able to reproduce the bounds from searches for the SUSY process $\tilde{g} \to t\bar{t}\tilde{\chi}_1^0$, we studied the decay channels via π_3 and π_8 separately at first (see Figs. 4.5 and 4.6), followed by a combined analysis in Fig. 4.8 where both channels occur with equal probability for $m_8 \to \infty$. Gluoni masses up to 2.7 TeV are excluded for a massless boni, the bounds on the boni mass reach almost up to 1.7 TeV. These results along with some further investigations are going to be published in [52].

As discussed in Section 4.3, the scenarios (S1a) and (S2a) have the same final state but differ in the kinematics. It would be interesting to study this difference in more detail by comparing distributions of the angle between the top quarks and the invariant mass. Firstly, one would have to see whether the two scenarios can be distinguished at all. If they can be, the next step might be to check if and how precisely the branching ratios of the $\tilde{g}$ can be recovered from the distributions. This could be guidance for designing searches that are sensitive to our model.

The phenomenology depends crucially on the assumption that the color singlets are the lightest BSM particles. However, this goes against the generic situation in composite Higgs models of top partners with mass $\sim \Lambda_{\mathrm{HC}}$ and the pNGB masses well below that. It might therefore be more natural to take $m_1 > m_{\pi_3,\pi_8}$. The decay $\pi_3 \to t\tilde{B}$ is then no longer possible. We find an interesting alternative by allowing lepton number violating terms in the Lagrangian. This opens up the possibility of adding terms that induce a mixing between one higgsoni doublet $\tilde{h}_d \in \mathbf{2}_{-1/2}$ of $\mathrm{SU}(2)_L \times \mathrm{U}(1)_Y$ with the lepton doublet $\ell_L = (\nu_\tau, \tau_L^-)$, which would offer an explanation for the neutrino masses. The mixing of the other generations is suppressed by their smaller Yukawa couplings. The derivative couplings in Eq. (3.60) now contain the operator (neglecting prefactors)

$$Q_3\sigma^\mu\bar{Q}_1\partial_\mu\pi_3^\dagger \supset (T\sigma^\mu\bar{\tilde{h}}_d^0 + B\sigma^\mu\bar{\tilde{h}}_d^-)\partial_\mu\pi_3^\dagger \xrightarrow{\text{mix}} (t_L\sigma^\mu\bar{\nu}_\tau + b_L\sigma^\mu\bar{\tau}_L^-)\partial_\mu\pi_3^\dagger, \tag{5.1}$$

which opens the decay channels

$$\pi_3 \to t_L\bar{\nu}_\tau,\, b_L\tau_L^+. \tag{5.2}$$

The bounds for (S1) with $m_1 \to 0$ are still applicable in the case of $\pi_3 \to t_L\bar{\nu}_\tau$ but not for the decay into the τ. The final states for $Q_8 \to \pi_8 Q_1$ also differ from (S2) since

$$\tilde{h}^+ \to \bar{b}_L\pi_3, \quad \tilde{h}^0 \to \bar{t}_L\pi_3, \quad \tilde{B} \to \bar{t}_R\pi_3, \tag{5.3}$$

which introduces additional t and/or b quarks. A natural extension of the present work would therefore be to determine the bounds for the case where the pNGBs are the lightest BSM particles. To this end, it might prove useful to recast searches for gluinos in the context of R-parity violating SUSY searches, e.g. [101].

In this thesis we have limited ourselves to the pair production of the gluonis. However, to test the viability of the full model, different sectors should also be studied. A possibilty for further investigation is the phenomenology of the EW pNGBs. For example, one could continue the classification of the scalar potential using the spurion method, building on the results obtained in Section 3.4, or determine bounds on the pNGB masses with numerical methods. In addition to the pNGBs, the VLQs are an interesting object of study. As discussed in Section 4.5, for the scenarios considered in this thesis, the current searches for VLQs yield weaker bounds than we can derive from the gluonis. However, this was based on $m_8 \approx m_3$, which in turn implicitly assumes that the hyperquarks are mass degenerate. If we instead introduced a mass splitting between the hyperquarks, this would translate to a mass difference for the top partners. The VLQ searches would then be relevant again, and limits could be set analogously to the gluonis. Besides the standard decays of a VLQ to a SM quark and an EW boson, the model also includes exotic decays [50, 53] such as

$$T \to b\eta^+ \to b\bar{b}t,\, bW^+\gamma,\, bW^+Z, \qquad X_{5/3} \to b\eta^{++} \to bW^+W^+. \tag{5.4}$$

Furthermore, if $m_8 > m_3$, the decay channels

$$\tilde{g} \to \pi_3\bar{T}_i,\, \pi_3^* T_i, \qquad \tilde{G}^0 \to \pi_3\bar{T}_i, \qquad \tilde{G}^+ \to \pi_3^* X_{5/3} \tag{5.5}$$

have to be taken into account when determining the bounds for the gluonis.

A | Details on the Classification of Top Coupling Operators

In Section 3.4.3, we abbreviated the classification of the color sector operators that contribute to V_{top}. Here, we provide more details and show that the classification is complete.

Tab. 3.3 lists the SU(6) invariant traces that serve as building blocks for the color sector operators. In Tab. A.1, we combine them into all possible operators with four spurions, i.e. to order $\mathcal{O}(p^2)$ in the chiral expansion, which have two P and two $P^\dagger$. This matches the classification given in [56]. We then construct all SM invariant operators by forming color singlets out of $P_L \in \overline{\mathbf{3}}$ and $P_R \in \mathbf{3}$, where each projector must occur an even number of times. The results are presented in Tabs. A.2 and A.3.

Our method for classifying the operators was based on the mixing Lagrangian

$$\mathcal{L}_{\text{mix}} \sim -\lambda_L \mathcal{O}_F \zeta_L - \lambda_R \mathcal{O}_F \zeta_R^c + \text{h.c.}\,. \tag{A.1}$$

However, $\mathcal{O}_F \in (\mathbf{5},\mathbf{15})_{\mathcal{G}}$ can be split into $\mathcal{B}_{14} \in (\mathbf{5},\mathbf{14})_{\mathcal{H}}$ and $\mathcal{B}_1 \in (\mathbf{5},\mathbf{1})_{\mathcal{H}}$, and the $\mathcal{H}$ multiplets can couple separately to the quarks,

$$\mathcal{L}_{\text{mix}} = -\lambda_{L,14} \mathcal{O}_{14} \zeta_L - \lambda_{R,14} \mathcal{O}_{14} \zeta_R^c - \lambda_{L,1} \mathcal{O}_1 \zeta_L - \lambda_{R,1} \mathcal{O}_1 \zeta_R^c + \text{h.c.}\,, \tag{A.2}$$

where $\lambda_{X,14} = c\lambda_{X,1}$ with $X = L, R$ and a group theory factor c. Instead of constructing $\mathcal{G}$ invariants, we should therefore classify the $\mathcal{H}$ invariant operators. This makes no difference in the EW sector as there is a unique SO(5) irrep, $\mathbf{5}_{\text{SU(5)}} \to \mathbf{5}_{\text{SO(5)}}$. In the color sector on the other hand, we have $\mathbf{15}_{\text{SU(6)}} \to \mathbf{14}_{\text{Sp(6)}} + \mathbf{1}_{\text{Sp(6)}}$, so we have to show that our classification is equivalent to one based on Sp(6) invariants. To this end, we can apply the proof in [53] with minor modifications. The SU(6) invariants are all constructed from operators of the form ΣP

Number of traces	Operators
1	$\text{Tr}\big(PP^\dagger PP^\dagger\big)$, $\text{Tr}\big(PP^\dagger\Sigma^\dagger P^\dagger P\Sigma\big)$
2	$\text{Tr}\big(P^\dagger P\big)\,\text{Tr}\big(P^\dagger P\big)$, $\text{Tr}(P\Sigma P\Sigma)\,\text{Tr}\big(P^\dagger\Sigma^\dagger P^\dagger\Sigma^\dagger\big)$, $\text{Tr}(P\Sigma)\,\text{Tr}\big(PP^\dagger\Sigma^\dagger P^\dagger\big) + \text{h.c.}$
3	$\text{Tr}(P\Sigma)\,\text{Tr}(P\Sigma)\,\text{Tr}\big(P^\dagger\Sigma^\dagger P^\dagger\Sigma^\dagger\big) + \text{h.c.}$, $\text{Tr}(P\Sigma)\,\text{Tr}\big(P^\dagger\Sigma^\dagger\big)\,\text{Tr}\big(P^\dagger P\big)$
4	$\text{Tr}(P\Sigma)\,\text{Tr}(P\Sigma)\,\text{Tr}\big(P^\dagger\Sigma^\dagger\big)\,\text{Tr}\big(P^\dagger\Sigma^\dagger\big)$

Table A.1: SU(6) invariants with four spurions P in the antisymmetric $\overline{\mathbf{15}}$. We show only the operators with two P and two $P^\dagger$.

Name	Operator	Expansion to $\mathcal{O}(\Pi_\chi^2)$
$O^{\mathrm{C}}_{L,1}$	$\mathrm{Tr}(P_L^i\Sigma_\chi)\,\mathrm{Tr}\Big(P_L^{i\dagger}\Sigma_\chi^\dagger\Big)$	$\pi_3^\dagger\pi_3/(4f_\chi^2)$
$O^{\mathrm{C}}_{L,2}$	$\mathrm{Tr}\Big(P_L^{i\dagger}P_L^i\Big)$	$3/2$
$O^{\mathrm{C}}_{LL,1}$	$\mathrm{Tr}(P_L^i\Sigma_\chi)\,\mathrm{Tr}\big(P_L^j\Sigma_\chi\big)\,\mathrm{Tr}\Big(P_L^{i\dagger}\Sigma_\chi^\dagger\Big)\,\mathrm{Tr}\Big(P_L^{j\dagger}\Sigma_\chi^\dagger\Big)$	0
$O^{\mathrm{C}}_{LL,2}$	$\mathrm{Tr}(P_L^i\Sigma_\chi)\,\mathrm{Tr}\Big(P_L^{i\dagger}\Sigma_\chi^\dagger\Big)\,\mathrm{Tr}\Big(P_L^{j\dagger}P_L^j\Big)$	$3\pi_3^\dagger\pi_3/(8f_\chi^2)$
$O^{\mathrm{C}}_{LL,3}$	$\mathrm{Tr}(P_L^i\Sigma_\chi)\,\mathrm{Tr}\Big(P_L^{j\dagger}\Sigma_\chi^\dagger\Big)\,\mathrm{Tr}\Big(P_L^{j\dagger}P_L^i\Big)+\mathrm{h.c.}$	$\pi_3^\dagger\pi_3/(8f_\chi^2)$
$O^{\mathrm{C}}_{LL,4}$	$\mathrm{Tr}(P_L^i\Sigma_\chi)\,\mathrm{Tr}\big(P_L^j\Sigma_\chi\big)\,\mathrm{Tr}\Big(P_L^{i\dagger}\Sigma_\chi^\dagger P_L^{j\dagger}\Sigma_\chi^\dagger\Big)+\mathrm{h.c.}$	0
$O^{\mathrm{C}}_{LL,5}$	$\mathrm{Tr}\Big(P_L^{i\dagger}P_L^i\Big)\,\mathrm{Tr}\Big(P_L^{j\dagger}P_L^j\Big)$	$9/4$
$O^{\mathrm{C}}_{LL,6}$	$\mathrm{Tr}\Big(P_L^{i\dagger}P_L^j\Big)\,\mathrm{Tr}\Big(P_L^{j\dagger}P_L^i\Big)$	$3/4$
$O^{\mathrm{C}}_{LL,7}$	$\mathrm{Tr}\big(P_L^i\Sigma P_L^j\Sigma\big)\,\mathrm{Tr}\Big(P_L^{i\dagger}\Sigma_\chi^\dagger P_L^{j\dagger}\Sigma_\chi^\dagger\Big)$	0
$O^{\mathrm{C}}_{LL,8}$	$\mathrm{Tr}(P_L^i\Sigma_\chi)\,\mathrm{Tr}\Big(P_L^jP_L^{j\dagger}\Sigma_\chi^\dagger P_L^{i\dagger}\Big)+\mathrm{h.c.}$	$\pi_3^\dagger\pi_3/(8f_\chi^2)$
$O^{\mathrm{C}}_{LL,9}$	$\mathrm{Tr}\Big(P_L^{i\dagger}P_L^iP_L^{j\dagger}P_L^j\Big)$	$3/4$
$O^{\mathrm{C}}_{LL,10}$	$\mathrm{Tr}\Big(P_L^iP_L^{i\dagger}\Sigma_\chi^\dagger P_L^{j\dagger}P_L^j\Sigma_\chi\Big)$	$\pi_3^\dagger\pi_3/(8f_\chi^2)$
$O^{\mathrm{C}}_{LL,11}$	$\mathrm{Tr}\Big(P_L^iP_L^{j\dagger}\Sigma_\chi^\dagger P_L^{i\dagger}P_L^j\Sigma_\chi\Big)$	0

Table A.2: Color singlet operators with up to four spurions $P_L \in \overline{\mathbf{3}}$. We also show the expansion to second order in the pNGBs. The operators for the right-handed spurions $P_R \in \mathbf{3}$ are identical after replacing $L \to R$.

and $P^\dagger\Sigma^\dagger$ that transform like an adjoint. Where this form is not obvious, like $P^\dagger P$, it can be recovered by inserting $\mathbb{1} = \Sigma^\dagger\Sigma$. We now separate ΣP into its trace and the traceless part,

$$\Sigma P = \Sigma P\Big|_{\not\mathrm{tr}} + \frac{1}{6}\,\mathrm{Tr}(\Sigma P)\mathbb{1}_6. \tag{A.3}$$

Since the adjoint decomposes as $\mathbf{35}_{\mathrm{SU}(6)} \to \mathbf{14}_{\mathrm{Sp}(6)} + \mathbf{21}_{\mathrm{Sp}(6)}$, of which only $\mathbf{14}_{\mathrm{Sp}(6)}$ appears in P, the traceless part of ΣP must contain the $\mathbf{14}_{\mathrm{Sp}(6)}$ while the second term is the $\mathbf{1}_{\mathrm{Sp}(6)}$. The same reasoning applies to $P^\dagger\Sigma^\dagger$ and the matrices with the reversed order. Thus, the trace $\mathrm{Tr}(\Sigma P)$ only contains the singlet. The trace of a product,

$$\mathrm{Tr}(\Sigma P\Sigma P) = \mathrm{Tr}(\Sigma P\Big|_{\not\mathrm{tr}}\Sigma P\Big|_{\not\mathrm{tr}}) + \frac{1}{6}\,\mathrm{Tr}(\Sigma P)\,\mathrm{Tr}(\Sigma P), \tag{A.4}$$

can be built from a trace of two $\mathbf{14}_{\mathrm{Sp}(6)}$ and the square of the singlet. Such a decomposition can be performed for all operators in Tab. A.1, which shows that our SU(6) invariant basis is equivalent to determining the Sp(6) invariants, so no operators are missing.

Name	Operator	Expansion to $\mathcal{O}(\Pi_\chi^2)$
$O^{\mathrm{C}}_{LR,1}$	$\mathrm{Tr}(P_L^i\Sigma_\chi)\,\mathrm{Tr}(P_R^i\Sigma_\chi)\,\mathrm{Tr}\Big(P_L^{j\dagger}\Sigma_\chi^\dagger\Big)\,\mathrm{Tr}\Big(P_R^{j\dagger}\Sigma_\chi^\dagger\Big)$	0
$O^{\mathrm{C}}_{LR,2}$	$\mathrm{Tr}(P_L^i\Sigma_\chi)\,\mathrm{Tr}\big(P_R^j\Sigma_\chi\big)\,\mathrm{Tr}\Big(P_L^{i\dagger}\Sigma_\chi^\dagger\Big)\,\mathrm{Tr}\Big(P_R^{j\dagger}\Sigma_\chi^\dagger\Big)$	0
$O^{\mathrm{C}}_{LR,3}$	$\mathrm{Tr}(P_L^i\Sigma_\chi)\,\mathrm{Tr}\Big(P_L^{i\dagger}\Sigma_\chi^\dagger\Big)\,\mathrm{Tr}\Big(P_R^{j\dagger}P_R^j\Big)$	$3\pi_3^\dagger\pi_3/(8f_\chi^2)$
$O^{\mathrm{C}}_{LR,4}$	$\mathrm{Tr}(P_R^i\Sigma_\chi)\,\mathrm{Tr}\Big(P_R^{i\dagger}\Sigma_\chi^\dagger\Big)\,\mathrm{Tr}\Big(P_L^{j\dagger}P_L^j\Big)$	$3\pi_3^\dagger\pi_3/(8f_\chi^2)$
$O^{\mathrm{C}}_{LR,5}$	$\mathrm{Tr}(P_L^i\Sigma_\chi)\,\mathrm{Tr}\Big(P_R^{j\dagger}\Sigma_\chi^\dagger\Big)\,\mathrm{Tr}\Big(P_L^{j\dagger}P_R^i\Big)+\mathrm{h.c.}$	0
$O^{\mathrm{C}}_{LR,6}$	$\mathrm{Tr}(P_L^i\Sigma_\chi)\,\mathrm{Tr}\Big(P_R^{j\dagger}\Sigma_\chi^\dagger\Big)\,\mathrm{Tr}\Big(P_L^{i\dagger}P_R^j\Big)+\mathrm{h.c.}$	0
$O^{\mathrm{C}}_{LR,7}$	$\mathrm{Tr}(P_L^i\Sigma_\chi)\,\mathrm{Tr}(P_R^i\Sigma_\chi)\,\mathrm{Tr}\Big(P_L^{j\dagger}\Sigma_\chi^\dagger P_R^{j\dagger}\Sigma_\chi^\dagger\Big)+\mathrm{h.c.}$	$-3\pi_3^\dagger\pi_3/(8f_\chi^2)$
$O^{\mathrm{C}}_{LR,8}$	$\mathrm{Tr}(P_L^i\Sigma_\chi)\,\mathrm{Tr}\big(P_R^j\Sigma_\chi\big)\,\mathrm{Tr}\Big(P_L^{i\dagger}\Sigma_\chi^\dagger P_R^{j\dagger}\Sigma_\chi^\dagger\Big)+\mathrm{h.c.}$	$-\pi_3^\dagger\pi_3/(8f_\chi^2)$
$O^{\mathrm{C}}_{LR,9}$	$\mathrm{Tr}\Big(P_L^{i\dagger}P_L^i\Big)\,\mathrm{Tr}\Big(P_R^{j\dagger}P_R^j\Big)$	9/4
$O^{\mathrm{C}}_{LR,10}$	$\mathrm{Tr}\Big(P_L^{i\dagger}P_L^j\Big)\,\mathrm{Tr}\Big(P_R^{j\dagger}P_R^i\Big)$	3/4
$O^{\mathrm{C}}_{LR,11}$	$\mathrm{Tr}\Big(P_L^{i\dagger}P_R^j\Big)\,\mathrm{Tr}\Big(P_R^{j\dagger}P_L^i\Big)$	0
$O^{\mathrm{C}}_{LR,12}$	$\mathrm{Tr}\Big(P_L^{i\dagger}P_R^j\Big)\,\mathrm{Tr}\Big(P_R^{i\dagger}P_L^j\Big)$	0
$O^{\mathrm{C}}_{LR,13}$	$\mathrm{Tr}(P_L^i\Sigma P_R^i\Sigma)\,\mathrm{Tr}\Big(P_L^{j\dagger}\Sigma_\chi^\dagger P_R^{j\dagger}\Sigma_\chi^\dagger\Big)$	$9/4-(3\pi_8^a\pi_8^a+12\pi_3^\dagger\pi_3)/(16f_\chi^2)$
$O^{\mathrm{C}}_{LR,14}$	$\mathrm{Tr}\big(P_L^i\Sigma P_R^j\Sigma\big)\,\mathrm{Tr}\Big(P_L^{i\dagger}\Sigma_\chi^\dagger P_R^{j\dagger}\Sigma_\chi^\dagger\Big)$	$3/4-\pi_3^\dagger\pi_3/(4f_\chi^2)$
$O^{\mathrm{C}}_{LR,15}$	$\mathrm{Tr}(P_L^i\Sigma_\chi)\,\mathrm{Tr}\Big(P_R^jP_R^{j\dagger}\Sigma_\chi^\dagger P_L^{i\dagger}\Big)+\mathrm{h.c.}$	0
$O^{\mathrm{C}}_{LR,16}$	$\mathrm{Tr}(P_L^i\Sigma_\chi)\,\mathrm{Tr}\Big(P_R^iP_R^{j\dagger}\Sigma_\chi^\dagger P_L^{j\dagger}\Big)+\mathrm{h.c.}$	0
$O^{\mathrm{C}}_{LR,17}$	$\mathrm{Tr}(P_R^i\Sigma_\chi)\,\mathrm{Tr}\Big(P_L^jP_L^{j\dagger}\Sigma_\chi^\dagger P_R^{i\dagger}\Big)+\mathrm{h.c.}$	0
$O^{\mathrm{C}}_{LR,18}$	$\mathrm{Tr}(P_R^i\Sigma_\chi)\,\mathrm{Tr}\Big(P_L^iP_L^{j\dagger}\Sigma_\chi^\dagger P_R^{j\dagger}\Big)+\mathrm{h.c.}$	0
$O^{\mathrm{C}}_{LR,19}$	$\mathrm{Tr}\Big(P_L^{i\dagger}P_L^iP_R^{j\dagger}P_R^j\Big)$	0
$O^{\mathrm{C}}_{LR,20}$	$\mathrm{Tr}\Big(P_L^{i\dagger}P_L^jP_R^{i\dagger}P_R^j\Big)$	0
$O^{\mathrm{C}}_{LR,21}$	$\mathrm{Tr}\Big(P_L^iP_L^{i\dagger}\Sigma_\chi^\dagger P_R^{j\dagger}P_R^j\Sigma_\chi\Big)$	$3/4-\pi_3^\dagger\pi_3/(8f_\chi^2)$
$O^{\mathrm{C}}_{LR,22}$	$\mathrm{Tr}\Big(P_L^iP_L^{j\dagger}\Sigma_\chi^\dagger P_R^{j\dagger}P_R^i\Sigma_\chi\Big)$	$3/4-(3\pi_8^a\pi_8^a+8\pi_3^\dagger\pi_3)/(64f_\chi^2)$
$O^{\mathrm{C}}_{LR,23}$	$\mathrm{Tr}\Big(P_L^iP_R^{j\dagger}\Sigma_\chi^\dagger P_L^{i\dagger}P_R^j\Sigma_\chi\Big)$	0
$O^{\mathrm{C}}_{LR,24}$	$\mathrm{Tr}\Big(P_L^iP_R^{j\dagger}\Sigma_\chi^\dagger P_L^{j\dagger}P_R^i\Sigma_\chi\Big)$	0

Table A.3: Mixed color singlet operators with two $P_L \in \overline{\mathbf{3}}$ and two $P_R \in \mathbf{3}$. We also show the expansion to second order in the pNGBs. The operators are separated into panels according to the underlying SU(6) invariants in Tab. A.1.

B | Documentation of the CHM5 FeynRules Implementation

We document the CHM5 FeynRules implementation, which extends the eVLQ library [71] by the fields and interactions necessary to describe the composite Higgs model M5. The basis are the files sm.fr and VLQ_v4.fr, which adds VLQs X, T, B, Y with charges $5/3, 2/3, -1/3, -4/3$, respectively. Additional fields can be added by including different independent modules, which include the interactions with the SM and the VLQs. The following modules are available:

- eVLQ_S10.fr: Adds neutral color singlet scalar S_1^0. This extension was already implemented [69].
- eVLQ_S11.fr: Adds singly charged color singlet scalar S_1^1. This extension was already implemented [69].
- eVLQ_S12.fr: Adds doubly charged color singlet scalar S_1^2.
- eVLQ_Q1.fr: Adds color singlet fermions with charges $Q = 1$ (Q_1^1), $Q = 0$ (Q_1^0) and a Majorana ($Q_{1,M}^0$).
- eVLQ_Q8.fr: Adds color octet fermions with charges $Q = 1$ (Q_8^1), $Q = 0$ (Q_8^0) and a Majorana ($Q_{8,M}^0$).
- eVLQ_S80.fr: Adds neutral color octet scalar S_8^0.
- eVLQ_S323.fr: Adds color triplet scalar with charge $Q = 2/3$ ($S_3^{2/3}$).

An overview of the notation for the fields is given in Tab. B.1, where we also indicate the corresponding fields in M5. For modules that correspond to multiple fields, e.g. S10, we add copies of the corresponding files with the replacements S10 → S102,S103 etc.

In the following we present the Lagrangians for the new fields, excluding lepton and baryon number violating terms. The Lagrangians are formulated in the mass eigenbasis, so the fields are eigenstates of $\mathrm{SU}(3)_c \times \mathrm{U}(1)_{\mathrm{em}}$. We have summarized our notational conventions at the end of this chapter.

Field	Spin	$\mathrm{SU}(3)_c \times \mathrm{U}(1)_{\mathrm{em}}$	In FR	FR numbering	PDG code	BSM fields in M5
ν_ℓ	1/2	$\mathbf{1}_0$	`vl`	`F[1]`	12, 14, 16	
ℓ	1/2	$\mathbf{1}_{-1}$	`vl`	`F[2]`	11, 13, 15	
q_u	1/2	$\mathbf{3}_{+2/3}$	`uq`	`F[3]`	2, 4, 6	
q_d	1/2	$\mathbf{3}_{-1/3}$	`dq`	`F[4]`	1, 3, 5	
h	0	$\mathbf{1}_0$	`H`	`S[1]`	25	
A	1	$\mathbf{1}_0$	`A`	`V[1]`	22	
Z	1	$\mathbf{1}_0$	`Z`	`V[2]`	23	
W	1	$\mathbf{1}_{+1}$	`W`	`V[3]`	24	
g	1	$\mathbf{8}_0$	`G`	`V[4]`	21	
X	1/2	$\mathbf{3}_{+5/3}$	`x`	`F[5]`	6000005	$X_{5/3}$
T	1/2	$\mathbf{3}_{+2/3}$	`tp`	`F[6]`	6000006	T_1, T_2, T_3
B	1/2	$\mathbf{3}_{-1/3}$	`bp`	`F[7]`	6000007	B
Y	1/2	$\mathbf{3}_{-4/3}$	`y`	`F[8]`	6000008	–
S_1^0	0	$\mathbf{1}_0$	`S10`	`S[100]`	6100001	$a, \eta, \eta_1^0, \eta_3^0, \eta_5^0$
S_1^1	0	$\mathbf{1}_{+1}$	`S11`	`S[101]`	6100002	η_3^+, η_5^+
S_1^2	0	$\mathbf{1}_{+2}$	`S12`	`S[102]`	6100003	η_5^{++}
S_8^0	0	$\mathbf{8}_0$	`S80`	`S[800]`	6100800	π_8
$S_3^{2/3}$	0	$\mathbf{3}_{+2/3}$	`S323`	`S[323]`	6100300	π_3
Q_1^1	1/2	$\mathbf{1}_{+1}$	`Q11`	`F[1010]`	6000011	$\tilde{h}^+$
Q_1^0	1/2	$\mathbf{1}_0$	`Q10`	`F[1000]`	6000010	$\tilde{h}^0$
$Q_{1,M}^0$	1/2	$\mathbf{1}_0$	`Q10M`	`F[1001]`	6001010	$\tilde{B}$
Q_8^1	1/2	$\mathbf{8}_{+1}$	`Q81`	`F[8010]`	6000081	$\tilde{G}^+$
Q_8^0	1/2	$\mathbf{8}_0$	`Q80`	`F[8000]`	6000080	$\tilde{G}^0$
$Q_{8,M}^0$	1/2	$\mathbf{8}_0$	`Q80M`	`F[8001]`	6001080	$\tilde{g}$

Table B.1: FeynRules (FR) notation for SM and BSM fields. The `sm.fr` and `VLQ_v4.fr` (upper two panels) form the basis of the implementation. For the fields in the lower panel, the interactions with the upper two are implemented. The right most column shows the fields in M5 that can be described with the respective module.

Coupling	FeynRules	LH Block
$\Gamma^{Xd,L}_{S_1^2}$	`GS12XDL`	`GS12XDL`
$\Gamma^{Xd,R}_{S_1^2}$	`GS12XDR`	`GS12XDR`
$\Gamma^{Yu,L}_{S_1^2}$	`GS12YUL`	`GS12YUL`
$\Gamma^{Yu,R}_{S_1^2}$	`GS12YUR`	`GS12YUR`
$\Gamma^{XB,L}_{S_1^2}$	`GS12XBL`	`GS12XBL`
$\Gamma^{XB,R}_{S_1^2}$	`GS12XBR`	`GS12XBR`
$\Gamma^{YT,L}_{S_1^2}$	`GS12YTL`	`GS12YTL`
$\Gamma^{YT,R}_{S_1^2}$	`GS12YTR`	`GS12YTR`

Coupling	FeynRules	LH Block	LH counter
$\kappa^{W}_{S_1^2}$	`KS12W`	`KS12W`	
$\tilde{\kappa}^{W}_{S_1^2}$	`KP12W`	`KP12W`	
$\kappa^{h,(1)}_{S_1^2}$	`KS12H1`	`KS12H`	1
$\kappa^{h,(2)}_{S_1^2}$	`KS12H2`	`KS12H`	2
$\kappa^{hh}_{S_1^2}$	`KS12HH`	`KS12H`	3

Table B.2: FeynRules notation for the coupling parameters for S_1^2 in Eq. (B.1). $\Gamma^{Xd,L/R}_{S_1^2}$, $\Gamma^{Yu,L/R}_{S_1^2}$ are vectors in flavor space, the remaining couplings are scalars.

Doubly charged scalar singlets: `eVLQ_S12.fr` General Lagrangian for $S_1^2 \in \mathbf{1}_2$:

$$\begin{aligned}
\mathcal{L}_{S_1^2} = {} & (D_\mu S_1^2)^\dagger D^\mu S_1^2 - m^2_{S_1^2}(S_1^2)^\dagger S_1^2 && \text{(B.1a)}\\
& + \left[S_1^2 \overline{X}\left(\Gamma^{Xd,L}_{S_1^1} P_L + \Gamma^{Xd,R}_{S_1^1} P_R\right) q_d + (S_1^2)^\dagger \overline{Y}\left(\Gamma^{Yu,L}_{S_1^1} P_L + \Gamma^{Yu,R}_{S_1^1} P_R\right) q_u + \text{h.c.}\right] && \text{(B.1b)}\\
& + \left[S_1^2 \overline{X}\left(\Gamma^{XB,L}_{S_1^1} P_L + \Gamma^{XB,R}_{S_1^1} P_R\right) B + (S_1^2)^\dagger \overline{Y}\left(\Gamma^{YT,L}_{S_1^1} P_L + \Gamma^{YT,R}_{S_1^1} P_R\right) T + \text{h.c.}\right] && \text{(B.1c)}\\
& + \left[\kappa^{W}_{S_1^2} \frac{g^2}{16\pi^2 v} S_1^2 W^{-,\mu\nu} W^-_{\mu\nu} + \tilde{\kappa}^{W}_{S_1^2} \frac{g^2}{16\pi^2 v} S_1^2 W^{-,\mu\nu} \tilde{W}^-_{\mu\nu} + \text{h.c.}\right] && \text{(B.1d)}\\
& + \frac{1}{v}\kappa^{h,(1)}_{S_1^2} h (D_\mu S_1^2)^\dagger D^\mu S_1^2 + \kappa^{h,(2)}_{S_1^2} v h (S_1^2)^\dagger S_1^2 + \kappa^{hh}_{S_1^2} h^2 (S_1^2)^\dagger S_1^2 && \text{(B.1e)}
\end{aligned}$$

The FeynRules notation for the couplings is shown in Tab. B.2.

Scalar triplets: `eVLQ_S323.fr` General Lagrangian for $S_3^{2/3} \in \mathbf{1}_2$:

$$\begin{aligned}
\mathcal{L}_{S_3^{2/3}} = {} & (D_\mu S_3^{2/3})^\dagger D^\mu S_3^{2/3} - m^2_{S_3^{2/3}} (S_3^{2/3})^\dagger S_3^{2/3} && \text{(B.2a)}\\
& + \frac{1}{v}\kappa^{h,(1)}_{S_3^{2/3}} h (D_\mu S_3^{2/3})^\dagger D^\mu S_3^{2/3} + \kappa^{h,(2)}_{S_3^{2/3}} v h (S_3^{2/3})^\dagger S_3^{2/3} + \kappa^{hh}_{S_3^{2/3}} h^2 (S_3^{2/3})^\dagger S_3^{2/3} && \text{(B.2b)}
\end{aligned}$$

The FeynRules notation for the couplings is shown in Tab. B.3.

Coupling	FeynRules	LH Block	LH counter
$\kappa^{h,(1)}_{S_3^{2/3}}$	KS323H1	KS323H	1
$\kappa^{h,(2)}_{S_3^{2/3}}$	KS323H2	KS323H	2
$\kappa^{hh}_{S_3^{2/3}}$	KS323HH	KS323H	3

Table B.3: FeynRules notation for the coupling parameters for $S_3^{2/3}$ in Eq. (B.2). All couplings are scalars in flavor space.

Scalar octets: `eVLQ_S8.fr` General Lagrangian for $S_8^0 = S_8^{0,a}T^a \in \mathbf{8}_0$:

$$\begin{aligned}
\mathcal{L}_{S_8^0} = {} & \frac{1}{2}D_\mu S_8^{0,a} D^\mu S_8^{0,a} - \frac{1}{2}m^2_{S_8^0} S_8^{0,a} S_8^{0,a} && \text{(B.3a)}\\
& + \left[\overline{B}\left(\Gamma^{Bd,L}_{S_8^0}P_L + \Gamma^{Bd,R}_{S_8^0}P_R\right) S_8^0 q_d + \overline{T}\left(\Gamma^{Tu,L}_{S_8^0}P_L + \Gamma^{Tu,R}_{S_8^0}P_R\right) S_8^0 q_u + \text{h.c.}\right] && \text{(B.3b)}\\
& + \left[\overline{q}_u\left(\Gamma^{u}_{S_8^0} + \mathrm{i}\gamma_5\tilde{\Gamma}^{u}_{S_8^0}\right) S_8^0 q_u + \overline{q}_d\left(\Gamma^{d}_{S_8^0} + \mathrm{i}\gamma_5\tilde{\Gamma}^{d}_{S_8^0}\right) S_8^0 q_d + \text{h.c.}\right] && \text{(B.3c)}\\
& + \Big[\overline{X}\left(\Gamma^{X}_{S_8^0} + \mathrm{i}\gamma_5\tilde{\Gamma}^{X}_{S_8^0}\right) S_8^0 X + \overline{T}\left(\Gamma^{T}_{S_8^0} + \mathrm{i}\gamma_5\tilde{\Gamma}^{T}_{S_8^0}\right) S_8^0 T \\
& \quad + \overline{B}\left(\Gamma^{B}_{S_8^0} + \mathrm{i}\gamma_5\tilde{\Gamma}^{B}_{S_8^0}\right) S_8^0 B + \overline{Y}\left(\Gamma^{Y}_{S_8^0} + \mathrm{i}\gamma_5\tilde{\Gamma}^{Y}_{S_8^0}\right) S_8^0 Y + \text{h.c.}\Big] && \text{(B.3d)}\\
& + \kappa^{G}_{S_8^0}\frac{g_s^2}{16\pi^2 v}\,\mathrm{Tr}\big(S_8^0 G^{\mu\nu}G_{\mu\nu}\big) + \tilde{\kappa}^{G}_{S_8^0}\frac{g_s^2}{16\pi^2 v}\,\mathrm{Tr}\Big(S_8^0 G^{\mu\nu}\tilde{G}_{\mu\nu}\Big) && \text{(B.3e)}\\
& + \kappa^{GZ}_{S_8^0}\frac{g_s e/s_W c_W}{16\pi^2 v} S_8^{0,a} G^{a,\mu\nu} Z_{\mu\nu} + \kappa^{GA}_{S_8^0}\frac{g_s e}{16\pi^2 v} S_8^{0,a} G^{a,\mu\nu} A_{\mu\nu} && \text{(B.3f)}\\
& + \tilde{\kappa}^{GZ}_{S_8^0}\frac{g_s e/s_W c_W}{16\pi^2 v} S_8^{0,a} G^{a,\mu\nu} \tilde{Z}_{\mu\nu} + \tilde{\kappa}^{GA}_{S_8^0}\frac{g_s e}{16\pi^2 v} S_8^{0,a} G^{a,\mu\nu} \tilde{A}_{\mu\nu} && \text{(B.3g)}\\
& + \frac{1}{v}\kappa^{h,(1)}_{S_8^0} h (D_\mu S_8^0)^a (D^\mu S_8^0)^a + \kappa^{h,(2)}_{S_8^0} v h S_8^{0,a} S_8^{0,a} + \kappa^{hh}_{S_8^0} h^2 S_8^{0,a} S_8^{0,a} && \text{(B.3h)}
\end{aligned}$$

The FeynRules notation for the couplings is shown in Tab. B.4.

Fermion singlets: `VLQ1.fr` General Lagrangian for Dirac fermion $Q_1^1 \in \mathbf{1}_{+1}$:

$$\mathcal{L}_{Q_1^1} = \overline{Q}_1^1\left(\mathrm{i}\not{D} - m_{Q_1^1}\right) Q_1^1 + \left(\frac{g}{2c_W}\overline{Q}_1^1 \not{Z}\left[\kappa^{Z}_{Q_1^1} + \mathrm{i}\gamma_5\tilde{\kappa}^{Z}_{Q_1^1}\right] Q_1^1 + \text{h.c.}\right) \tag{B.4}$$

General Lagrangian for Dirac fermion $Q_1^0 \in \mathbf{1}_0$:

$$\mathcal{L}_{Q_1^0} = \overline{Q}_1^0\left(\mathrm{i}\not{\partial} - m_{Q_1^0}\right) Q_1^0 + \left(\frac{g}{2c_W}\overline{Q}_1^0 \not{Z}\left[\kappa^{Z}_{Q_1^0} + \mathrm{i}\gamma_5\tilde{\kappa}^{Z}_{Q_1^0}\right] Q_1^0 + \text{h.c.}\right) \tag{B.5}$$

General Lagrangian for Majorana fermion $Q^0_{1,M} \in \mathbf{1}_0$:

$$\mathcal{L}_{Q^0_{1,M}} = \frac{1}{2}\overline{Q}^0_{1,M}\left(\mathrm{i}\not{\partial} - m_{Q^0_{1,M}}\right) Q^0_{1,M} + \left(\tilde{\kappa}^{Z}_{Q^0_{1,M}}\frac{g}{4c_W}\overline{Q}^0_{1,M}\not{Z}\,\mathrm{i}\gamma_5 Q^0_{1,M} + \text{h.c.}\right) \tag{B.6}$$

The FeynRules notation for the couplings is shown in Tab. B.5.

Coupling	FeynRules	LH Block
$(\Gamma^u_{S_8^0})_{ij}$	`GS80U`	`GS80U`
$(\tilde{\Gamma}^u_{S_8^0})_{ij}$	`GP80U`	`GP80U`
$(\Gamma^d_{S_8^0})_{ij}$	`GS80D`	`GS80D`
$(\tilde{\Gamma}^d_{S_8^0})_{ij}$	`GP80D`	`GP80D`
$\Gamma^X_{S_8^0}$	`GS80X`	`GS80X`
$\tilde{\Gamma}^X_{S_8^0}$	`GP80X`	`GP80X`
$\Gamma^T_{S_8^0}$	`GS80T`	`GS80T`
$\tilde{\Gamma}^T_{S_8^0}$	`GP80T`	`GP80T`
$\Gamma^B_{S_8^0}$	`GS80B`	`GS80B`
$\tilde{\Gamma}^B_{S_8^0}$	`GP80B`	`GP80B`
$\Gamma^Y_{S_8^0}$	`GS80Y`	`GS80Y`
$\tilde{\Gamma}^Y_{S_8^0}$	`GP80Y`	`GP80Y`

Coupling	FeynRules	LH Block	LH counter
$\kappa^G_{S_8^0}$	`KS80G`	`KS80VV`	1
$\tilde{\kappa}^G_{S_8^0}$	`KP80G`	`KP80VV`	1
$\kappa^{GZ}_{S_8^0}$	`KS80GZ`	`KS80VV`	2
$\tilde{\kappa}^{GZ}_{S_8^0}$	`KP80GZ`	`KP80VV`	2
$\kappa^{GA}_{S_8^0}$	`KS80GA`	`KS80VV`	3
$\tilde{\kappa}^{GA}_{S_8^0}$	`KP80GA`	`KP80VV`	3
$\kappa^{h,(1)}_{S_8^0}$	`KS80H1`	`KS80H`	1
$\kappa^{h,(2)}_{S_8^0}$	`KS80H2`	`KS80H`	2
$\kappa^{hh}_{S_8^0}$	`KS80HH`	`KS80H`	3

Coupling	FeynRules	LH Block
$\Gamma^{Bd,L}_{S_8^0}$	`GS80BDL`	`GS80BDL`
$\Gamma^{Bd,R}_{S_8^0}$	`GS80BDR`	`GS80BDR`
$\Gamma^{Tu,L}_{S_8^0}$	`GS80TUL`	`GS80TUL`
$\Gamma^{Tu,R}_{S_8^0}$	`GS80TUL`	`GS80TUL`

Table B.4: FeynRules notation for the coupling parameters for S_8^0 as defined in Eq. (B.3). All κ are scalars. Γ^f and $\tilde{\Gamma}^f$ are matrices in flavor space for $f = u, d$ and scalars for $f = X, T, B, Y$. $\Gamma^{Bd,L/R}, \Gamma^{Tu,L/R}$ are vectors in flavor space.

Coupling	FeynRules	LH Block	Coupling	FeynRules	LH Block
$\kappa^Z_{Q^1_1}$	KQ11Z	KQ11Z	$\kappa^Z_{Q^1_8}$	KQ81Z	KQ81Z
$\tilde{\kappa}^Z_{Q^1_1}$	K5Q11Z	K5Q11Z	$\tilde{\kappa}^Z_{Q^1_8}$	K5Q81Z	K5Q81Z
$\kappa^Z_{Q^0_1}$	KQ10Z	KQ10Z	$\kappa^Z_{Q^0_8}$	KQ80Z	KQ80Z
$\tilde{\kappa}^Z_{Q^0_1}$	K5Q10Z	K5Q10Z	$\tilde{\kappa}^Z_{Q^0_8}$	K5Q80Z	K5Q80Z
$\tilde{\kappa}^Z_{Q^0_{1,M}}$	K5Q10MZ	K5Q10MZ	$\tilde{\kappa}^Z_{Q^0_{8,M}}$	K5Q80MZ	K5Q80MZ

Table B.5: FeynRules notation for the coupling parameters for Q_1 and Q_8 as defined in Eqs. (B.4)-(B.9). All couplings are scalars parameters.

Fermion octets: `VLQ8.fr` General Lagrangian for Dirac fermion $Q^1_8 \in \mathbf{8}_{+1}$:

$$\mathcal{L}_{Q^1_8} = \overline{Q}^{1,a}_8 \left(\mathrm{i}\not{D} - m_{Q^1_8}\right) Q^{1,a}_8 + \left(\frac{g}{2c_W}\overline{Q}^{1,a}_8 \not{Z} \left[\kappa^Z_{Q^1_8} + \mathrm{i}\gamma_5\tilde{\kappa}^Z_{Q^1_8}\right] Q^{1,a}_8 + \mathrm{h.c.}\right) \tag{B.7}$$

General Lagrangian for Dirac fermion $Q^0_8 \in \mathbf{8}_0$:

$$\mathcal{L}_{Q^0_8} = \overline{Q}^{0,a}_8 \left(\mathrm{i}\not{D} - m_{Q^0_8}\right) Q^{0,a}_8 + \left(\frac{g}{2c_W}\overline{Q}^{0,a}_8 \not{Z} \left[\kappa^Z_{Q^0_8} + \mathrm{i}\gamma_5\tilde{\kappa}^Z_{Q^0_8}\right] Q^{0,a}_8 + \mathrm{h.c.}\right) \tag{B.8}$$

General Lagrangian for Majorana fermion $Q^0_{8,M} \in \mathbf{8}_0$:

$$\mathcal{L}_{Q^0_{8,M}} = \frac{1}{2}\overline{Q}^{0,a}_{8,M} \left(\mathrm{i}\not{D} - m_{Q^0_{8,M}}\right) Q^{0,a}_{8,M} + \left(\tilde{\kappa}^Z_{Q^0_{8,M}} \frac{g}{4c_W}\overline{Q}^{0,a}_{8,M} \not{Z}\, \mathrm{i}\gamma_5 Q^{0,a}_{8,M} + \mathrm{h.c.}\right) \tag{B.9}$$

The FeynRules notation for the parameters is shown in Table B.5.

Model-specific interactions: `CHM5.fr` We have implemented selected vertices that mix different modules:

$$\begin{aligned}
\mathcal{L}_{\mathrm{M5}} = {} & C^{S_3^{2/3}t}_{Q^0_{8,M}} (S_3^{2/3})^\dagger \overline{Q}^0_{8,M} P_R t + C^{S_3^{2/3}t}_{Q^0_8} (S_3^{2/3})^\dagger \overline{Q}^{0,c}_{8,M} P_L t + C^{S_3^{2/3}t}_{Q^1_8} (S_3^{2/3})^\dagger \overline{Q}^{1,c}_8 P_L b && \text{(B.10a)}\\
& + \frac{1}{2} C^{S_8^0 Q^0_{1,M}}_{Q^0_{8,M}} S_8^{0,a} \overline{Q}^{0,a}_{8,M} Q^0_{1,M} + C^{S_8^0 Q^0_1}_{Q^0_8} S_8^{0,a} \overline{Q}^{0,a}_8 Q^0_1 + C^{S_8^0 Q^1_1}_{Q^1_8} S_8^{0,a} \overline{Q}^{0,a}_8 Q^1_1 && \text{(B.10b)}\\
& + \frac{g}{2c_W} C^{Q^0_{1,M} Z}_{Q^0_1} \overline{Q}^0_1 \not{Z} Q^0_{1,M} + \frac{g}{\sqrt{2}} C^{Q^0_1 W}_{Q^1_1} \overline{Q}^1_1 \not{W}^+ Q^0_1 + C^{Q^0_{1,M} t}_{S_3^{2/3}} (S_3^{2/3})^\dagger \overline{Q}^0_{1,M} P_R t + \mathrm{h.c.} && \text{(B.10c)}
\end{aligned}$$

These are necessary for describing the gluoni and stop decays studied in Chapter 4. The FeynRules notation for the parameters is shown in Table B.6. The implemented vertices differ slightly from the simplified models in Section 4.1.3 in that the coupling to S^0_8 does not have a $\mathrm{i}\gamma_5$. This does not affect the results since the differences can be absorbed in the coupling constants and the branching ratios remain the same.

For scenario (S3), we used the following auxiliary vertex,

$$\mathcal{L}_{\mathrm{aux}} = C^{S^1_1 Q^0_{1,M}}_{Q^1_1} \overline{Q}^1_1 Q^0_{1,M} S^1_1 + \mathrm{h.c.}\,, \tag{B.11}$$

with a very light S^1_1 for the decay $Q^1_1 \to Q^0_{1,M} S^1_1 \to Q^0_{1,M} e^+ \nu_e$ instead of an off-shell W^+. The decay $S^1_1 \to e^+\nu_e$ is implemented in `eVLQ_S10.fr`.

Coupling	FeynRules	LH Block
$C^{S_3^{2/3}t}_{Q^0_{8,M}}$	CQ80MS323t	CQ80MS323t
$C^{S_3^{2/3}t}_{Q^0_8}$	CQ80S323t	CQ80S323t
$C^{S_3^{2/3}t}_{Q^1_8}$	CQ81S323t	CQ81S323t
$C^{S_8^0 Q^0_{1,M}}_{Q^0_{8,M}}$	CQ80MS80Q10M	CQ80MS80Q10M
$C^{S_8^0 Q_1^0}_{Q_8^0}$	CQ80S80Q10	CQ80S80Q10
$C^{S_8^0 Q_1^1}_{Q_8^1}$	CQ81S80Q11	CQ81S80Q11
$C^{Q^0_{1,M}t}_{S_3^{2/3}}$	CS323Q10Mt	CS323Q10Mt
$C^{S_1^1 Q^0_{1,M}}_{Q_1^1}$	CQ11Q10MS11	CQ11Q10MS11

Table B.6: FeynRules notation for the coupling parameters in Eqs. (B.10) and (B.11). All couplings are scalar parameters.

FeynRules Conventions We mostly follow the notation of [69].

- $X^B_A \to$ XAB. Exception: Majorana fermion $Q^0_{1,M} \to$ Q10M
- Field names are of the form $Q^{e_Q}_{\mathbf{C}}$ for fermions and $S^{e_S}_{\mathbf{C}}$ for scalars, where $\mathbf{C}$ is the color irrep and $e_{Q,S}$ the field's electric charge. For example, a color octet fermion with electric charge 1 is denoted by Q^1_8.
- Coupling constants for a scalar to two fermions are denoted by Γ, couplings of a scalar to two vector bosons are κ. The index of the coupling constant is the scalar, the superscript specifies the fermions/vector bosons.
- Couplings for a (Γ) or pseudoscalar ($\tilde{\Gamma}$) to fermions are called GS10... and GP10..., respectively, for S^0_1.
- Notwithstanding the previous points, the model-specific couplings in CHM5.fr that facilitate the decay $X \to YZ$ are denoted by C^{YZ}_X.
- For a duplicate field, e.g. a second copy of the neutral scalar S^0_1, the file is copied and the field and couplings are renamed by replacing S10 $\to$ S102.

List of Abbreviations

ABJ	Adler-Bell-Jackiw
BSM	Beyond the Standard Model
CCWZ	Callan-Coleman-Wess-Zumino
CHM	Composite Higgs model
CL	Confidence level
CM	CheckMATE
CP	Charge-Parity
DM	Dark matter
EW	Electroweak
EWSB	Electroweak symmetry breaking
FR	FeynRules
IR	Infrared
irrep	Irreducible representation
HC	Hypercolor
LEC	Low-energy constant
LH	Les Houches
LO	Leading order
MA	MadAnalysis5
MAC	Maximally attractive channel
MC	Monte Carlo
MCHM	Minimal composite Higgs model
MET	Missing transverse energy
MG	MadGraph5_aMC@NLO
PDF	Parton distribution function
PDG	Particle Data Group
NLO	Next-to-leading order
pNGB	pseudo Nambu-Goldstone boson
QCD	Quantum chromodynamics
RGE	Renormalization group equation
SM	Standard model
SR	Signal region
SUSY	Supersymmetry
UFO	Universal FeynRules Output
UV	Ultraviolet
VLQ	Vector-like quark
WZW	Wess-Zumino-Witten

Bibliography

[1] **ATLAS** Collaboration, G. Aad *et al.*, "Observation of a new particle in the search for the Standard Model Higgs boson with the ATLAS detector at the LHC," *Phys. Lett. B* **716** (2012) 1–29, arXiv:1207.7214 [hep-ex].

[2] **CMS** Collaboration, S. Chatrchyan *et al.*, "Observation of a New Boson at a Mass of 125 GeV with the CMS Experiment at the LHC," *Phys. Lett. B* **716** (2012) 30–61, arXiv:1207.7235 [hep-ex].

[3] G. Panico and A. Wulzer, *The Composite Nambu-Goldstone Higgs*, vol. 913 of *Lect. Notes Phys.* Springer, 2016. arXiv:1506.01961 [hep-ph].

[4] G. F. Giudice, "Naturally Speaking: The Naturalness Criterion and Physics at the LHC," in *Perspectives on LHC Physics*, G. Kane and A. Pierce, eds., pp. 155–178. World Scientific, 2008. arXiv:0801.2562 [hep-ph].

[5] G. 't Hooft, "Naturalness, chiral symmetry, and spontaneous chiral symmetry breaking," *NATO Sci. Ser. B* **59** (1980) 135–157.

[6] L. Susskind, "Dynamics of Spontaneous Symmetry Breaking in the Weinberg-Salam Theory," *Phys. Rev. D* **20** (1979) 2619–2625.

[7] D. B. Kaplan and H. Georgi, "SU(2)×U(1) breaking by vacuum misalignment," *Phys. Lett. B* **136** no. 3, (1984) 183–186.

[8] D. B. Kaplan, H. Georgi, and S. Dimopoulos, "Composite Higgs scalars," *Phys. Lett. B* **136** no. 3, (1984) 187–190.

[9] M. J. Dugan, H. Georgi, and D. B. Kaplan, "Anatomy of a composite Higgs model," *Nucl. Phys. B* **254** (1985) 299–326.

[10] D. B. Kaplan, "Flavor at SSC energies: A New mechanism for dynamically generated fermion masses," *Nucl. Phys. B* **365** (1991) 259–278.

[11] G. Ferretti and D. Karateev, "Fermionic UV completions of Composite Higgs models," *JHEP* **03** (2014) 077, arXiv:1312.5330 [hep-ph].

[12] G. Ferretti, "Gauge theories of Partial Compositeness: Scenarios for Run-II of the LHC," *JHEP* **06** (2016) 107, arXiv:1604.06467 [hep-ph].

[13] A. Belyaev, G. Cacciapaglia, H. Cai, G. Ferretti, T. Flacke, A. Parolini, and H. Serodio, "Di-boson signatures as Standard Candles for Partial Compositeness," *JHEP* **01** (2017) 094, arXiv:1610.06591 [hep-ph]. [Erratum: *JHEP* **12** (2017) 088].

[14] A. Alloul, N. D. Christensen, C. Degrande, C. Duhr, and B. Fuks, "FeynRules 2.0 - A complete toolbox for tree-level phenomenology," *Comput. Phys. Commun.* **185** (2014) 2250–2300, arXiv:1310.1921 [hep-ph].

[15] J. Alwall, R. Frederix, S. Frixione, V. Hirschi, F. Maltoni, O. Mattelaer, H. S. Shao, T. Stelzer, P. Torrielli, and M. Zaro, "The automated computation of tree-level and next-to-leading order differential cross sections, and their matching to parton shower simulations," *JHEP* **07** (2014) 079, arXiv:1405.0301 [hep-ph].

[16] E. Conte, B. Fuks, and G. Serret, "MadAnalysis 5, A User-Friendly Framework for Collider Phenomenology," *Comput. Phys. Commun.* **184** (2013) 222–256, arXiv:1206.1599 [hep-ph].

[17] E. Conte, B. Dumont, B. Fuks, and C. Wymant, "Designing and recasting LHC analyses with MadAnalysis 5," *Eur. Phys. J. C* **74** no. 10, (2014) 3103, arXiv:1405.3982 [hep-ph].

[18] B. Dumont, B. Fuks, S. Kraml, S. Bein, G. Chalons, E. Conte, S. Kulkarni, D. Sengupta, and C. Wymant, "Toward a public analysis database for LHC new physics searches using MadAnalysis 5," *Eur. Phys. J. C* **75** no. 2, (2015) 56, arXiv:1407.3278 [hep-ph].

[19] E. Conte and B. Fuks, "Confronting new physics theories to LHC data with MadAnalysis 5," *Int. J. Mod. Phys. A* **33** no. 28, (2018) 1830027, arXiv:1808.00480 [hep-ph].

[20] M. Drees, H. Dreiner, D. Schmeier, J. Tattersall, and J. S. Kim, "CheckMATE: Confronting your Favourite New Physics Model with LHC Data," *Comput. Phys. Commun.* **187** (2015) 227–265, arXiv:1312.2591 [hep-ph].

[21] D. Dercks, N. Desai, J. S. Kim, K. Rolbiecki, J. Tattersall, and T. Weber, "CheckMATE 2: From the model to the limit," *Comput. Phys. Commun.* **221** (2017) 383–418, arXiv:1611.09856 [hep-ph].

[22] R. Contino, "The Higgs as a Composite Nambu-Goldstone Boson," in *Physics of the Large and the Small. TASI 2009*, C. Csaki and S. Dodelson, eds. World Scientific, 2010. arXiv:1005.4269 [hep-ph].

[23] S. Weinberg, "Implications of dynamical symmetry breaking," *Phys. Rev. D* **13** no. 4, (1976) 974.

[24] S. Weinberg, "Implications of dynamical symmetry breaking: an addendum," *Phys. Rev. D* **19** no. 4, (1979) 1277.

[25] T. Plehn, *Lectures on LHC Physics*, vol. 844 of *Lect. Notes Phys.* Springer, 2012. arXiv:0910.4182 [hep-ph].

[26] J. Erdmenger, N. Evans, W. Porod, and K. S. Rigatos, "Gauge/gravity dual dynamics for the strongly coupled sector of composite Higgs models," *JHEP* **02** (2021) 058, arXiv:2010.10279 [hep-ph].

[27] J. Goldstone, "Field Theories with Superconductor Solutions," *Nuovo Cim.* **19** (1961) 154–164.

[28] J. Goldstone, A. Salam, and S. Weinberg, "Broken Symmetries," *Phys. Rev.* **127** (1962) 965–970.

[29] L.-X. Xu, J.-H. Yu, and S.-H. Zhu, "Holographic Completion of Minimal Neutral Naturalness Model and Deconstruction," arXiv:1905.12796 [hep-ph].

[30] K. Agashe, R. Contino, and A. Pomarol, "The Minimal composite Higgs model," *Nucl. Phys. B* **719** (2005) 165–187, arXiv:hep-ph/0412089.

[31] S. R. Coleman, J. Wess, and B. Zumino, "Structure of phenomenological Lagrangians. 1.," *Phys. Rev.* **177** (1969) 2239–2247.

[32] C. G. Callan, Jr., S. R. Coleman, J. Wess, and B. Zumino, "Structure of phenomenological Lagrangians. 2.," *Phys. Rev.* **177** (1969) 2247–2250.

[33] A. Agugliaro, *Composite Higgs: Theory and Phenomenology*. PhD thesis, Florence U., 2019.

[34] J. Wess and B. Zumino, "Consequences of anomalous Ward identities," *Phys. Lett. B* **37** (1971) 95–97.

[35] E. Witten, "Global Aspects of Current Algebra," *Nucl. Phys. B* **223** (1983) 422–432.

[36] J. Davighi, *Topological effects in particle physics phenomenology*. PhD thesis, Cambridge U., DAMTP, 2020.

[37] O. Kaymakcalan, S. Rajeev, and J. Schechter, "Nonabelian Anomaly and Vector Meson Decays," *Phys. Rev. D* **30** (1984) 594.

[38] S. Dimopoulos and L. Susskind, "Mass Without Scalars," *Nucl. Phys. B* **155** (1979) 237–252.

[39] E. Eichten and K. D. Lane, "Dynamical Breaking of Weak Interaction Symmetries," *Phys. Lett. B* **90** (1980) 125–130.

[40] R. Contino, L. Da Rold, and A. Pomarol, "Light custodians in natural composite Higgs models," *Phys. Rev. D* **75** (2007) 055014, arXiv:hep-ph/0612048.

[41] J. M. Maldacena, "The Large N limit of superconformal field theories and supergravity," *Adv. Theor. Math. Phys.* **2** (1998) 231–252, arXiv:hep-th/9711200.

[42] R. Contino, Y. Nomura, and A. Pomarol, "Higgs as a holographic pseudoGoldstone boson," *Nucl. Phys. B* **671** (2003) 148–174, arXiv:hep-ph/0306259.

[43] S. Raby, S. Dimopoulos, and L. Susskind, "Tumbling Gauge Theories," *Nucl. Phys. B* **169** (1980) 373–383.

[44] K. Agashe, R. Contino, L. Da Rold, and A. Pomarol, "A Custodial symmetry for $Zb\bar{b}$," *Phys. Lett. B* **641** (2006) 62–66, arXiv:hep-ph/0605341.

[45] J. Barnard, T. Gherghetta, and T. S. Ray, "UV descriptions of composite Higgs models without elementary scalars," *JHEP* **02** (2014) 002, arXiv:1311.6562 [hep-ph].

[46] G. Ferretti, "UV Completions of Partial Compositeness: The Case for a SU(4) Gauge Group," *JHEP* **06** (2014) 142, arXiv:1404.7137 [hep-ph].

[47] G. Cacciapaglia, G. Ferretti, T. Flacke, and H. Serôdio, "Light scalars in composite Higgs models," *Front. in Phys.* **7** (2019) 22, arXiv:1902.06890 [hep-ph].

[48] G. Cacciapaglia, A. Deandrea, T. Flacke, and A. M. Iyer, "Gluon-Photon Signatures for color octet at the LHC (and beyond)," *JHEP* **05** (2020) 027, arXiv:2002.01474 [hep-ph].

[49] N. Bizot, G. Cacciapaglia, and T. Flacke, "Common exotic decays of top partners," *JHEP* **06** (2018) 065, arXiv:1803.00021 [hep-ph].

[50] K.-P. Xie, G. Cacciapaglia, and T. Flacke, "Exotic decays of top partners with charge 5/3: bounds and opportunities," *JHEP* **10** (2019) 134, arXiv:1907.05894 [hep-ph].

[51] G. Cacciapaglia, T. Flacke, M. Park, and M. Zhang, "Exotic decays of top partners: mind the search gap," *Phys. Lett. B* **798** (2019) 135015, arXiv:1908.07524 [hep-ph].

[52] G. Cacciapaglia, T. Flacke, M. Kunkel, and W. Porod, "Phenomenology of unusual top-partners in composite Higgs models." In preparation, 2021.

[53] A. Agugliaro, G. Cacciapaglia, A. Deandrea, and S. De Curtis, "Vacuum misalignment and pattern of scalar masses in the SU(5)/SO(5) composite Higgs model," *JHEP* **02** (2019) 089, arXiv:1808.10175 [hep-ph].

[54] A. Karle, *Elektroschwache Wechselwirkungen der pseudo-Nambu-Goldstone-Bosonen.* Bachelor thesis, Würzburg, 2021.

[55] G. Cacciapaglia, H. Cai, T. Flacke, S. J. Lee, A. Parolini, and H. Serôdio, "Anarchic Yukawas and top partial compositeness: the flavour of a successful marriage," *JHEP* **06** (2015) 085, arXiv:1501.03818 [hep-ph].

[56] T. Alanne, N. Bizot, G. Cacciapaglia, and F. Sannino, "Classification of NLO operators for composite Higgs models," *Phys. Rev. D* **97** no. 7, (2018) 075028, arXiv:1801.05444 [hep-ph].

[57] G. Cacciapaglia, H. Cai, A. Deandrea, T. Flacke, S. J. Lee, and A. Parolini, "Composite scalars at the LHC: the Higgs, the Sextet and the Octet," *JHEP* **11** (2015) 201, arXiv:1507.02283 [hep-ph].

[58] H. Georgi, "Generalized dimensional analysis," *Phys. Lett. B* **298** (1993) 187–189, arXiv:hep-ph/9207278.

[59] G. Buchalla, O. Catá, and C. Krause, "On the Power Counting in Effective Field Theories," *Phys. Lett. B* **731** (2014) 80–86, arXiv:1312.5624 [hep-ph].

[60] C. Degrande, C. Duhr, B. Fuks, D. Grellscheid, O. Mattelaer, and T. Reiter, "UFO - The Universal FeynRules Output," *Comput. Phys. Commun.* **183** (2012) 1201–1214, arXiv:1108.2040 [hep-ph].

[61] J. Huston, "LHC Guide to Parton Distributions and Cross Sections,". ATL-PHYS-99-008.

[62] **LHC SUSY Cross Section Working Group** Collaboration, C. Borschensky *et al.* https://twiki.cern.ch/twiki/bin/view/LHCPhysics/SUSYCrossSections. Accessed 23.08.21.

[63] **CMS** Collaboration, A. M. Sirunyan *et al.*, "Search for vector-like T and B quark pairs in final states with leptons at $\sqrt{s} = 13$ TeV," *JHEP* **08** (2018) 177, arXiv:1805.04758 [hep-ex].

[64] M. Czakon and A. Mitov, "Top++: A Program for the Calculation of the Top-Pair Cross-Section at Hadron Colliders," *Comput. Phys. Commun.* **185** (2014) 2930, arXiv:1112.5675 [hep-ph].

[65] W. Beenakker, C. Borschensky, M. Krämer, A. Kulesza, and E. Laenen, "NNLL-fast: predictions for coloured supersymmetric particle production at the LHC with threshold and Coulomb resummation," *JHEP* **12** (2016) 133, arXiv:1607.07741 [hep-ph].

[66] J. Erdmenger, N. Evans, W. Porod, and K. S. Rigatos, "Gauge/gravity dynamics for composite Higgs models and the top mass," *Phys. Rev. Lett.* **126** no. 7, (2021) 071602, arXiv:2009.10737 [hep-ph].

[67] J. Alwall, P. Schuster, and N. Toro, "Simplified Models for a First Characterization of New Physics at the LHC," *Phys. Rev. D* **79** (2009) 075020, arXiv:0810.3921 [hep-ph].

[68] **LHC New Physics Working Group** Collaboration, D. Alves, "Simplified Models for LHC New Physics Searches," *J. Phys. G* **39** (2012) 105005, arXiv:1105.2838 [hep-ph].

[69] B. Fuks, "Documentation on the eVLQ FeynRules implementation,". Unpublished documentation, 2019.

[70] C. Duhr, N. Christensen, B. Fuks, and C. Degrande, "Standard model FeynRules implementation." https://feynrules.irmp.ucl.ac.be/wiki/StandardModel.

[71] B. Fuks and H.-S. Shao, "QCD next-to-leading-order predictions matched to parton showers for vector-like quark models," *Eur. Phys. J. C* **77** no. 2, (2017) 135, arXiv:1610.04622 [hep-ph].

[72] C. Uhlemann, *Narrow-width approximation in the Minimal Supersymmetric Standard Model*. Diplomarbeit, Würzburg, 2007.

[73] **NNPDF** Collaboration, R. D. Ball, V. Bertone, S. Carrazza, L. Del Debbio, S. Forte, A. Guffanti, N. P. Hartland, and J. Rojo, "Parton distributions with QED corrections," *Nucl. Phys. B* **877** (2013) 290–320, arXiv:1308.0598 [hep-ph].

[74] A. Buckley, J. Ferrando, S. Lloyd, K. Nordström, B. Page, M. Rüfenacht, M. Schönherr, and G. Watt, "LHAPDF6: parton density access in the LHC precision era," *Eur. Phys. J. C* **75** (2015) 132, arXiv:1412.7420 [hep-ph].

[75] J. Alwall, C. Duhr, B. Fuks, O. Mattelaer, D. G. Öztürk, and C.-H. Shen, "Computing decay rates for new physics theories with FeynRules and MadGraph5_aMC@NLO," *Comput. Phys. Commun.* **197** (2015) 312–323, arXiv:1402.1178 [hep-ph].

[76] P. Artoisenet, R. Frederix, O. Mattelaer, and R. Rietkerk, "Automatic spin-entangled decays of heavy resonances in Monte Carlo simulations," *JHEP* **03** (2013) 015, arXiv:1212.3460 [hep-ph].

[77] T. Sjöstrand, S. Ask, J. R. Christiansen, R. Corke, N. Desai, P. Ilten, S. Mrenna, S. Prestel, C. O. Rasmussen, and P. Z. Skands, "An introduction to PYTHIA 8.2" *Comput. Phys. Commun.* **191** (2015) 159–177, arXiv:1410.3012 [hep-ph].

[78] M. Dobbs and J. B. Hansen, "The HepMC C++ Monte Carlo event record for High Energy Physics," *Comput. Phys. Commun.* **134** (2001) 41–46.

[79] M. Cacciari, G. P. Salam, and G. Soyez, "The anti-k_t jet clustering algorithm," *JHEP* **04** (2008) 063, arXiv:0802.1189 [hep-ph].

[80] M. Cacciari, G. P. Salam, and G. Soyez, "FastJet User Manual," *Eur. Phys. J. C* **72** (2012) 1896, arXiv:1111.6097 [hep-ph].

[81] A. L. Read, "Presentation of search results: The CL_s technique," *J. Phys. G* **28** (2002) 2693–2704.

[82] **DELPHES 3** Collaboration, J. de Favereau, C. Delaere, P. Demin, A. Giammanco, V. Lemaître, A. Mertens, and M. Selvaggi, "DELPHES 3, A modular framework for fast simulation of a generic collider experiment," *JHEP* **02** (2014) 057, arXiv:1307.6346 [hep-ex].

[83] M. Chakraborti *et al.* https://checkmate.hepforge.org/. Accessed 25.08.21.

[84] "MadAnalysis 5 Public Analysis Database (PAD) for recasting LHC results." http://madanalysis.irmp.ucl.ac.be/wiki/PublicAnalysisDatabase. Accessed 25.08.21.

[85] J. D. Hunter, "Matplotlib: A 2d graphics environment," *Comput. Sci. Eng.* **9** no. 3, (2007) 90–95.

[86] **ATLAS** Collaboration, "Search for supersymmetry in final states with missing transverse momentum and multiple b-jets in proton-proton collisions at $\sqrt{s} = 13$ TeV with the ATLAS detector,". ATLAS-CONF-2018-041.

[87] **CMS** Collaboration, A. M. Sirunyan *et al.*, "Search for supersymmetry in proton-proton collisions at 13 TeV in final states with jets and missing transverse momentum," *JHEP* **10** (2019) 244, arXiv:1908.04722 [hep-ex].

[88] **ATLAS** Collaboration, "Search for squarks and gluinos in final states with jets and missing transverse momentum using 139 fb^{-1} of $\sqrt{s}$ =13 TeV pp collision data with the ATLAS detector,". ATLAS-CONF-2019-040.

[89] M. Mrowietz, S. Bein, and J. Sonneveld, "Implementation of the CMS-SUS-19-006 analysis in the MadAnalysis 5 framework (supersymmetry with large hadronic activity and missing transverse energy; 137 fb^{-1})," *Mod. Phys. Lett. A* **36** no. 01, (2021) 2141007.

[90] **ATLAS** Collaboration, G. Aad *et al.*, "Search for bottom-squark pair production with the ATLAS detector in final states containing Higgs bosons, b-jets and missing transverse momentum," *JHEP* **12** (2019) 060, arXiv:1908.03122 [hep-ex].

[91] **ATLAS** Collaboration, M. Aaboud *et al.*, "Search for squarks and gluinos in final states with jets and missing transverse momentum using 36 fb^{-1} of $\sqrt{s} = 13$ TeV pp collision data with the ATLAS detector," *Phys. Rev. D* **97** no. 11, (2018) 112001, arXiv:1712.02332 [hep-ex].

[92] **CMS** Collaboration, A. M. Sirunyan *et al.*, "Search for supersymmetry in multijet events with missing transverse momentum in proton-proton collisions at 13 TeV," *Phys. Rev. D* **96** no. 3, (2017) 032003, arXiv:1704.07781 [hep-ex].

[93] **ATLAS** Collaboration, G. Aad *et al.*, "Search for squarks and gluinos in final states with one isolated lepton, jets, and missing transverse momentum at $\sqrt{s} = 13$ TeV with the ATLAS detector," *Eur. Phys. J. C* **81** no. 7, (2021) 600, arXiv:2101.01629 [hep-ex].

[94] **ATLAS** Collaboration, G. Aad *et al.*, "Search for a scalar partner of the top quark in the all-hadronic $t\bar{t}$ plus missing transverse momentum final state at $\sqrt{s} = 13$ TeV with the ATLAS detector," *Eur. Phys. J. C* **80** no. 8, (2020) 737, arXiv:2004.14060 [hep-ex].

[95] **CMS** Collaboration, A. M. Sirunyan *et al.*, "Search for top squark production in fully-hadronic final states in proton-proton collisions at $\sqrt{s} = 13$ TeV," *Phys. Rev. D* **104** no. 5, (2021) 052001, arXiv:2103.01290 [hep-ex].

[96] G. Cacciapaglia, A. Deandrea, T. Flacke, and A. M. Iyer, "Gluon-Photon Signatures for color octet at the LHC (and beyond)," *JHEP* **05** (2020) 027, arXiv:2002.01474 [hep-ph].

[97] **ATLAS** Collaboration, "Search for pair-production of vector-like quarks in pp collision events at $\sqrt{s} = 13$ TeV with at least one leptonically-decaying Z boson and a third-generation quark with the ATLAS detector,". ATLAS-CONF-2021-024.

[98] **CMS** Collaboration, A. M. Sirunyan *et al.*, "A search for bottom-type, vector-like quark pair production in a fully hadronic final state in proton-proton collisions at $\sqrt{s} =$ 13 TeV," *Phys. Rev. D* **102** (2020) 112004, `arXiv:2008.09835 [hep-ex]`.

[99] **CMS** Collaboration, A. M. Sirunyan *et al.*, "A search for bottom-type, vector-like quark pair production in a fully hadronic final state in proton-proton collisions at $\sqrt{s} =$ 13 TeV," *Phys. Rev. D* **102** (2020) 112004, `arXiv:2008.09835 [hep-ex]`.

[100] **CMS** Collaboration, A. M. Sirunyan *et al.*, "Search for top quark partners with charge 5/3 in the same-sign dilepton and single-lepton final states in proton-proton collisions at $\sqrt{s} = 13$ TeV," *JHEP* **03** (2019) 082, `arXiv:1810.03188 [hep-ex]`.

[101] **ATLAS** Collaboration, G. Aad *et al.*, "Search for R-parity violating supersymmetry in a final state containing leptons and many jets with the ATLAS experiment using $\sqrt{s} = 13$ TeV proton-proton collision data," `arXiv:2106.09609 [hep-ex]`.

Ich versichere, dass ich die vorliegende Masterarbeit selbstständig verfasst und nur die angegebenen Quellen und Hilfsmittel verwendet habe. Weiterhin versichere ich, dass ich die Arbeit bisher oder gleichzeitig keiner anderen Prüfungsbehörde zur Erlangung eines akademischen Grades vorgelegt habe.

Würzburg, den 27.09.2021

(Manuel Kunkel)

Acknowledgment

I would like to thank my supervisor, Prof. Dr. Werner Porod, for teaching me the inner workings of the standard model and its extensions, for always being open to my questions, and for his patience when I came back with the same questions again the following week.

I am grateful to Giacomo Cacciapaglia and Thomas Flacke, as well as Markus Feld, Andreas Karle, Leonard Schwarze and Michael Sittinger, for making our weekly meetings something I was always looking forward to. I am also thankful to Yang Liu for helping me with the installation of CheckMATE.

Finally, I could not have finished this thesis without the love and support of my family and friends. I would like to particularly thank my parents for always believing in me, as well as Tim Janiak, Lea Janiak and Tim Ammerer for helping me take my mind off of physics every once in a while.